Functional Renormalization-Group Analysis of Luttinger Liquids with Impurities

Von der Fakultät Mathematik und Physik der Universität Stuttgart
zur Erlangung der Würde eines Doktors der Naturwissenschaften
(Dr. rer. nat.) genehmigte Abhandlung

vorgelegt von

Sabine Andergassen

aus Bozen (Italien)

Hauptberichter: Prof. Dr. Walter Metzner
Mitberichter: Prof. Dr. Ulrich Weiss

Tag der mündlichen Prüfung: 20. Januar 2006

Max-Planck-Institut für Festkörperforschung

Stuttgart 2005

Für meine Eltern und Susanne

Acknowledgments

Several people contributed to the realization of the present thesis, and I would like to express my gratitude for their support during the last years.

First of all, I would like to thank my supervisor Prof. Walter Metzner, who taught me to appreciate the beauty of simple ideas. I would like to thank him for his heedful supervision, for guiding my first steps in scientific research, for always having time for discussions, the numerous valuable suggestions, for his constant encouragement and support, and for the opportunity to attend several international workshops and conferences. It has been a great pleasure to work in his theory group, and I wish to thank for the opportunity to join his collaboration with Prof. Kurt Schönhammer and Prof. Volker Meden in Göttingen, and Prof. Uli Schollwöck in Aachen. It has been a particularly enriching experience and fruitful collabaration. I would like to thank Prof. Kurt Schönhammer and Prof. Volker Meden for their support, the numerous discussions and encouragement, the stimulating correspondence, the careful proofreading of the manuscript, and the warm hospitality. To Prof. Uli Schollwöck I would like to express my thanks for his precious suggestions.

I would like to thank Prof. Ulrich Weiss for his willingness to co-report on the thesis.

I wish to thank Prof. Manfred Salmhofer for the excellent lectures on the functional renormalization-group technique, and Prof. Carsten Honerkamp for his support and suggestions of further extensions and applications.

A special thank goes to my officemate Dr. Tilman Enss, for the numerous discussions, his helpfulness and patient assistence in computer issues. It was a great pleasure to share these years. I would also like to thank him for a critical reading of the manuscript.

Let me also commemorate Xavier Barnabé-Thériault from Göttingen, with whom I started, together with Dr. Tilman Enss, to implement a small shared library, and who unfortunately died in a tragic accident on August 15, 2004. He conveyed the curiosity and enthusiasm in approaching open problems.

I wish to thank Dr. Daniel Rohe for always finding time for my questions, his encouragement and a critical proofreading, Julius Reiss for his assistence and his sociocultural activities at the institute, Roland Gersch for a careful reading of the manuscript, Dr. habil. Karsten Held and Dr. habil. Dirk Manske for their help and encouragement, as well as all other members of the Department Metzner, for the numerous discussions and interesting conversations, their support and the friendly atmosphere. I would also like to thank our secretary Mrs. Ingrid Knapp for her help in all organizational matters, and the Computer Department of the Max Planck Institute for their support.

I owe particular thanks to Prof. Carlo Di Castro, Prof. Claudio Castellani, and Dr. Massimo Capone in Rome for advices and valuable discussions.

Abstract

In one-dimensional quantum wires the interplay of electron correlations and impurities strongly influences the low-energy physics. The diversity of energy scales and the competition of correlations in interacting Fermi systems can be treated very efficiently with the functional renormalization group (fRG), describing the gradual evolution from a microscopic model Hamiltonian to the effective low-energy action as a function of a continuously decreasing energy cutoff. The fRG provides the universal low-energy asymptotics as well as nonuniversal properties, and in particular an answer to the important question at what scale the ultimate asymptotics sets in.

The lowest order truncation of the fRG hierarchy of flow equations considered previously for spinless fermions is generalized to spin-$\frac{1}{2}$ systems and extended including renormalization of the two-particle interaction, in addition to renormalization of the impurity potential. The underlying approximations are devised for weak interactions and arbitrary impurity strengths. A comparison with numerical density-matrix renormalization results for systems with up to 1000 sites shows that the fRG is remarkably accurate even for intermediate interaction strengths.

We investigate the influence of impurities on spectral and transport properties of fermionic lattice models with short-range interactions. The results capture relevant energy scales and crossover phenomena, in addition to the universal low-energy asymptotics. For weak and intermediate impurity strengths the asymptotic behavior is approached only at rather low energy scales, accessible only for very large systems. For spin-$\frac{1}{2}$ systems two-particle backscattering leads to striking effects, which are not captured if the bulk system is approximated by its low-energy fixed point, the Luttinger model. In particular, the expected decrease of spectral weight near the impurity and of the conductance at low energy scales is often preceded by a pronounced increase, and the asymptotic power laws are modified by logarithmic corrections.

Contents

1 Introduction

In one dimension metallic electron systems are strongly affected by interactions. Differently from the conventional Fermi-liquid behavior, the generic low-energy physics is described by the Luttinger-liquid phenomenology [Giamarchi 2004]. For various correlation functions Luttinger-liquid theory predicts anomalous power laws; for spin-rotation invariant systems the exponents can be expressed in terms of a single interaction-dependent parameter K_ρ. An important aspect concerns the peculiar effects due to the interplay of impurities and interactions. For Luttinger liquids with repulsive interactions already a single static impurity has a strong effect [Luther and Peschel 1974; Mattis 1974; Apel and Rice 1982; Giamarchi and Schulz 1988]. At low energy scales even a weak impurity effectively "cuts" the system into two parts with open boundary conditions at the end points, and physical observables are controlled by the open chain fixed point [Kane and Fisher 1992a,c]. In particular, the impurity potential becomes dressed by long-range oscillations leading to a characteristic power-law suppression of the local density of states near the impurity and the conductance through the impurity down to zero in the low-energy limit. The asymptotic behavior is universal in the sense that the exponents depend only on the properties of the bulk system via K_ρ, while they do not depend on the impurity strength or shape. These power laws are generally modified by logarithmic corrections in the presence of two-particle backscattering.

The *asymptotic* low-energy properties of Luttinger liquids with a single impurity are rather well understood. Universal power laws and scaling functions have been obtained by bosonization, conformal field theory and exact solutions for the low-energy asymptotics in special integrable cases [Giamarchi 2004]. Numerical methods as exact diagonalization and the density-matrix renormalization group (DMRG) confirm the field-theoretical predictions and the validity of the underlying assumptions for microscopic fermionic systems with Luttinger-liquid behavior. The limited system size accessible to numerical solutions is however a serious constraint for a systematic analysis beyond the perturbatively accessible weak and strong-impurity regimes. The important question arises at what *scale* the ultimate asymptotics sets

in and asymptotic power laws are actually valid. That scale can indeed be surprisingly low, and the properties above it very different from the asymptotic behavior. Recently a functional renormalization group (fRG) method has been introduced for a direct treatment of *microscopic* models of interacting fermions, which does not only capture correctly the universal low-energy asymptotics, but allows to compute observables on all energy scales, providing thus also *nonuniversal* properties, and a possible key to the understanding of the behavior at intermediate scales accessible in experiments. Some of the nonuniversal properties can be computed numerically by the DMRG, but this method is limited to lattice systems with about 1000 sites, and only a restricted set of observables can be evaluated with affordable computational effort.

The fRG provides a powerful computational tool to study interacting Fermi systems, especially low-dimensional systems with competing instabilities and entangled infrared singularities. Starting point is an exact hierarchy of differential flow equations for the Green or vertex functions of the system, describing the gradual evolution from the microscopic model Hamiltonian to the effective action as a function of a continuously decreasing energy cutoff introduced in the free propagator [Salmhofer 1998]. Approximations are then constructed by truncating the hierarchy and parametrizing the vertex functions with a manageable set of variables or functions. The fRG captures the expected universal power laws at low energy, as well as relevant energy scales and nonuniversal crossover phenomena at intermediate scales, as for the temperature dependence of the conductance through a double barrier [Enss et al. 2005; Meden et al. 2005]. The direct application to microscopic models allows for a flexible modeling of different geometries, as mesoscopic rings threaded by a magnetic flux [Meden and Schollwöck 2003a,b] and Y junctions [Barnabé-Thériault et al. 2005a,b].

In previous applications to spinless Luttinger liquids with impurities [Meden et al. 2002a,b] the fRG hierarchy of flow equations was truncated at first order, where the renormalized vertex is approximated by the bare interaction. Despite the simplicity of this scheme the effects of a single static impurity are captured qualitatively, and for spinless fermions in the weak coupling limit also quantitatively. It turned out that the asymptotic behavior typically holds only at very low energy scales and for very large systems, except for very strong bare impurities.

In the present work we further develop and extend the fRG approach for Luttinger liquids with impurities to spin-$\frac{1}{2}$ fermions and include two-particle vertex

renormalization, in addition to the renormalization of the impurity potential. The underlying approximations are devised for weak interactions and arbitrary impurity strength. A comparison with exact numerical DMRG results for systems with up to 1000 sites shows however that the fRG with the inclusion of vertex renormalization is remarkably accurate even for intermediate interaction strengths. For spinless fermions this extension improves considerably the quantitative accuracy of the results in particular at intermediate interaction strengths, whereas for spin-$\frac{1}{2}$ systems vertex renormalization is necessary to take into account that backscattering of particles with opposite spins at opposite Fermi points scales to zero in the low-energy limit. Explicit flow equations are derived for various lattice fermion models supplemented by different types of impurity potentials. We present results for spectral properties of single-particle excitations, the oscillations in the density profile induced by impurities or boundaries and the linear conductance for chains with up to 10^6 lattice sites. Two-particle backscattering leads to peculiar effects, which are not captured if the bulk system is approximated by its low-energy fixed point, the Luttinger model. In particular, the expected decrease of spectral weight near the impurity and of the conductance at low energy scales is often preceded by a pronounced increase, and the asymptotic power laws are modified by logarithmic corrections.

The outline of the thesis is as follows.

- In Chapter 2 we give a short overview on general aspects of Luttinger liquids with impurities.

- The fRG formalism is developed in Chapter 3. We briefly review the fRG for interacting Fermi systems, and derive the hierarchy of differential flow equations for the one-particle irreducible (1PI) vertex functions.

- In Chapter 4 we describe the implementation of the fRG technique for various one-dimensional microscopic lattice models with impurities, providing details on the parametrization of the two-particle vertex and different truncation schemes. Parts of this chapter are published in

  S. Andergassen, T. Enss, V. Meden, W. Metzner, U. Schollwöck, and K. Schönhammer, *Functional renormalization group for Luttinger liquids with impurities*, Phys. Rev. B **70**, 075102 (2004), `cond-mat/0403517`;

S. Andergassen, T. Enss, V. Meden, W. Metzner, U. Schollwöck, and K. Schönhammer, *Renormalization group analysis of the one-dimensional extended Hubbard model with a single impurity*, cond-mat/0509021.

- In Chapter 5 we present results for spectral properties of single-particle excitations near an impurity or boundary, the density profile, and transport properties in the presence of a single and a double barrier. In the first part we focus on spinless fermions; the modifications due to the spin degree of freedom are addressed in the second part. Parts of this chapter are presented in the above publications, and for the conductance in

  V. Meden, S. Andergassen, W. Metzner, U. Schollwöck, and K. Schönhammer, *Scaling of the conductance in a quantum wire*, Europhys. Lett. **64**, 769 (2003), cond-mat/0303460;

  V. Meden, T. Enss, S. Andergassen, W. Metzner, and K. Schönhammer, *Correlation effects on resonant tunneling in one-dimensional quantum wires*, Phys. Rev. B **71**, 041302(R) (2005), cond-mat/0403655;

  T. Enss, V. Meden, S. Andergassen, X. Barnabé-Thériault, W. Metzner, and K. Schönhammer, *Impurity and correlation effects on transport in one-dimensional quantum wires*, Phys. Rev. B **71**, 155401 (2005), cond-mat/0411310;

  S. Andergassen, T. Enss, and V. Meden, *Kondo physics in transport through a quantum dot with Luttinger liquid leads*, cond-mat/0509576.

- We conclude in Chapter 6 with a summary and an outlook on further applications and extensions of the present work.

2 Impurities in Luttinger liquids

The exactly soluble Luttinger model provides a generic scenario for one-dimensional Fermi systems with repulsive interactions, denoted as "Luttinger liquid". The low-energy physics is completely determined by a few interaction-dependent characteristic parameters describing the power-law exponents of the correlation functions. Already a single static impurity leads to peculiar modifications of the electronic properties of Luttinger liquids. Even for a weak impurity potential, physical observables behave as if the system is split into two parts in the low-energy limit. The local density of states near the impurity and the conductance through the impurity vanish as power laws.

2.1 Luttinger liquids

In one-dimensional interacting Fermi systems Fermi-liquid theory is not valid. The breakdown of Fermi-liquid theory is indicated already in second order perturbation theory, where the reduction of the quasi-particle weight at the Fermi surface due to interactions diverges logarithmically. These divergencies can be treated by a weak-coupling renormalization-group method applied to an effective low-energy theory known as g-ology model [Sólyom 1979]. Depending on the values of the bare couplings, the renormalized couplings flow either to strong coupling, and hence out of the perturbatively controlled regime, or to a fixed-point Hamiltonian, the exactly soluble Luttinger model [Tomonaga 1950; Luttinger 1963; Mattis and Lieb 1965]. The term "Luttinger liquid" has been introduced for the latter systems, in analogy with the mapping of low-energy states of interacting electron systems onto the Fermi gas in higher dimensions for Fermi liquids [Haldane 1981b]. The normal

gapless metallic phase is characterized by *i)* a continuous momentum distribution with a power-law singularity at the Fermi surface, described by a nonuniversal exponent α; *ii)* a single-particle density of states which vanishes as $|\omega|^\alpha$ near the Fermi energy, implying the absence of fermionic quasi-particles; *iii)* finite charge and spin-density responses for long wavelengths and the existence of collective bosonic charge and spin-density modes; *iv)* power-law singularities in various correlation functions with interaction-dependent exponents; *v)* separation of spin and charge degrees of freedom. There are several good reviews on one-dimensional Fermi systems, recent reviews are presented in Refs. [Voit 1995; Giamarchi 2004]. In the following we will summarize the most important results.

Theoretical work on interacting fermions in one dimension has progressed along different lines. Besides the perturbative investigation of the weak-coupling limit [Sólyom 1979], Luttinger-liquid theory is usually formulated using the bosonization technique [Mattis and Lieb 1965; Haldane 1980, 1981a,b; Luther and Peschel 1974; Mattis 1974]. A different approach is based on the Bethe-ansatz method for special integrable models [Giamarchi 2004]. The computation of correlation functions is however very difficult from the complicated expressions for the eigenfunctions.

As proposed in a seminal work by Haldane [Haldane 1981b], the low-energy physics of the Luttinger model is generic for interacting fermions in one dimension with repulsive interactions. In the language of the renormalization group the Luttinger model Hamiltonian is the fixed-point Hamiltonian for a large class of one-dimensional fermions with repulsive interactions. The Luttinger model can be solved exactly at any interaction; it is characterized by a linear dispersion relation, and the electron-electron interaction is limited to forward scattering only [Giamarchi 2004]. Umklapp and backscattering processes, as well as additional terms for more general models arising from band curvature are irrelevant and vanish in the low-energy limit [Haldane 1981b]. As in the Landau Fermi liquid a few parameters completely determine the low-energy physics. The charge degrees of freedom of Luttinger liquids are described by a sound velocity v_ρ and the dimensionless parameter K_ρ, and the spin degrees of freedom are characterized by a spin-wave velocity v_σ and K_σ. All correlation functions are uniquely parametrized by K_ν and the velocities of the collective modes v_ν, with $\nu = \rho, \sigma$, in the low-energy limit; the corresponding exponents are determined by K_ν. For noninteracting particles $K_\rho = K_\sigma = 1$. In the absence of a magnetic field, the ground state is spin-rotationally invariant and $K_\sigma = 1$, while $K_\rho < 1$ (> 1) for repulsive (attractive) forces.

For $K_\sigma = 1$ the momentum distribution function exhibits a power-law singularity at the Fermi level with exponent $\alpha = (K_\rho + K_\rho^{-1} - 2)/4$ for any nonvanishing interaction [Giamarchi 2004]. For $\alpha < 1$ the momentum distribution function near k_F obeys a power law

$$|n(k) - n(k_F)| \sim |k - k_F|^\alpha \; . \tag{2.1}$$

The spectral function has the form

$$N(\omega) \sim |\omega|^\alpha \tag{2.2}$$

in the low-energy limit. Landau quasi-particle excitations are absent in the Luttinger liquid. The power laws hold also for nonsoluble generalizations of the model with a nonlinear dispersion [Haldane 1981b].

In the Luttinger model the charge and spin density modes are exact undamped eigenstates, and any excited state of the model is a superposition of these elementary excitations. This becomes particularly explicit in the bosonized form of the Luttinger model [Mattis and Lieb 1965]. The Luttinger model Hamiltonian conserves charge and the z component of spin separately on each Fermi point. Charge and spin excitations are completely independent, as the respective terms in the Hamiltonian commute. This phenomenon is called "spin-charge separation" [Giamarchi 2004], charge and spin propagate with different velocities.

Concerning the leading low-energy long-wavelength response functions there is no difference between Fermi and Luttinger liquids [Giamarchi 2004]. Thermodynamic properties as the compressibility and the susceptibility do not differ from the Fermi-liquid description and the modification due to the interaction leads to renormalized coefficients depending on K_ν and v_ν. Differences between Fermi and Luttinger-liquid behavior arise only from the enhanced phase space for forward scattering in one dimension. Marked differences appear in the single-particle propagator, which determines the momentum distribution function and the spectral density for single-particle excitations. In a Fermi liquid residual interactions modify the propagator only on a subleading level, leading for example to a small quasi-particle decay rate, while in a Luttinger liquid forward scattering affects the leading low-energy behavior. Another distinctive feature of Luttinger liquids is the singular behavior of density correlations with momenta near $2k_F$ [Giamarchi 2004].

Conservation laws play a crucial role in one-dimensional Fermi systems [Metzner et al. 1998]. In addition to the usual charge and spin conservation the discrete

structure of the Fermi surface in one dimension leads to an additional conservation law: separate charge conservation in low-energy scattering processes for particles near the left and right Fermi points, respectively. Separate spin conservation is spoiled by the backscattering process generally present in models of spin-$\frac{1}{2}$ fermions. In most cases of interest, in particular for the models considered in the present work, the backscattering amplitude scales to zero at low energies, and the separate spin conservation is restored asymptotically. The velocities associated with the corresponding conserved currents provide a complete parametrization of the low-energy physics [Haldane 1981b; Metzner and Di Castro 1993].

2.2 Impurity effects

An important aspect of Luttinger-liquid behavior concerns the peculiar modification of the electronic properties in the presence of impurities. For Luttinger liquids with repulsive interactions ($K_\rho < 1$) already a single static impurity has a strong effect at low energy scales, even if the impurity potential is relatively weak [Luther and Peschel 1974; Mattis 1974; Apel and Rice 1982; Giamarchi and Schulz 1988; Kane and Fisher 1992a,c; Furusaki and Nagaosa 1993a,b; Yue et al. 1994]. In general the interplay of disorder and interactions is still a challenging issue, although the properties of noninteracting disordered electronic systems are rather well understood. In one-dimensional noninteracting systems disorder leads to localization of all electrons; the localization length characterizing the exponential decay of the wave function is of the same order as the mean free path [Giamarchi 2004]. On the other hand interactions strongly affect the properties of the pure system, leading to Luttinger-liquid behavior. Thus in one dimension a particularly strong mutual influence of disorder and interactions is expected.

Relevant parameters in the description of disorder are the strength of the individual impurity V and the impurity density n_{imp}. The variation of these two parameters leads to different physical effects. In the limiting case of very weak individual impurities with a dense distribution the effect of a single impurity is negligible and collective effects dominate; the corresponding relevant length scale is $\sim 1/n_{\mathrm{imp}}$. As a consequence of the central-limit theorem, for continuous systems the disorder can be described by a Gaussian distribution in the limit $n_{\mathrm{imp}} \to \infty$ and $V \to 0$ for constant $n_{\mathrm{imp}}V^2$ measuring the disorder strength [Giamarchi 2004]. The main results

for Gaussian disorder from a perturbative treatment can be summarized as follows [Giamarchi 2004]. Interactions are effectively renormalized by disorder, which is reversely affected by interactions. Repulsive interactions generally enhance localization whereas attractive ones reduce this effect. For spinless fermions attractive interactions enhance superconducting fluctuations, leading to an effective screening of the disorder. For spin-$\frac{1}{2}$ fermions a competing effect arises. The tendency towards a uniform charge distribution inhibits the coupling to disorder, leading to an increase in the localization length for strong interactions in the pure Hubbard model. For the extended Hubbard model with a local as well as nearest-neighbor interaction this effect is reduced. The opposite limit examined in the present work corresponds to strong and dilute impurities. In this case collective effects do not play any role and the problem essentially reduces to a single isolated impurity. An interesting unsolved problem concerns the combination of single impurity and collective effects at intermediate scales: depending on whether collective effects become important before the individual impurities renormalize to high barriers, a different characteristic behavior is expected.

In the following we consider the case of a single or double impurity, where the effects of coherent scattering from many impurities are absent. The asymptotic low-energy properties of Luttinger liquids with a single impurity have been investigated by mapping the problem onto an effective field theory, where terms which are expected to be irrelevant in the low-energy limit are neglected. For attractive interactions the impurity is irrelevant in the renormalization-group sense and scales to zero at low energies. For repulsive electron systems with $K_\rho < 1$ the essential properties from the perturbative bosonic renormalization-group calculation and the boundary conformal field-theory analysis can be summarized as follows. The backscattering amplitude generated by a weak impurity is a relevant perturbation which grows as $\Lambda^{(K_\rho - 1)/z}$, for a decreasing energy scale Λ, where z is the number of spin components. This behavior can be traced back to the power-law singularity of the $2k_F$ density response function in a Luttinger liquid. On the other hand, the tunneling amplitude through a weak link between two otherwise separate wires is irrelevant and scales to zero as Λ^{α_B}, with the boundary exponent

$$\alpha_B = \frac{1}{z}(K_\rho^{-1} - 1) \tag{2.3}$$

depending only on the interaction strength and band filling, but not on the impurity parameters. At low energy scales any impurity thus effectively "cuts" the system into

two parts with open boundary conditions at the end points, and physical observables are controlled by the open chain fixed point.

In particular, the local density of states near the impurity is suppressed as

$$\rho(\omega) \sim |\omega|^{\alpha_B} \tag{2.4}$$

for $|\omega| \to 0$.

Long-range Friedel oscillations in the density profile induced by boundaries or impurities decay with a power law at long distances [Egger and Grabert 1995] as

$$n(x) \sim x^{-K_\rho} \tag{2.5}$$

for spinless fermions, where x measures the distance from the impurity or boundary. For spin-$\frac{1}{2}$ fermions K_ρ is replaced by $(K_\rho + 1)/2$ in Eq. (2.5).

The conductance through an infinite Luttinger liquid with a single impurity vanishes at low temperatures as

$$G(T) \sim T^{2\alpha_B} \ . \tag{2.6}$$

The conductance through a single impurity of variable strength can be collapsed onto a single curve by a one-parameter scaling ansatz. For resonant scattering at double barriers the distance between the two barriers and the detuning from resonance introduce additional scales and a more complex behavior is observed. The Lorentzian resonance line shape for noninteracting electrons is modified by the interaction, and for appropriate parameters the conductance exhibits distinctive power-law scaling as a function of temperature [Kane and Fisher 1992b; Furusaki and Nagaosa 1993a; Furusaki 1998; Nazarov and Glazman 2003; Polyakov and Gornyi 2003; Yue et al. 1994].

Note that the above power laws are strictly valid only in the absence of two-particle backscattering. For spin-$\frac{1}{2}$ fermions they are in general modified by logarithmic corrections. The asymptotic behavior is universal in the sense that the exponents depend only on the properties of the bulk system, via K_ρ, while they do not depend on the impurity strength or shape, except in special cases such as resonant scattering at double barriers, which require fine-tuning of parameters.

The asymptotic low-energy properties of Luttinger liquids with a single impurity are rather well understood. Universal power laws and scaling functions have been obtained by bosonization, conformal field theory, and exact solutions for the

low-energy asymptotics in special integrable cases [Giamarchi 2004]. Numerical results from exact diagonalization and DMRG applied to the lattice model of spinless fermions with nearest-neighbor interaction confirmed the field theoretical scenario and the validity of the underlying assumptions [Eggert and Affleck 1992; Meden et al. 1998]. These methods are however limited to lattice systems with about 1000 sites and do not allow for a systematic analysis of the crossover between the weak and strong-impurity limit. Moreover, only a restricted set of observables can be evaluated with affordable computational effort. In this context the fRG provides a complementary technique for microscopic models of interacting fermions with impurities, which does not only capture correctly the universal low-energy asymptotics, but allows one to compute observables on all energy scales, providing thus also nonuniversal properties, and in particular an answer to the important question at what scale the ultimate asymptotics sets in. That scale can indeed be surprisingly low, and the properties above it very different from the asymptotic behavior.

2.3 Experimental realization

The progress in the fabrication of artificial low-dimensional structures led to advanced experimental verification of the theoretical predictions. We present a short list of the most promising systems and of the employed experimental techniques. For a detailed discussion and references to the most recent publications and review articles on the subject we refer to Ref. [Schönhammer 2004].

Strictly one-dimensional systems are a theoretical idealization, the coupling to an experimental probe as well as the coupling between several Luttinger liquids is not completely understood [Giamarchi 2004]. The coupling between the chains in a strongly anisotropic three-dimensional compound leads to the development of long-range order at very low temperatures in the phase for which the algebraic decay of the corresponding correlation function of the single-chain Luttinger liquid is the slowest. In appropriate temperature and energy regimes Luttinger-liquid behavior can be expected in several systems with a predominantly one-dimensional character, as highly anisotropic quasi one-dimensional conductors, organic conductors like the Bechgaard salts, as well as inorganic materials, artificial quantum wires in semiconductor heterostructures or on surface substrates, carbon nanotubes, and fractional quantum Hall fluids [Schönhammer 2004]. In particular, single-wall carbon nan-

otubes are expected to show Luttinger-liquid behavior with $K_\rho \sim 0.2 - 0.3$ down to very low temperatures, despite the presence of two low-energy channels [Egger and Gogolin 1997; Kane et al. 1997].

Experimental techniques used to verify Luttinger-liquid behavior involve mainly high resolution photoemission and transport measurements, in addition to optical properties [Schönhammer 2004]. A careful analysis of experimental data indicating power-law behavior and signatures of spin-charge separation reveals partly inconsistent interpretations. The discussion on the modification of the quantized value e^2/h for noninteracting electrons in a single channel by the interaction to $K_\rho\,(e^2/h)$ indicates a sensitive dependence on the schematization of the contacts, a challenging theoretical as well as experimental problem [Schönhammer 2004]. Experimental results for cleaved-edge overgrowth quantum wires and carbon nanotubes indicate power laws of the conductance consistent with Luttinger-liquid behavior. In the last few years, ultracold gases in optical lattices have opened up an entirely new area of physics, where strong correlations can be studied with unprecedented flexibility and control of the parameters. Further work is necessary for clear experimental evidence of Luttinger-liquid behavior.

3 Functional RG technique: a short overview

We review the functional renormalization-group approach for interacting Fermi systems in the 1PI version. Introducing an infrared cutoff Λ in the free propagator and differentiating the effective action with respect to Λ, an exact hierarchy of differential flow equations for the 1PI vertex functions is derived, describing the gradual evolution from the microscopic model Hamiltonian to the effective action as a function of the continuously decreasing energy cutoff. We briefly discuss the relation to alternative formulations of the fRG approach.

3.1 Introduction

The renormalization-group is a powerful method in the study of low-dimensional Fermi systems, providing in particular a systematic and unbiased method to study competing instabilities and entangled infrared singularities at weak coupling. Early renormalization-group approaches for one-dimensional systems, combined with exact solutions of fixed-point models, have been a major source of physical insight [Sólyom 1979; Giamarchi 2004]. From the renormalization-group point of view, the existence of the Luttinger liquid requires the cancellation of contributions to the flow of the two-particle vertex to all orders [Metzner et al. 1998]. This is a one-dimensional phenomenon, in higher dimensions the interactions in general diverge and the flow in the fermionic variables breaks down indicating a possible opening of a gap in the fermionic excitation spectrum.

Wilson's renormalization-group approach [Wilson 1971; Wilson and Kogut 1974] of successive integration of degrees of freedom with different energy scales determines the evolution of the bare action of the system, given by the microscopic Hamilto-

nian, to the final effective action, from which all physical quantities can be extracted. The hierarchy of coupled differential flow equations for the Green or vertex functions describing the full functional evolution of the effective action has been first implemented for bosonic field theories in the context of critical phenomena [Wegner and Houghton 1973; Polchinski 1984; Wetterich 1993]. The intuition of the relevance of fRG methods for interacting Fermi systems followed in the 1990s [Benfatto and Gallavotti 1990; Feldman and Trubowitz 1990; Shankar 1991, 1994], together with important rigorous work [Salmhofer 1999]. The infinite hierarchy of flow equations can be solved exactly only in special cases, for instance the Luttinger model [Schütz et al. 2004]. Truncations however preserve the successive handling of energy scales and the consequent treatment of infrared singularities, characteristic of a renormalization-group treatment.

There are several variants of the fRG flow equations. The flow equations for the connected amputated Green functions correspond to the Polchinski scheme, first derived in Ref. [Polchinski 1984; Keller et al. 1992]. The expansion of the connected amputated Green functions in 1PI vertex functions led to the respective flow equations [Wegner and Houghton 1973; Weinberg 1976], subsequently derived from the Legendre transform of the generating functional [Wetterich 1993; Morris 1994; Salmhofer and Honerkamp 2001]. The Wick-ordered scheme is obtained from the Polchinski scheme by expanding the generating functional of the connected amputated Green functions in Wick-ordered polynomials [Wieczerkowski 1988; Salmhofer 1998, 1999]. Important applications of the fRG in condensed-matter physics include the two-dimensional Hubbard model using the Polchinski scheme [Zanchi and Schulz 1998, 2000], the Wick-ordered scheme [Halboth and Metzner 2000] and also the 1PI scheme [Honerkamp et al. 2001]. In the context of classical disordered systems a fRG approach is necessary to overcome the problem of dimensional reduction [Wiese 2003]. One-dimensional impurity problems and Luttinger-liquid physics are most conveniently investigated in the 1PI scheme, as self-energy contributions are included to all orders.

In the following the hierarchy of differential flow equations for the 1PI vertex functions is derived, which is obtained by differentiating the corresponding generating functional with respect to an infrared cutoff introduced in the free propagator [Salmhofer 1998].

3.2 Generating functional

We consider a system of interacting fermions with single-particle propagator of the noninteracting system G_0. The properties of the system are determined by the action

$$S[\psi,\bar{\psi}] = (\bar{\psi}, G_0^{-1}\psi) - V[\psi,\bar{\psi}] \;, \tag{3.1}$$

where $\bar{\psi}$ and ψ are Grassmann variables associated with creation and annihilation operators, and $V[\psi,\bar{\psi}]$ is an arbitrary many-body interaction. Here we introduced the short-hand notation $(\bar{\psi}, G_0^{-1}\psi) = \sum_{K,K'} \bar{\psi}_K [G_0^{-1}]_{K,K'} \psi_{K'}$, where K contains the Matsubara frequency in addition to the single-particle quantum numbers and $\sum_K$ stands for summation over the discrete indices and integrals over the continuous ones.

All connected Green functions are obtained from the generating functional [Negele and Orland 1987] defined by

$$\begin{aligned} e^{-\mathcal{G}[\eta,\bar{\eta}]} &= \frac{1}{\mathcal{Z}_0} \int d\psi d\bar{\psi}\, e^{S[\psi,\bar{\psi}]}\, e^{-(\bar{\psi},\eta)-(\bar{\eta},\psi)} \\ &= \int d\mu_Q[\psi,\bar{\psi}]\, e^{-V[\psi,\bar{\psi}]}\, e^{-(\bar{\psi},\eta)-(\bar{\eta},\psi)} \;, \end{aligned} \tag{3.2}$$

with Grassmann source terms η and $\bar{\eta}$. The normalized Gaussian measure with covariance $Q = G_0^{-1}$

$$d\mu_Q[\psi,\bar{\psi}] = \frac{1}{\mathcal{Z}_0}\, d\psi d\bar{\psi}\, e^{(\bar{\psi},Q\psi)} \tag{3.3}$$

includes the exponential of the quadratic part of the action and the noninteracting partition function $\mathcal{Z}_0$, such that $\int d\mu_Q[\psi,\bar{\psi}] = 1$. The generating functional for the connected Green functions is related to the partition function of the physical system with action (3.1) by

$$\mathcal{G}[\eta,\bar{\eta}] = -\ln \mathcal{Z}[\eta,\bar{\eta}] \;. \tag{3.4}$$

In the noninteracting case $V[\psi,\bar{\psi}] = 0$, and the Gaussian integral

$$\int d\mu_Q[\psi,\bar{\psi}]\, e^{-(\bar{\psi},\eta)-(\bar{\eta},\psi)} = e^{-(\bar{\eta},G_0\eta)} \tag{3.5}$$

implies that $\mathcal{G}[\eta,\bar{\eta}] = (\bar{\eta}, G_0\eta)$.

The connected m-particle Green functions are given by the derivatives of the generating functional $\mathcal{G}[\eta,\bar{\eta}]$ with respect to the source terms at $\eta=\bar{\eta}=0$

$$\begin{aligned} G_m(K'_1,\ldots,K'_m;K_1,\ldots,K_m) &= (-1)^m\langle\psi_{K'_1}\ldots\psi_{K'_m}\bar{\psi}_{K_m}\ldots\bar{\psi}_{K_1}\rangle_c \\ &= \frac{\partial^m}{\partial\eta_{K'_1}\ldots\partial\eta_{K'_m}}\frac{\partial^m}{\partial\bar{\eta}_{K_m}\ldots\partial\bar{\eta}_{K_1}}\mathcal{G}[\eta,\bar{\eta}]\Big|_{\eta=\bar{\eta}=0}\,, \end{aligned} \tag{3.6}$$

where $\langle\ldots\rangle_c$ is the connected average of the product of Grassmann variables between the brackets.

The connected amputated Green functions are generated by the *effective interaction* $\mathcal{V}[\chi,\bar{\chi}]$ defined by

$$e^{-\mathcal{V}[\chi,\bar{\chi}]} = \int d\mu_Q[\psi,\bar{\psi}]\, e^{-V[\psi+\chi,\bar{\psi}+\bar{\chi}]}\,. \tag{3.7}$$

The substitution $\chi = G_0\eta$ and $\bar{\chi} = G_0^T\bar{\eta}$, where G_0^T is the transposed propagator, relates $\mathcal{V}[\chi,\bar{\chi}]$ to the functional $\mathcal{G}[\eta,\bar{\eta}]$ by

$$\mathcal{V}[\chi,\bar{\chi}] = \mathcal{G}[\eta,\bar{\eta}] - (\bar{\eta},G_0\eta)\,. \tag{3.8}$$

The functional derivatives of $\mathcal{V}[\chi,\bar{\chi}]$ generate connected Green functions divided by $G_0(K_1)\ldots G_0(K_m)\,G_0(K'_1)\ldots G_0(K'_m)$, that is, propagators amputated from external legs in the corresponding Feynman diagrams. The term $(\bar{\eta},G_0\eta)$ cancels the noninteracting part of $\mathcal{G}[\eta,\bar{\eta}]$ such that $\mathcal{V}[\chi,\bar{\chi}]=0$ for $V[\psi,\bar{\psi}]=0$. Hence, the noninteracting propagator is subtracted from the one-particle Green function generated by $\mathcal{V}[\chi,\bar{\chi}]$.

The generating functional $\Gamma[\phi,\bar{\phi}]$ for the *1PI* vertex functions γ_m is derived from the Legendre transform of $\mathcal{G}[\eta,\bar{\eta}]$ by

$$\Gamma[\phi,\bar{\phi}] + (\bar{\phi},Q\phi) = \mathcal{G}[\eta,\bar{\eta}] + (\bar{\phi},\eta) - (\bar{\eta},\phi)\,, \tag{3.9}$$

with

$$\begin{aligned} \phi &= \frac{\partial\mathcal{G}}{\partial\bar{\eta}} & \eta &= \frac{\partial\Gamma}{\partial\bar{\phi}} + Q\phi \\ \bar{\phi} &= \frac{\partial\mathcal{G}}{\partial\eta} & \bar{\eta} &= \frac{\partial\Gamma}{\partial\phi} - Q^T\bar{\phi} \end{aligned} \tag{3.10}$$

and

$$\frac{\delta^2\mathcal{G}}{\delta\eta\,\delta\bar{\eta}} = \Big(\frac{\delta^2\Gamma}{\delta\phi\,\delta\bar{\phi}} + Q\Big)^{-1} . \tag{3.11}$$

For the special case without interaction $\mathcal{G}[\eta,\bar{\eta}] = (\bar{\eta}, G_0\eta)$ leads to $\Gamma[\phi,\bar{\phi}] = 0$.

The choice of the appropriate generating functional for a convenient formulation of a renormalization-group approach depends on the physical problem under investigation. For a detailed description of the different schemes we refer to Ref. [Enss 2005]; here we will concentrate on the 1PI version of the fRG.

3.3 RG differential flow equation for Γ

In this section we briefly review the general renormalization-group setup, introduced as a transformation that leaves the generating functional for the correlation functions invariant, and concentrate subsequently on the derivation of a continuous renormalization-group equation for the 1PI functions, following the derivation in the context of interacting Fermi systems in Ref. [Salmhofer and Honerkamp 2001].

The addition principle for Gaussian fields implies that for the decomposition $G_0 = G_0^< + G_0^>$ the corresponding Gaussian measure factorizes as

$$\begin{aligned} e^{-\mathcal{W}[\Phi,\bar{\Phi}]} &= \int d\mu_Q[\Psi,\bar{\Psi}] e^{-\mathcal{Y}[\Psi+\Phi,\bar{\Psi}+\bar{\Phi}]} \\ &= \int d\mu_{Q^<}[\Psi_<,\bar{\Psi}_<] \int d\mu_{Q^>}[\Psi_>,\bar{\Psi}_>] e^{-\mathcal{Y}[\Psi_<+\Psi_>+\Phi,\bar{\Psi}_<+\bar{\Psi}_>+\bar{\Phi}]} , \end{aligned} \tag{3.12}$$

with $\Psi = \Psi_< + \Psi_>$. The generating functional $\mathcal{W}$ corresponds to $\mathcal{W} = \mathcal{V}$ for the particular choice $\mathcal{Y} = V$. This leads to the semigroup law of the renormalization group

$$e^{-\mathcal{W}[\Phi,\bar{\Phi}]} = \int d\mu_{Q^<}[\Psi',\bar{\Psi}'] e^{-\mathcal{W}_>[\Psi'+\Phi,\bar{\Psi}'+\bar{\Phi}]} , \tag{3.13}$$

where in $\mathcal{W}_> = \mathcal{W}(Q^>,\mathcal{Y})$ the fields with propagator $Q^>$ have been integrated out. The semigroup law implies that the system $(Q,\mathcal{Y})$ under analysis is exactly equivalent to the system $(Q^<,\mathcal{W}(Q^>,\mathcal{Y}))$. In the present case $Q^>$ is a covariance with infrared cutoff Λ, and $Q^<$ has support only for fields with energies smaller than Λ.

Set up in this way, the renormalization group is simply a symmetry of the generating functional $\mathcal{W}(Q, \mathcal{Y})$. In differential form $\mathcal{W}(Q, \mathcal{Y})$ is independent of Λ, that is,

$$\frac{\partial}{\partial \Lambda} \mathcal{W}(Q, \mathcal{Y}) = 0 \, . \tag{3.14}$$

Inserting the right-hand side of Eq. (3.13) leads to the flow equation describing the gradual evolution from $\mathcal{Y}$ to the effective functional $\mathcal{W}$ as a function of the continuously decreasing energy cutoff Λ. $\mathcal{W}_>$ is an infinite power series in the fields; the quadratic and quartic terms correspond to the self-energy and the effective interaction, higher order terms are however always present and the convergence of the infinite series is a nontrivial problem [Salmhofer and Honerkamp 2001].

In the following the differential equation for the generating functional $\Gamma^\Lambda[\phi, \bar{\phi}]$ of the 1PI functions, starting point for the hierarchy of differential flow equations, is derived. Introducing an infrared cutoff at an energy scale $\Lambda > 0$ in the bare propagator leads to a Λ-dependent generating functional for the connected Green functions defined by

$$e^{-\mathcal{G}^\Lambda[\eta,\bar{\eta}]} = \int d\mu_{Q^\Lambda}[\psi, \bar{\psi}] \, e^{-V[\psi,\bar{\psi}]} \, e^{-\left(\bar{\psi},\eta\right) - (\bar{\eta},\psi)} \, . \tag{3.15}$$

The original functional is recovered in the limit $\Lambda \to 0$. Similarly the functional $\Gamma^\Lambda[\phi, \bar{\phi}]$ generating the 1PI vertex functions is constructed with G_0^Λ replacing G_0 in Eqs. (3.9 - 3.11). Differentiating the above Eq. (3.15) for $\mathcal{G}^\Lambda[\eta, \bar{\eta}]$ with respect to Λ yields

$$\begin{aligned} -\frac{\partial \mathcal{G}^\Lambda[\eta,\bar{\eta}]}{\partial \Lambda} \, e^{-\mathcal{G}^\Lambda[\eta,\bar{\eta}]} &= -\operatorname{Tr}\left(G_0^\Lambda \dot{Q}^\Lambda\right) e^{-\mathcal{G}^\Lambda[\eta,\bar{\eta}]} \\ &\quad + \int d\mu_{Q^\Lambda}[\psi, \bar{\psi}] \, (\bar{\psi}, \dot{Q}^\Lambda \psi) \, e^{-V_0[\psi,\bar{\psi}]} \, e^{-(\bar{\psi},\eta)-(\bar{\eta},\psi)} \\ &= -\left[\operatorname{Tr}\left(G_0^\Lambda \dot{Q}^\Lambda\right) + \Delta_{\dot{Q}^\Lambda} \right] e^{-\mathcal{G}^\Lambda[\eta,\bar{\eta}]} \, , \end{aligned} \tag{3.16}$$

where the first term comes from the derivative of the normalization factor (3.3), and Tr denotes the sum over all space-time indices. The functional Laplace operator Δ_Q is defined as

$$\Delta_Q = \left(\frac{\delta}{\delta \eta}, Q \frac{\delta}{\delta \bar{\eta}} \right) = \sum_K \frac{\delta}{\delta \eta_K} \, Q_K \, \frac{\delta}{\delta \bar{\eta}_K} \, . \tag{3.17}$$

The flow of $\mathcal{G}^\Lambda[\eta,\bar\eta]$ is then

$$\frac{\partial\mathcal{G}^\Lambda[\eta,\bar\eta]}{\partial\Lambda} = \mathrm{Tr}\,(G_0^\Lambda\dot Q^\Lambda) - \mathrm{Tr}\left[\dot Q^\Lambda\,\frac{\delta^2\mathcal{G}^\Lambda[\eta,\bar\eta]}{\delta\eta\,\delta\bar\eta}\right] + \left(\frac{\delta\mathcal{G}^\Lambda[\eta,\bar\eta]}{\delta\eta},\dot Q^\Lambda\frac{\delta\mathcal{G}^\Lambda[\eta,\bar\eta]}{\delta\bar\eta}\right). \tag{3.18}$$

Using the Legendre transform (3.9) the derivative of $\Gamma^\Lambda[\phi,\bar\phi]$ reads

$$\begin{aligned}\frac{\partial\Gamma^\Lambda[\phi,\bar\phi]}{\partial\Lambda} &= \frac{\partial\mathcal{G}^\Lambda[\eta,\bar\eta]}{\partial\Lambda} - (\bar\phi,\dot Q^\Lambda\phi)\\ &= \Big(\frac{\delta\mathcal{G}^\Lambda[\eta,\bar\eta]}{\delta\eta},\dot Q^\Lambda\frac{\delta\mathcal{G}^\Lambda[\eta,\bar\eta]}{\delta\bar\eta}\Big)\\ &\quad - \mathrm{Tr}\left[\dot Q^\Lambda\Big(\frac{\delta^2\mathcal{G}^\Lambda[\eta,\bar\eta]}{\delta\eta\,\delta\bar\eta} - G_0^\Lambda\Big)\right] - (\bar\phi,\dot Q^\Lambda\phi)\\ &= -\mathrm{Tr}\Big[\dot Q^\Lambda\Big(\Big(\frac{\delta^2\Gamma^\Lambda[\phi,\bar\phi]}{\delta\phi\,\delta\bar\phi}+Q^\Lambda\Big)^{-1} - G_0^\Lambda\Big)\Big],\end{aligned} \tag{3.19}$$

leading to the exact renormalization-group equation

$$\frac{\partial}{\partial\Lambda}\Gamma^\Lambda[\phi,\bar\phi] = \mathrm{Tr}\Big[G_0^\Lambda\frac{\partial(G_0^\Lambda)^{-1}}{\partial\Lambda}\Big] - \mathrm{Tr}\Big[\Big(\frac{\delta^2\Gamma^\Lambda[\phi,\bar\phi]}{\delta\phi\,\delta\bar\phi}+(G_0^\Lambda)^{-1}\Big)^{-1}\frac{\partial(G_0^\Lambda)^{-1}}{\partial\Lambda}\Big]. \tag{3.20}$$

With the initial condition

$$\Gamma^{\Lambda_0}[\phi,\bar\phi] = V[\phi,\bar\phi] \tag{3.21}$$

Eq. (3.20) determines the flow of Γ^Λ uniquely for all $\Lambda<\Lambda_0$.

3.4 Expansion in the fields and exact hierarchy of flow equations

The renormalization-group equations for the 1PI m-particle vertex functions γ_m^Λ are derived by expanding $\Gamma^\Lambda[\phi,\bar\phi]$ in Eq. (3.20) as a power series in the fields. The coefficients in the expansion of $\Gamma^\Lambda[\phi,\bar\phi]$ determine γ_m^Λ by

$$\Gamma^\Lambda[\phi,\bar\phi] = \sum_{m=0}^\infty\frac{1}{(m!)^2}\sum_{K_1\ldots K_m}\sum_{K_1'\ldots K_m'}\gamma_m^\Lambda(K_1',\ldots,K_m';K_1,\ldots,K_m)\prod_{j=1}^m\bar\phi_{K_j'}\phi_{K_j}. \tag{3.22}$$

Due to the antisymmetry properties of the Grassmann variables only antisymmetric vertex functions contribute.

Similarly the second derivative on the right-hand side of Eq. (3.20) can be expanded. Separating the ϕ-independent part corresponding to the self-energy yields

$$\frac{\delta^2\Gamma^\Lambda[\phi,\bar\phi]}{\delta\phi\,\delta\bar\phi} = \frac{\delta^2\Gamma^\Lambda[\phi,\bar\phi]}{\delta\phi\,\delta\bar\phi}\Big|_{\phi=\bar\phi=0} + \tilde\Gamma^\Lambda[\phi,\bar\phi] = -\Sigma^\Lambda + \tilde\Gamma^\Lambda[\phi,\bar\phi]\;, \tag{3.23}$$

where the remaining functional $\tilde\Gamma^\Lambda[\phi,\bar\phi]$ is defined by Eq. (3.22) with indices m and j starting from 2. The second term on the right-hand side of the flow equation (3.20) then reads

$$\begin{aligned}\Big(\frac{\delta^2\Gamma^\Lambda[\phi,\bar\phi]}{\delta\phi\,\delta\bar\phi} + (G_0^\Lambda)^{-1}\Big)^{-1} &= \big(\tilde\Gamma^\Lambda + (G^\Lambda)^{-1}\big)^{-1} \\ &= G^\Lambda \sum_{l=0}^{\infty}(-1)^l\big(\tilde\Gamma^\Lambda\, G^\Lambda\big)^l\;,\end{aligned} \tag{3.24}$$

with the full propagator G^Λ defined via the Dyson equation $(G^\Lambda)^{-1} = (G_0^\Lambda)^{-1} - \Sigma^\Lambda$. Introducing the *single-scale propagator* S^Λ as

$$S^\Lambda = G^\Lambda\,\frac{\partial(G_0^\Lambda)^{-1}}{\partial\Lambda}\,G^\Lambda \tag{3.25}$$

the differential equation (3.20) for Γ^Λ is

$$\begin{aligned}\frac{\partial}{\partial\Lambda}\Gamma^\Lambda &= \mathrm{Tr}\Big[G_0^\Lambda\frac{\partial(G_0^\Lambda)^{-1}}{\partial\Lambda}\Big] + \sum_{l=0}^{\infty}(-1)^{l+1}\,\mathrm{Tr}\,\Big[G^\Lambda\frac{\partial}{\partial\Lambda}[G_0^\Lambda]^{-1}\big(G^\Lambda\,\tilde\Gamma^\Lambda\big)^l\Big] \\ &= \mathrm{Tr}\Big[\big(G_0^\Lambda - G^\Lambda\big)\frac{\partial(G_0^\Lambda)^{-1}}{\partial\Lambda}\Big] + \sum_{l=0}^{\infty}(-1)^l\,\mathrm{Tr}\,\Big[S^\Lambda\tilde\Gamma^\Lambda\,\big(G^\Lambda\,\tilde\Gamma^\Lambda\big)^l\Big]\;.\end{aligned} \tag{3.26}$$

The first term corresponds to a vacuum energy not entering the correlation functions, while the second one contains one-loop diagrams with $(l+1)$ vertices $\tilde\Gamma^\Lambda$ connected by one single-scale propagator S^Λ and l full propagators G^Λ. The term linear in $\tilde\Gamma^\Lambda$ generates self-energy corrections.

Inserting the components γ_m^Λ on the left-hand side and the components $\tilde\gamma_m^\Lambda$ on the right-hand side of the flow equation (3.26) for Γ^Λ we obtain a system of equations

for γ_m^Λ. In a graphical representation the equations for $m \leq 3$ are

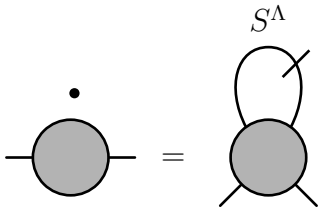

(3.27)

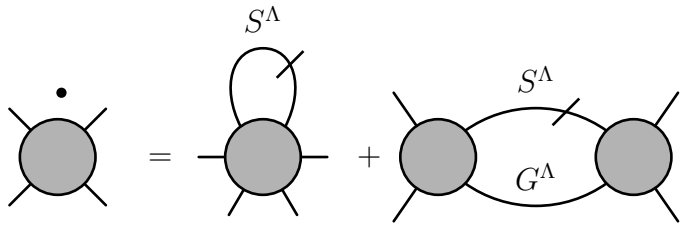

(3.28)

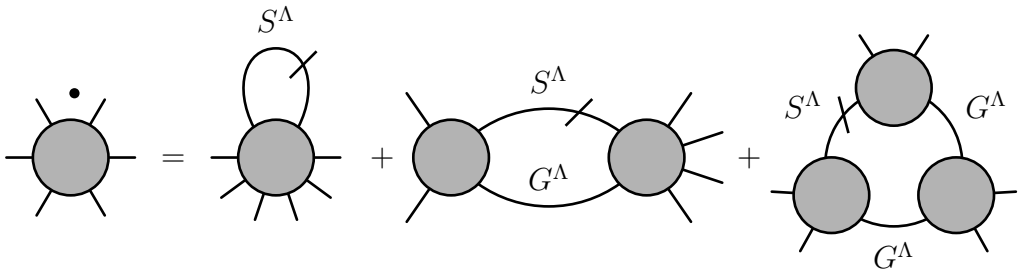

(3.29)

The initial conditions for the vertex functions at $\Lambda = \infty$ are given by the bare interactions of the system. In particular, the flow of the two-particle vertex starts from the antisymmetrized bare two-particle interaction while m-particle vertices of higher order vanish at $\Lambda = \infty$, in the absence of bare m-body interactions with $m > 2$.

Note that the right-hand side of the equation for γ_m contains γ_{m+1}. The infinite system of differential equations contains only one-loop terms in every equation, as the differential formulation of Eq. (3.20) contains only a single trace, and for the 1PI scheme no tree terms appear. The infinite hierarchy produces the full Green functions, generating graphs with an arbitrary number of loops; truncations amount to a partial inclusion of higher order contibutions generated during the flow, where the internal lines contain only modes above the cutoff scale Λ. Consequences of symmetries are discussed in Ref. [Salmhofer and Honerkamp 2001].

3.5 Comparison to other RG schemes

Infrared divergencies arising in the context of perturbative expansions or in proximity of phase transitions can alternatively be regularized by temperature, a weak coupling strength or a finite system size. In the fRG approach the cutoff scale is introduced only in the quadratic part of the bare action, and the regularization is implemented with respect to energy scales. The temperature and interaction flows are derived in Refs. [Honerkamp and Salmhofer 2001; Honerkamp et al. 2004] respectively, a pedagogic introduction is given in Ref. [Enss 2005]. The renormalization-group equations describe the flow of the correlation functions as the cutoff scale is lowered. The choice of the basis set for the correlation functions determines a particular scheme.

In addition to the 1PI scheme described previously, the various generating functionals introduced in Sec. 3.2 correspond to different schemes. Starting point for the *Polchinski scheme* is the effective interaction, generating functional of the connected amputated Green functions. The flow equation for $\mathcal{V}^\Lambda[\chi,\bar{\chi}]$ is derived by replacing Q by Q^Λ in Eq. (3.7) and taking the derivative with respect to Λ. An expansion in powers of χ and $\bar{\chi}$ of the functional $\mathcal{V}^\Lambda[\chi,\bar{\chi}]$ in the renormalization-group equation leads to Polchinski's flow equations for amputated connected Green functions [Polchinski 1984; Keller et al. 1992], with a similar structure as for the connected Green functions. The connected amputated Green functions are the expansion coefficients of the generating functional $\mathcal{V}^\Lambda[\chi,\bar{\chi}]$ in terms of monomials of the source fields χ and $\bar{\chi}$. Alternatively, one can also expand $\mathcal{V}^\Lambda[\chi,\bar{\chi}]$ with respect to *Wick-ordered* polynomials, leading to the Wick-ordered Green functions as expansion coefficients [Wieczerkowski 1988; Salmhofer 1998, 1999]. The flow equations are characterized by a bilinear structure in the vertices on the right-hand side connected by bare Λ-dependent propagators. The Wick ordering also implies that except for the differentiated propagator the internal lines are supported below scale Λ instead of above it. Thus, for a momentum cutoff only momenta close to the Fermi surface contribute at low cutoff scale Λ. This justifies a parametrization of the coupling functions by projecting onto the Fermi surface [Halboth and Metzner 2000]. Self-energy corrections are however most conveniently taken into account in the 1PI formalism with full propagators on the internal lines.

In an exact treatment all schemes are equivalent, differences arise with truncations of the infinite hierarchy of flow equations. While the full hierarchy of flow

equations leads to the correct solution to all orders in perturbation theory independently of the scheme, in the computation of the lowest orders a particular scheme might be more suitable than others, depending on the considered physical problem and properties. An important point for the choice concerns the possibility of an efficient parametrization of the effective interactions by a manageable number of variables.

Continuous symmetries in the bare action lead to conservation laws and Ward identities relating Green and response functions, as a consequence of the Noether theorem. These are generally not preserved for the truncated flow equations, in contrast to the solution of the infinite flow-equation hierarchy, as shown in detail in Ref. [Enss 2005]. For a gauge-invariant construction however, as for the temperature-flow scheme, the Ward identities between Green and response functions are satisfied exactly despite truncations. The related property of self-consistency is satisfied by construction in conserving approximations [Baym and Kadanoff 1961], but generally violated in truncated fRG flows. However, in the one-dimensional lattice models for Luttinger liquids, the truncated fRG is nevertheless surprisingly successful and self-consistency does not appear to play an important role.

4 Functional RG for Luttinger liquids

We apply the fRG in the one-particle irreducible version to one-dimensional Fermi systems with impurities. The lowest order truncation of the fRG hierarchy of flow equations, where the two-particle vertex is approximated by the bare interaction, considered previously for spinless fermions, is extended including two-particle vertex renormalization, and generalized to spin-$\frac{1}{2}$ systems. For spinless fermions the quantitative accuracy of the results improves considerably, whereas for spin-$\frac{1}{2}$ systems vertex renormalization is necessary to take into account that backscattering of particles with opposite spins at opposite Fermi points scales to zero in the low-energy limit. The underlying approximations are devised for weak interactions and arbitrary impurity strengths. Details on the computation of the relevant observables from the solution of the flow equations are presented.

4.1 Microscopic models

We consider various lattice fermion systems with spinless and spin-$\frac{1}{2}$ fermions supplemented by different types of impurity potentials. The Hamiltonian has the form

$$H = H_0 + H_I + H_{\text{imp}} \tag{4.1}$$

where H_0 is the kinetic energy, H_I a short-range interaction, and H_{imp} a static local or nonlocal impurity potential.

We distinguish between spinless and spin-$\frac{1}{2}$ fermions.

4.1.1 Spinless fermions

For the spinless fermion model

$$H_0 = -t \sum_j \left(c_{j+1}^\dagger c_j + c_j^\dagger c_{j+1} \right) \tag{4.2}$$

describes nearest-neighbor hopping processes with an amplitude t and

$$H_I = U \sum_j n_j \, n_{j+1} \tag{4.3}$$

is a nearest-neighbor interaction of strength U, as shown in Fig. 4.1. We use standard second quantization notation, where $c_j^\dagger$ and c_j are creation and annihilation operators on site j respectively, and $n_j = c_j^\dagger \, c_j$ is the local density operator. The impurity is represented by

$$H_{\rm imp} = \sum_{j,j'} V_{j'j} \; c_{j'}^\dagger \, c_j \; , \tag{4.4}$$

where $V_{j'j}$ is a static potential. For "site impurities"

$$V_{j'j} = V_j \, \delta_{jj'} \tag{4.5}$$

this potential is local. For the special case of a single site impurity

$$V_j = V \, \delta_{jj_0} \tag{4.6}$$

the potential acts only on one site j_0. We also consider "hopping impurities" described by the nonlocal potential

$$V_{j'j} = V_{jj'} = -t_{j,j+1} \, \delta_{j',j+1} \; . \tag{4.7}$$

For a single hopping impurity

$$t_{j,j+1} = (t' - t) \, \delta_{jj_0} \tag{4.8}$$

the hopping amplitude t is replaced by t' on the bond linking the sites j_0 and $j_0 + 1$. In the following we will set the bulk hopping amplitude t equal to one, that is, all energies are expressed in units of t.

The clean spinless fermion model $H_0 + H_I$ is exactly soluble via the Bethe ansatz [Yang and Yang 1966]. The system is a Luttinger liquid for all particle densities n

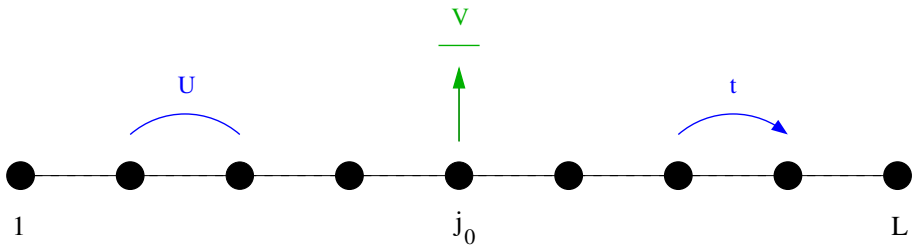

Figure 4.1: *Spinless fermion model with nearest-neighbor hopping amplitude t, nearest-neighbor interaction U, and a local site potential V on site j_0.*

and any interaction strength, except at half filling for $|U| > 2$. For $U > 2$ a charge density wave with wave vector π forms; for $U < -2$ the system undergoes phase separation. The Luttinger-liquid parameter K_ρ, which determines all the critical exponents of the liquid, can be computed exactly from the Bethe ansatz solution [Haldane 1980]. At half filling K_ρ is related to U by the simple explicit formula

$$K_\rho^{-1} = \frac{2}{\pi} \arccos\left(-\frac{U}{2}\right) \tag{4.9}$$

for $|U| \leq 2$.

4.1.2 Spin-$\frac{1}{2}$ fermions

For spin-$\frac{1}{2}$ fermions, the kinetic energy is given by

$$H_0 = -t \sum_{j,\sigma} \left(c^\dagger_{j+1,\sigma} c_{j\sigma} + c^\dagger_{j\sigma}\, c_{j+1,\sigma} \right) , \tag{4.10}$$

where $c^\dagger_{j\sigma}$ and $c_{j\sigma}$ are creation and annihilation operators for fermions with spin projection σ on site j. The interaction term of the extended Hubbard model contains a local interaction U and a nearest-neighbor interaction U'

$$H_I = U \sum_j n_{j\uparrow}\, n_{j\downarrow} + U' \sum_j n_j\, n_{j+1} , \tag{4.11}$$

with $n_{j\sigma} = c^\dagger_{j\sigma}\, c_{j\sigma}$ and $n_j = n_{j\uparrow} + n_{j\downarrow}$, as shown in Fig. 4.2. For the pure Hubbard model only the local interaction U is finite, while $U' = 0$. The impurity term

$$H_{\text{imp}} = \sum_{j,j'} \sum_\sigma V_{j'j}\; c^\dagger_{j'\sigma}\, c_{j\sigma} \tag{4.12}$$

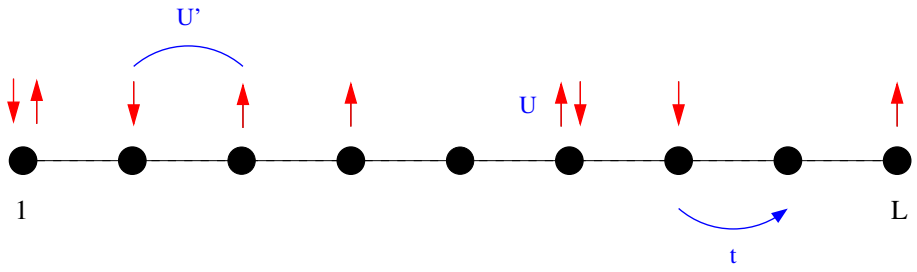

Figure 4.2: *Extended Hubbard model with nearest-neighbor hopping amplitude t, local interaction U and nearest-neighbor interaction U'.*

differs from the spinless case only by the spin sum.

In the absence of impurities, the Hubbard model can be solved exactly using the Bethe-ansatz [Lieb and Wu 1968], while the extended Hubbard model is not integrable. The Hubbard model is a Luttinger liquid for arbitrary repulsive interactions at all particle densities except half filling, where the system becomes a Mott insulator [Voit 1995; Giamarchi 2004]. The phase diagram of the extended Hubbard model is more complex. Away from half filling it is a Luttinger liquid at least for sufficiently weak repulsive interactions [Voit 1995]. For the Hubbard model the Luttinger-liquid parameter K_ρ can be computed exactly from the Bethe ansatz solution [Frahm and Korepin 1990; Kawakami and Yang 1990; Schulz 1990].

4.2 Cutoff and flow equations

4.2.1 Cutoff

The cutoff introduced in Sec. 3.3 can be imposed in many different ways. The only requirement is that the infrared singularities must be regularized such that the flow equations allow for a regular perturbation expansion in powers of the renormalized two-particle vertex. Since translation invariance is spoiled by the impurity, a Matsubara frequency cutoff is the most efficient choice, while a momentum cutoff is less suitable. At $T = 0$ the cutoff is sharp [Andergassen et al. 2004], the extension to $T > 0$ will be addressed subsequently. The cutoff is imposed by excluding modes with frequencies below scale Λ from the functional integral representation of the system, or equivalently, by introducing a regularized bare propagator

$$G_0^\Lambda(i\omega) = \Theta(|\omega| - \Lambda)\, G_0(i\omega)\ . \tag{4.13}$$

Here G_0 is the bare propagator of the pure system, involving neither interactions nor impurities. Instead of the sharp cutoff imposed by the step function Θ one may also choose a smooth cutoff function, but the sharp cutoff has the advantage that it reduces the number of integration variables on the right-hand side of the flow equations. Note that we will frequently write expressions which are well defined only if the sharp cutoff is viewed as a limit of increasingly sharp smooth cutoff functions. The suppression of frequencies below scale Λ affects all Green and vertex functions of the interacting system, which become thus functions of Λ. The original system is recovered in the limit $\Lambda \to 0$.

4.2.2 Truncation schemes

The truncation of the fRG hierarchy of differential flow equations for the one-particle irreducible m-particle vertex functions and their parametrization with a manageable set of variables or functions leads to different approximation schemes.

In the lowest order truncation of the fRG hierarchy (cf. Sec. 3.4) the renormalized two-particle vertex is approximated by the bare interaction [Meden et al. 2002a,b]. This truncation scheme, denoted by *Scheme I*, includes only the first equation in the hierarchy for the one-particle vertex function $\Gamma_1^\Lambda = -\Sigma^\Lambda$, where the self-energy Σ^Λ is related to the interacting propagator by the usual Dyson equation

$$G^\Lambda = \left[(G_0^\Lambda)^{-1} - \Sigma^\Lambda\right]^{-1} \ . \tag{4.14}$$

Here and below G^Λ, Σ^Λ etc. are operators, which do not refer to any particular single-particle basis, unless we write matrix indices explicitly. The right-hand side of the flow equation for Σ^Λ (3.27) involves the two-particle vertex Γ^Λ and the single-scale propagator S^Λ introduced in Eq. (3.25) which has support only on a single frequency scale $|\omega| = \Lambda$. The flow equation for the self-energy reads

$$\frac{\partial}{\partial\Lambda}\Sigma^\Lambda(1',1) = -\frac{1}{\beta}\sum_{2,2'} e^{i\omega_2 0^+}\, S^\Lambda(2,2')\, \Gamma^\Lambda(1',2';1,2) \ , \tag{4.15}$$

where β is the inverse temperature. The numbers 1, 2, etc. are a shorthand for Matsubara frequencies and labels for single-particle states such as site and spin indices. Note that $\omega_1 = \omega_1'$ and $\omega_2 = \omega_2'$ due to Matsubara frequency conservation. The exponential factor in the above equation is irrelevant at any finite Λ, but is necessary to define the initial conditions of the flow at $\Lambda = \Lambda_0 \to \infty$.

For a sharp frequency cutoff the frequency sum on the right-hand side of the flow equation can be carried out analytically in the zero temperature limit, where the Matsubara sum becomes an integral. At this point one has to deal with products of delta functions $\delta(|\omega| - \Lambda)$ and expressions involving step functions $\Theta(|\omega| - \Lambda)$. These at first sight ambiguous expressions are well defined and unique if the sharp cutoff is implemented as a limit of increasingly sharp broadened cutoff functions Θ_ϵ, with the broadening parameter ϵ tending to zero. The expressions can then be conveniently evaluated by using the following relation [Morris 1994], valid for arbitrary continuous functions f:

$$\delta_\epsilon(x - \Lambda)\, f[\Theta_\epsilon(x - \Lambda)] \to \delta(x - \Lambda) \int_0^1 f(t)\, dt \;, \tag{4.16}$$

where $\delta_\epsilon = \Theta_\epsilon'$. Note that the functional form of Θ_ϵ for finite ϵ does not affect the result in the limit $\epsilon \to 0$.

In Scheme I Γ^Λ in Eq. (4.15) is replaced by the antisymmetrized bare two-particle interaction $\Gamma^{\Lambda_0}_{1',2';1,2} = I_{1',2';1,2}$, where the lower indices 1, 2, etc. label single-particle states (not frequencies). Since $I_{1',2';1,2}$ is frequency independent, no frequency dependence of the self-energy is generated in the flow. Carrying out the frequency integration in the flow equation for the self-energy (4.15) one obtains

$$\frac{\partial}{\partial\Lambda}\Sigma^\Lambda_{1',1} = -\frac{1}{2\pi} \sum_{\omega=\pm\Lambda} \sum_{2,2'} e^{i\omega 0^+}\, \tilde{G}^\Lambda_{2,2'}(i\omega)\, I_{1',2';1,2} \;, \tag{4.17}$$

where

$$\tilde{G}^\Lambda(i\omega) = \left[G_0^{-1}(i\omega) - \Sigma^\Lambda\right]^{-1} \;. \tag{4.18}$$

Note that $\tilde{G}^\Lambda$ has no jump at $|\omega| = \Lambda$, in contrast to G^Λ.

The flow is determined uniquely by the differential flow equation and the initial condition at $\Lambda = \infty$. The self-energy at $\Lambda = \infty$ is given by the bare impurity (site or hopping) potential V. In a numerical solution the flow starts at some large finite initial cutoff Λ_0. Here one has to take into account that, due to the slow decay of the right-hand side of the flow equation for Σ^Λ at large Λ, the integration of the flow from $\Lambda = \infty$ to $\Lambda = \Lambda_0$ yields a contribution which does not vanish in the limit $\Lambda_0 \to \infty$, but rather tends to a finite constant. Since $\tilde{G}^\Lambda_{2,2'}(i\omega) \to \delta_{2,2'}/(i\omega)$ for $|\omega| = \Lambda \to \infty$, this constant is determined as

$$-\frac{1}{2\pi} \lim_{\Lambda_0\to\infty} \int_\infty^{\Lambda_0} d\Lambda \sum_{\omega=\pm\Lambda} \sum_{2,2'} e^{i\omega 0^+}\, \frac{\delta_{2,2'}}{i\omega}\, I_{1',2';1,2} = \frac{1}{2} \sum_2 I_{1',2;1,2} \;. \tag{4.19}$$

Including the bare impurity potential $V_{1,1'}$, the initial conditions for the self-energy at $\Lambda = \Lambda_0 \to \infty$ is

$$\Sigma^{\Lambda_0}_{1,1'} = V_{1,1'} + \frac{1}{2}\sum_{2} I_{1',2;1,2} \; . \tag{4.20}$$

For the flow at $\Lambda < \Lambda_0$ the factor $e^{i\omega 0^+}$ in Eq. (4.17) can be discarded.

A further development of the fRG approach for impurities in Luttinger liquids includes the two-particle vertex renormalization, denoted by *Scheme II* and used in the following if not specified otherwise. For spinless fermions this extension does not matter qualitatively, but the quantitative accuracy of the results improves considerably, in particular at intermediate interaction strengths. By contrast, for spin-$\frac{1}{2}$ systems vertex renormalization is necessary to take into account that backscattering of particles with opposite spins at opposite Fermi points scales to zero in the low-energy limit. The right-hand side of the flow equation for the two-particle vertex Γ^Λ (3.28) involves Γ^Λ itself, but also the three-particle vertex Γ^Λ_3. Neglecting the contribution of the three-particle vertex to the flow of the two-particle vertex, the coupled system of flow equations for the two-particle vertex Γ^Λ and the self-energy Σ^Λ is closed. In terms of an expansion in the bare coupling function, this truncation is exact up to second order. However, the fRG provides more than just a second-order calculation: the evolution of the interaction and the self-energy is continually fed back into the fRG differential equation. This effectively sums up contributions from arbitrarily high orders and thus produces a scale-dependent resummation of perturbation theory. We note that it does not correspond to an expansion to a fixed loop order: the flow equations appear to be one loop, but they also take into account two-loop effects by iteration. The relevant question is whether higher orders significantly change the flow, they certainly do so if the coupling functions get too large. The contribution of Γ^Λ_3 to Γ^Λ is small as long as Γ^Λ is sufficiently small, because Γ^Λ_3 is initially (at Λ_0) zero and is generated only from terms of third order in Γ^Λ. A comparison of the fRG results to exact DMRG results and exact scaling properties shows that the truncation error is often surprisingly small, even for rather large interactions [Meden et al. 2002a,b]. The explicit form of the truncated flow equation for the two-particle vertex reads

$$\begin{aligned}\frac{\partial}{\partial\Lambda}\Gamma^\Lambda(1',2';1,2) = \; & \frac{1}{\beta}\sum_{3,3'}\sum_{4,4'} G^\Lambda(3,3')\,S^\Lambda(4,4')\Big[\Gamma^\Lambda(1',2';3,4)\,\Gamma^\Lambda(3',4';1,2) \\ & - \Gamma^\Lambda(1',4';1,3)\,\Gamma^\Lambda(3',2';4,2) - (3\leftrightarrow 4, 3'\leftrightarrow 4')\end{aligned}$$

$$+ \Gamma^{\Lambda}(2',4';1,3)\,\Gamma^{\Lambda}(3',1';4,2) + (3 \leftrightarrow 4, 3' \leftrightarrow 4') \Big] \,. \tag{4.21}$$

Diagrammatically, the individual contributions for the particle-particle and particle-hole channels written explicitly are

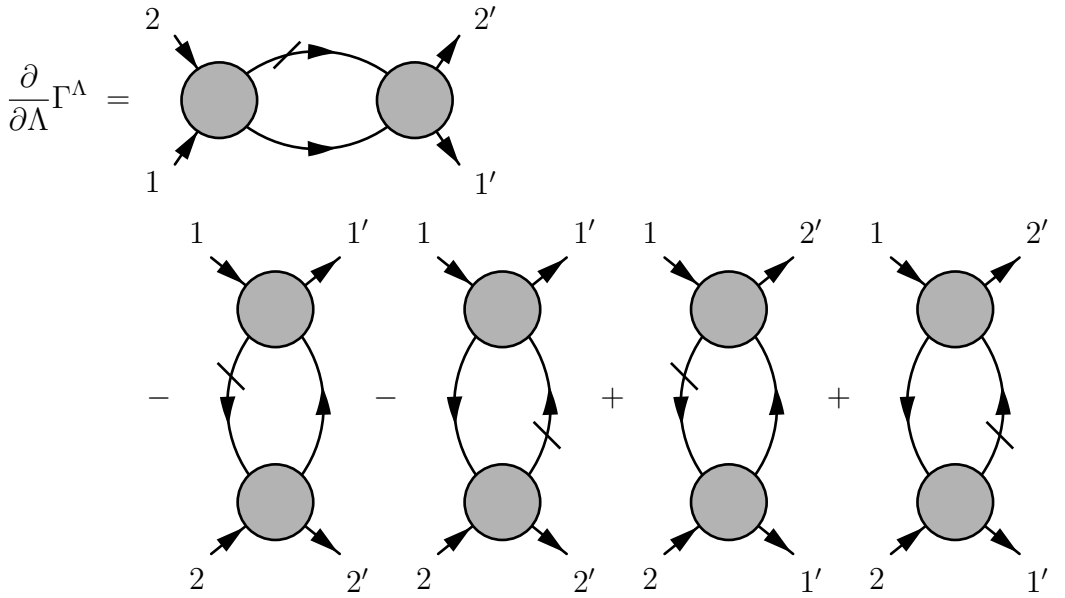

(4.22)

Instead of solving the frequency integrated flow equation in full generality, we implement the following approximation: the frequency-dependent flow of the renormalized two-particle vertex Γ^{Λ} is replaced by its value at vanishing (external) frequencies, such that Γ^{Λ} remains frequency independent. As a consequence, also the self-energy remains frequency independent. Since the bare interaction is frequency independent, neglecting the frequency dependence leads to errors only at second order (in the interaction strength) for the self-energy, and at third order for the vertex function at zero frequency. In addition to the quantitative errors we miss qualitative properties related to the frequency dependence of the self-energy, such as the suppression of the one-particle spectral weight in the bulk of a pure Luttinger liquid. On the other hand, a comparison with exact numerical results and asymptotic analytical results shows that the impurity effects are not qualitatively affected by the frequency dependence of Σ, at least for weak interactions.

The frequency-integrated flow equation for the two-particle vertex, evaluated at

vanishing external frequencies, has the form

$$\frac{\partial}{\partial\Lambda}\Gamma^{\Lambda}_{1',2';1,2} = \frac{1}{2\pi}\sum_{\omega=\pm\Lambda}\sum_{3,3'}\sum_{4,4'}\Big[\frac{1}{2}\,\tilde{G}^{\Lambda}_{3,3'}(i\omega)\,\tilde{G}^{\Lambda}_{4,4'}(-i\omega)\,\Gamma^{\Lambda}_{1',2';3,4}\,\Gamma^{\Lambda}_{3',4';1,2} + \tilde{G}^{\Lambda}_{3,3'}(i\omega)\,\tilde{G}^{\Lambda}_{4,4'}(i\omega)\,\left(-\Gamma^{\Lambda}_{1',4';1,3}\,\Gamma^{\Lambda}_{3',2';4,2} + \Gamma^{\Lambda}_{2',4';1,3}\,\Gamma^{\Lambda}_{3',1';4,2}\right)\Big]\,, \tag{4.23}$$

with the initial condition $\Gamma^{\Lambda_0}_{1',2';1,2} = I_{1',2';1,2}$.

A crucial point is to devise an efficient parametrization of the vertex by a manageable number of variables. For a finite lattice system with L sites the flow of the two-particle vertex $\Gamma^{\Lambda}_{1',2';1,2}$ involves $\mathcal{O}(L^3)$ independent flowing variables, if translation invariance is assumed, and $\mathcal{O}(L^4)$ variables, if the influence of the impurity on the flow of the two-particle vertex is taken into account. For a treatment of large systems it is therefore necessary to reduce the number of variables by a suitable approximate parametrization of the vertex. In the low-energy limit (small Λ) the flow is dominated by a very small number of variables, the others being irrelevant according to standard renormalization-group arguments [Voit 1995]. In particular, the frequency dependence of the vertex, discarded already above, is irrelevant for the flow of Γ^{Λ} at small Λ. For larger Λ one can use perturbation theory as a guide for a simple but efficient parametrization of Γ^{Λ}.

We neglect the influence of the impurity on the flow of the two-particle vertex, such that Γ^{Λ} remains translation invariant. While this is sufficient for capturing the effects of isolated impurities in otherwise pure systems, it is known that impurity contributions to vertex renormalization become important in macroscopically disordered systems [Giamarchi 2004]. We also neglect the feedback of the bulk self-energy into the flow of Γ^{Λ}, which yields higher order contributions in the renormalized interaction. The two-particle vertex is parametrized approximately by a renormalized static short-range interaction, which allows us to capture various features: the low-energy flow of the vertex at k_F in the pure system is obtained correctly to second order in the renormalized couplings; the nonuniversal contributions at finite energy scales are correct to second order in the bare interaction; the algorithm for the flow of the self-energy remains as fast as in the absence of vertex renormalization, such that one can easily deal with up to 10^7 lattice sites!

For a more concrete treatment of the vertex renormalization, we now focus on a specific model.

4.2.3 Spinless fermions

For spinless fermions the two-particle vertex and the self-energy are fully characterized by either site or momentum variables. In the low-energy limit, the flow of the vertex is dominated by contributions with momenta close to the Fermi points, such that the right-hand side of the flow equation is determined by momentum components of the vertex $\Gamma^{\Lambda}_{k_1',k_2';k_1,k_2}$ with $k_1, k_2, k_1', k_2' = \pm k_F$. Due to the antisymmetry of the vertex, there is only one such component which is nonzero:

$$g^{\Lambda} = \Gamma^{\Lambda}_{k_F,-k_F;k_F,-k_F} \, . \tag{4.24}$$

In the low-energy limit the momentum dependence of the vertex away from $\pm k_F$ is irrelevant. There are therefore many possible choices for the functional form of $\Gamma^{\Lambda}_{k_1',k_2';k_1,k_2}$, which all lead to the correct low-energy asymptotics. For a model with a bare nearest-neighbor interaction U, a natural and efficient choice is to parametrize the flowing vertex simply by a renormalized nearest-neighbor interaction U^{Λ}, which leads to a real space vertex of the form

$$\Gamma^{\Lambda}_{j_1',j_2';j_1,j_2} = U^{\Lambda}_{j_1,j_2} \left(\delta_{j_1,j_1'}\delta_{j_2,j_2'} - \delta_{j_1,j_2'}\delta_{j_2,j_1'}\right) , \tag{4.25}$$

with $U^{\Lambda}_{j_1,j_2} = U^{\Lambda} \left(\delta_{j_1,j_2-1} + \delta_{j_1,j_2+1}\right)$. This yields the following structure in momentum space:

$$\Gamma^{\Lambda}_{k_1',k_2';k_1,k_2} = 2U^{\Lambda} \left[\cos(k_1' - k_1) - \cos(k_2' - k_1)\right] \delta^{(2\pi)}_{k_1+k_2,k_1'+k_2'} \, , \tag{4.26}$$

where the Kronecker δ implements momentum conservation (modulo 2π). The flowing coupling constant U^{Λ} is linked to the value of the vertex at the Fermi points by the relation

$$g^{\Lambda} = 2U^{\Lambda} \left[1 - \cos(2k_F)\right] . \tag{4.27}$$

The flow equation for g^{Λ} becomes

$$\frac{\partial g^{\Lambda}}{\partial \Lambda} = \frac{1}{2\pi} \sum_{\omega=\pm\Lambda} \int \frac{dp}{2\pi} \left(PP + PH + PH' \right) , \tag{4.28}$$

with the particle-particle and particle-hole contributions

$$PP = \frac{1}{2} \, G^0_p(i\omega) \, G^0_{-p}(-i\omega) \, \Gamma^{\Lambda}_{k_F,-k_F;p,-p} \, \Gamma^{\Lambda}_{p,-p;k_F,-k_F}$$

$$
\begin{aligned}
PH =& -\left[G^0_p(i\omega)\right]^2 \Gamma^\Lambda_{k_F,p;k_F,p}\,\Gamma^\Lambda_{p,-k_F;p,-k_F} \\
PH' =& G^0_{p-k_F}(i\omega)\, G^0_{p+k_F}(i\omega)\, \Gamma^\Lambda_{-k_F,p+k_F;k_F,p-k_F}\,\Gamma^\Lambda_{p-k_F,k_F;p+k_F,-k_F}\ ,
\end{aligned}
\tag{4.29}
$$

where Γ^Λ on the right-hand side of the flow equation is given by Eq. (4.26). Using Eq. (4.27) to replace $\partial_\Lambda g^\Lambda$ by $\partial_\Lambda U^\Lambda$ on the left-hand side of Eq. (4.28), one obtains a flow equation for U^Λ of the simple form

$$
\partial_\Lambda U^\Lambda = h(\Lambda)\,(U^\Lambda)^2\ . \tag{4.30}
$$

The function $h(\Lambda)$ depends only on the cutoff Λ and the Fermi momentum k_F. An explicit formula for $h(\Lambda)$ can be obtained by carrying out the momentum integral in Eq. (4.28) using the residue theorem. For finite systems the momentum integral should be replaced by a discrete momentum sum; however, this leads to sizable corrections only for very small systems. Inserting the momentum structure of Γ^Λ (4.26) into the flow equation (4.28) and replacing g^Λ by U^Λ on the left-hand side yields

$$
\frac{\partial U^\Lambda}{\partial \Lambda} = \frac{(U^\Lambda)^2}{2\pi \sin^2 k_F} \sum_{\omega=\pm\Lambda} \int_0^{2\pi} \frac{dp}{2\pi}\, f(p,\omega)\ , \tag{4.31}
$$

where

$$
f(p,\omega) = \frac{2\sin^2 k_F\, \sin^2 p}{(i\omega-\xi^0_p)(-i\omega-\xi^0_{-p})} - \frac{(\cos k_F - \cos p)^2}{(i\omega-\xi^0_p)^2} + \frac{[\cos(2k_F)-\cos p]^2}{(i\omega-\xi^0_{p-k_F})(i\omega-\xi^0_{p+k_F})}\ . \tag{4.32}
$$

Here $\xi^0_k = -2\cos k - \mu_0$, with $\mu_0 = -2\cos k_F$, is the bare dispersion relation relative to the bare Fermi level. Since $f(p,\omega)$ can be written as a rational function of $\cos p$ and $\sin p$, the p-integral can be carried out analytically using the substitution $z = e^{ip}$ and the residue theorem. After a lengthy but straightforward calculation one obtains the following result for the coefficient $h(\Lambda)$ in (4.30):

$$
\begin{aligned}
h(\Lambda) = -\frac{1}{2\pi} - \mathrm{Re}\Bigg[& \frac{i}{2}\,(\mu_0+i\Lambda)\sqrt{1-\frac{4}{(\mu_0+i\Lambda)^2}} \\
& \times \frac{3i\mu_0^4 - 10\mu_0^3\Lambda - 12i\mu_0^2(\Lambda^2+1) + 6\Lambda^3\mu_0 + 18\Lambda\mu_0 + 6i\Lambda^2 + i\Lambda^4}{\pi(2\mu_0+i\Lambda)(4-\mu_0^2+\Lambda^2-2i\Lambda\mu_0)^2}\Bigg]\ .
\end{aligned}
\tag{4.33}
$$

The flow equation (4.30) can be integrated to

$$U^\Lambda = \frac{U}{1 - U\,H(\Lambda)}\,, \tag{4.34}$$

where $H(\Lambda)$ is the primitive function of $h(\Lambda)$ with $H(\Lambda) \to 0$ for $\Lambda \to \infty$. Integrating $h(\Lambda)$ one obtains

$$\begin{aligned} H(\Lambda) = -\frac{\Lambda}{2\pi} + \frac{1}{\pi}\,\mathrm{Re}\Big[& \frac{(4-\mu_0^2)\Lambda^2 - 2i\mu_0(2-\mu_0^2)\Lambda + \mu_0^4 - 6\mu_0^2 + 8}{2\,(4-\mu_0^2)\sqrt{\Lambda^2 - 2i\mu_0\Lambda + 4 - \mu_0^2}} \\ & + \frac{\mu_0^4}{2(4-\mu_0^2)^{3/2}}\,\tanh^{-1}\frac{4 + \mu_0^2 + i\mu_0\Lambda}{\sqrt{(4+\mu_0^2+i\mu_0\Lambda)^2 + 4(\Lambda - 2i\mu_0)^2}} \\ & - \frac{i\mu_0}{2}\,\sinh^{-1}\frac{\Lambda - i\mu_0}{2}\Big]\,, \end{aligned} \tag{4.35}$$

where $\sinh^{-1}$ and $\tanh^{-1}$ denote the main branch of the inverse of the complex functions sinh and tanh respectively.

At half filling, corresponding to $k_F = \pi/2$, the function $h(\Lambda)$ is particularly simple

$$h(\Lambda) = -\frac{1}{2\pi}\,\left[1 - \Lambda\,\frac{6 + \Lambda^2}{(4+\Lambda^2)^{3/2}}\right] \tag{4.36}$$

such that U^Λ reduces to

$$U^\Lambda = \frac{U}{1 + \left(\Lambda - \frac{2+\Lambda^2}{\sqrt{4+\Lambda^2}}\right)\,U/(2\pi)}\,. \tag{4.37}$$

In Fig. 4.3 we show results for the renormalized nearest-neighbor interaction U^Λ as obtained from the flow equation at various densities n, for a bare interaction $U = 1$. While the renormalization does not follow any simple rule at intermediate scales Λ, all curves saturate at a finite value U^* in the limit $\Lambda \to 0$, corresponding to a finite g^*, as expected for a Luttinger-liquid fixed point [Voit 1995].

Parametrizing Γ^Λ by a renormalized nearest-neighbor interaction has the enormous advantage that the self-energy, as determined by the flow equation (4.17), is a tridiagonal matrix in real space, that is, only the matrix elements $\Sigma^\Lambda_{j,j}$ and $\Sigma^\Lambda_{j,j\pm1}$ are nonzero. Inserting Γ^Λ from Eq. (4.25) into (4.17), one obtains the following simple coupled flow equations for the diagonal and off-diagonal matrix elements:

$$\frac{\partial}{\partial\Lambda}\,\Sigma^\Lambda_{j,j} = -\frac{U^\Lambda}{2\pi}\sum_{\omega=\pm\Lambda}\sum_{r=\pm1}\tilde{G}^\Lambda_{j+r,j+r}(i\omega)$$

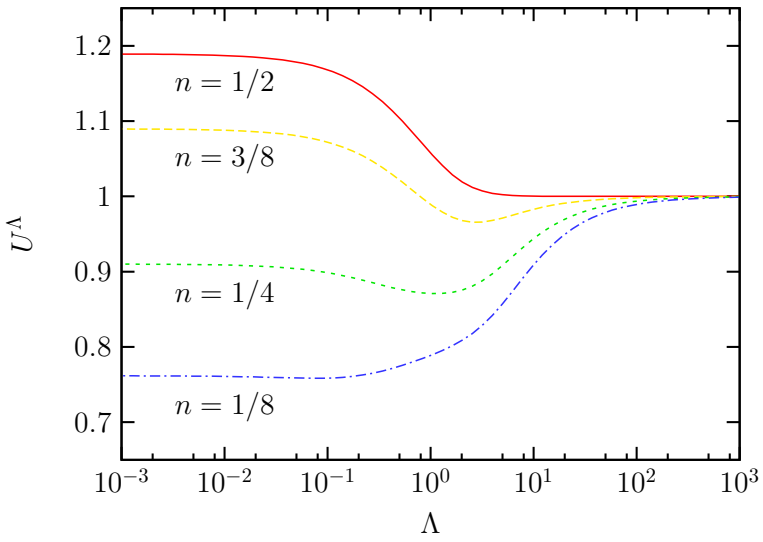

Figure 4.3: *Flow of the renormalized nearest-neighbor interaction U^Λ for the spinless fermion model, for $U = 1$ and various densities n.*

$$\frac{\partial}{\partial\Lambda}\,\Sigma^\Lambda_{j,j\pm1} \;=\; \frac{U^\Lambda}{2\pi}\sum_{\omega=\pm\Lambda}\tilde{G}^\Lambda_{j,j\pm1}(i\omega)\;. \tag{4.38}$$

Note that the self-energy enters also the right-hand side of these equations, via $\tilde{G}^\Lambda = (G_0^{-1} - \Sigma^\Lambda)^{-1}$. Since Σ^Λ and G_0^{-1} are both tridiagonal in real space, the matrix inversion required to compute the diagonal and first off-diagonal elements of $\tilde{G}^\Lambda$ from Σ^Λ can be carried out very efficiently. An algorithm for the numerical solution of the flow equation for Σ^Λ scaling linearly with the system size is described in Ref. [Andergassen et al. 2004; Enss 2005]. Very large systems with up to 10^7 sites can be treated without extensive numerical effort.

4.2.4 Spin-$\frac{1}{2}$ fermions

We now describe the parametrization of the spatial (or momentum) dependences of the two-particle vertex Γ^Λ for spin-$\frac{1}{2}$ fermions [Andergassen et al. 2005b], employing a natural extension of our previous parametrization for the spinless case in Sec. 4.2.3. We consider spin-rotation invariant lattice systems with local and nearest-neighbor interactions. This includes the extended Hubbard model.

For a spin-rotation invariant system the spin structure of the two-particle vertex

can be decomposed in a singlet and a triplet part:

$$\Gamma^\Lambda = \Gamma_s^\Lambda \, S_{\sigma_1',\sigma_2';\sigma_1,\sigma_2} + \Gamma_t^\Lambda \, T_{\sigma_1',\sigma_2';\sigma_1,\sigma_2} \; , \tag{4.39}$$

with

$$\begin{aligned} S_{\sigma_1',\sigma_2';\sigma_1,\sigma_2} &= \frac{1}{2} \left(\delta_{\sigma_1\sigma_1'} \delta_{\sigma_2\sigma_2'} - \delta_{\sigma_1\sigma_2'} \delta_{\sigma_2\sigma_1'} \right) \\ T_{\sigma_1',\sigma_2';\sigma_1,\sigma_2} &= \frac{1}{2} \left(\delta_{\sigma_1\sigma_1'} \delta_{\sigma_2\sigma_2'} + \delta_{\sigma_1\sigma_2'} \delta_{\sigma_2\sigma_1'} \right) \; . \end{aligned} \tag{4.40}$$

Since the total vertex is antisymmetric in the incoming and outgoing particles, the singlet part Γ_s^Λ has to be symmetric and the triplet part Γ_t^Λ antisymmetric.

Proceeding in analogy to the case of spinless fermions in Sec. 4.2.3, we first list momentum components of the vertex with all momenta at $\pm k_F$. For the triplet vertex the antisymmetry allows once again only one such component

$$g_t^\Lambda = \Gamma^\Lambda_{t|\, k_F,-k_F;k_F,-k_F} \; . \tag{4.41}$$

For the singlet vertex there are several distinct components at $\pm k_F$. Since we will neglect the influence of the impurity on the vertex renormalization, the renormalized vertex remains translation invariant. Hence the momentum components are restricted by momentum conservation: $k_1' + k_2' = k_1 + k_2$, modulo integer multiples of 2π. The remaining independent (not related by obvious symmetries) components are

$$\begin{aligned} g_{s2}^\Lambda &= \Gamma^\Lambda_{s|\, k_F,-k_F;k_F,-k_F} \\ g_{s4}^\Lambda &= \Gamma^\Lambda_{s|\, k_F,k_F;k_F,k_F} \end{aligned} \tag{4.42}$$

and in the case of half filling, for which $k_F = \pi/2$, also

$$g_{s3}^\Lambda = \Gamma^\Lambda_{s|\, \pi/2,\pi/2;-\pi/2,-\pi/2} \; . \tag{4.43}$$

The labels $2, 3, 4$ are chosen in analogy to the conventional g-ology notation for one-dimensional Fermi systems [Sólyom 1979]. In order to parametrize the vertex in a uniform way in all cases, we will include the umklapp component g_{s3}^Λ not only at half filling, but at any density. The effect on the other components is negligible for the range of interactions and fillings considered.

Extending our treatment of the spinless case in Sec. 4.2.3, we now parametrize the vertex by renormalized local and nearest-neighbor interactions in real space.

For the triplet part, there is no local component, and only one nearest-neighbor component compatible with the antisymmetry, namely

$$U_t'^{\Lambda} = \Gamma^{\Lambda}_{t|\,j,j+1;j,j+1} \,, \tag{4.44}$$

which has the same form as the nearest-neighbor interaction in the spinless case. Note that $\Gamma^{\Lambda}_{t|\,j,j+1;j,j+1}$ does not depend on j and is equal to $\Gamma^{\Lambda}_{t|\,j,j-1;j,j-1}$. For the symmetric singlet part, there is one local component

$$U_s^{\Lambda} = \Gamma^{\Lambda}_{s|\,j,j;j,j} \tag{4.45}$$

and three different components involving nearest neighbors:

$$\begin{aligned} U_s'^{\Lambda} &= \Gamma^{\Lambda}_{s|\,j,j+1;j,j+1} \\ P_s^{\Lambda} &= \Gamma^{\Lambda}_{s|\,j+1,j+1;j,j} \\ W_s^{\Lambda} &= \Gamma^{\Lambda}_{s|\,j+1,j;j,j} \,. \end{aligned} \tag{4.46}$$

For the Hubbard model, the bare vertex is purely local and the initial condition for the vertex is given by $U_s^{\Lambda_0} = 2U$, while all the other components vanish. For the extended Hubbard model, $U_s'^{\Lambda_0} = U_t'^{\Lambda_0} = U'$ are nonzero.

The triplet vertex is parametrized by only one renormalized real space coupling, which leads to a momentum representation of the form

$$\Gamma^{\Lambda}_{t|\,k_1',k_2';k_1,k_2} = 2U_t'^{\Lambda} \left[\cos(k_1' - k_1) - \cos(k_2' - k_1)\right] \delta^{(2\pi)}_{k_1+k_2,k_1'+k_2'} \,, \tag{4.47}$$

where the Kronecker δ implements momentum conservation (modulo 2π). The flowing coupling $U_t'^{\Lambda}$ is thus linked in a one-to-one correspondence to the Fermi momentum coupling g_t^{Λ} by

$$g_t^{\Lambda} = 2U_t'^{\Lambda} \left[1 - \cos(2k_F)\right] \tag{4.48}$$

as in the spinless case in Sec. 4.2.3. In the singlet channel we have found four real space couplings, that is, one more than necessary to match the three singlet couplings in momentum space, g_{s2}^{Λ}, g_{s3}^{Λ}, g_{s4}^{Λ}. We discard the interaction W_s^{Λ}, because it does not appear in the bare Hubbard model, where it is generated only at third order in U, while the pair hopping P_s^{Λ} appears already in second-order perturbation theory. Fourier transforming the remaining interactions yields the singlet vertex in k-space

$$\Gamma^{\Lambda}_{s|\,k_1',k_2';k_1,k_2} = \Big[U_s^{\Lambda} + 2U_s'^{\Lambda} \left[\cos(k_1' - k_1) + \cos(k_2' - k_1)\right]$$

$$+P_s^\Lambda \cos(k_1+k_2)\big]\ \delta^{(2\pi)}_{k_1+k_2,k_1'+k_2'} \tag{4.49}$$

from which we obtain a linear relation between the momentum space couplings g_{s2}^Λ, g_{s3}^Λ, g_{s4}^Λ and the renormalized interaction parameters U_s^Λ, $U_s'^\Lambda$, P_s^Λ:

$$\begin{aligned}
g_{s2}^\Lambda &= U_s^\Lambda + 2U_s'^\Lambda\,[1+\cos(2k_F)] + 2P_s^\Lambda \\
g_{s3}^\Lambda &= U_s^\Lambda - 4U_s'^\Lambda - 2P_s^\Lambda \\
g_{s4}^\Lambda &= U_s^\Lambda + 4U_s'^\Lambda + 2P_s^\Lambda\,\cos(2k_F)\ .
\end{aligned} \tag{4.50}$$

The determinant of this linear system is positive for all k_F, except for $k_F = 0$ and π. Hence the equations can be inverted for all densities except the trivial cases of an empty or completely filled band.

We can now set up the flow equations for the four independent couplings $U_t'^\Lambda$, U_s^Λ, $U_s'^\Lambda$, and P_s^Λ which parametrize the vertex. Consider the case $T = 0$ first. Inserting the spin structure (4.39) into the general flow equation for the two-particle vertex (4.23), and using the momentum representation for a translation invariant vertex, the flow equation for the singlet and triplet vertices Γ_a^Λ, for $a = s, t$, can be written as

$$\frac{\partial}{\partial\Lambda}\,\Gamma^\Lambda_{a|\,k_1',k_2';k_1,k_2} = -\frac{1}{2\pi}\sum_{\omega=\pm\Lambda}\sum_{b,b'=s,t}\int\frac{dp}{2\pi}\,(\,PP+PH+PH'\,)\ , \tag{4.51}$$

with the particle-particle and particle-hole contributions

$$\begin{aligned}
PP &= C^{PP}_{a,bb'}\,G^0_p(i\omega)\,G^0_{k_1+k_2-p}(-i\omega)\,\Gamma^\Lambda_{b|\,k_1',k_2';p,k_1+k_2-p}\,\Gamma^\Lambda_{b'|\,p,k_1+k_2-p;k_1,k_2} \\
PH &= C^{PH}_{a,bb'}\,G^0_p(i\omega)\,G^0_{p+k_1-k_1'}(i\omega)\,\Gamma^\Lambda_{b|\,k_1',p+k_1-k_1';k_1,p}\,\Gamma^\Lambda_{b'|\,p,k_2';p+k_1-k_1',k_2} \\
PH' &= C^{PH'}_{a,bb'}\,G^0_p(i\omega)\,G^0_{p+k_1-k_2'}(i\omega)\,\Gamma^\Lambda_{b|\,k_2',p+k_1-k_2';k_1,p}\,\Gamma^\Lambda_{b'|\,p,k_1';p+k_1-k_2',k_2}\ .
\end{aligned} \tag{4.52}$$

The coefficients $C_{a,bb'}$ are obtained from the spin sums as

$$\begin{aligned}
C^{PP}_{s,ss} &= 1 & C^{PP}_{s,st} &= C^{PP}_{s,ts} = C^{PP}_{s,tt} = 0 \\
C^{PP}_{t,tt} &= 1 & C^{PP}_{t,ss} &= C^{PP}_{t,st} = C^{PP}_{t,ts} = 0 \\
C^{PH}_{s,ss} &= -1/4 & C^{PH}_{s,st} &= C^{PH}_{s,ts} = C^{PH}_{s,tt} = 3/4 \\
C^{PH}_{t,tt} &= 5/4 & C^{PH}_{t,ss} &= C^{PH}_{t,st} = C^{PH}_{t,ts} = 1/4
\end{aligned}$$

$$C^{PH'}_{s,bb'} = -\,C^{PH}_{s,bb'} \qquad\qquad C^{PH'}_{t,bb'} = C^{PH}_{t,bb'}\ . \tag{4.53}$$

Note that we have neglected the self-energy feedback in the flow of Γ^Λ, such that only bare propagators G_0 enter. On the right-hand side of the flow equation we insert the parametrization (4.47) for Γ^Λ_t and (4.49) for Γ^Λ_s. The flow of the triplet vertex $\Gamma^\Lambda_{t|\,k_1',k_2';k_1,k_2}$ is evaluated only for $(k_1', k_2', k_1, k_2) = (k_F, -k_F, k_F, -k_F)$ as in Eq. (4.41), which yields the flow of g_t^Λ, while the flow of the singlet vertex $\Gamma^\Lambda_{s|\,k_1',k_2';k_1,k_2}$ is computed for the three choices of (k_1', k_2', k_1, k_2) which yield the flow of g_{s2}^Λ, g_{s3}^Λ, g_{s4}^Λ corresponding to Eqs. (4.42) and (4.43). Using the linear equations (4.48) and (4.50) to replace the couplings g^Λ by the renormalized real space interactions on the left-hand side of the flow equations, we obtain a complete set of flow equations for the four renormalized interactions $U_t'^\Lambda$, U_s^Λ, $U_s'^\Lambda$, and P_s^Λ of the form

$$\partial_\Lambda U_\alpha^\Lambda = \sum_{\alpha',\alpha''} h^\alpha_{\alpha'\alpha''}(\Lambda)\, U^\Lambda_{\alpha'}\, U^\Lambda_{\alpha''}\ , \tag{4.54}$$

where $\alpha = 1, 2, 3, 4$ labels the four different interactions. The functions $h^\alpha_{\alpha'\alpha''}(\Lambda)$ can be computed analytically by carrying out the momentum integrals in Eq. (4.51) via the residue theorem, details are reported in App. A.1. The flow equations can then be solved numerically very easily. For finite systems the momentum integral should be replaced by a discrete momentum sum; however, this leads only to negligible corrections for the physical observables presented in Sec. 4.4.

After computing the flow of the real space interactions, one can also calculate the flow of the momentum space couplings g^Λ by using the linear relation between the two. In the low-energy limit (small Λ) one recovers the one-loop flow of the g-ology model, the general effective low-energy model for one-dimensional fermions [Sólyom 1979], for details see Sec. A.2. In addition, our vertex renormalization captures also all nonuniversal second-order contributions to the vertex at $\pm k_F$ from higher energy scales.

In Fig. 4.4 we show results for the renormalized real space interactions together with the corresponding momentum space couplings, as obtained by integrating the flow equations for the Hubbard model at quarter filling and $T = 0$. Note that the couplings converge to finite fixed-point values in the limit $\Lambda \to 0$, but the convergence is very slow, except for the momentum space couplings g_{s3}^Λ and g_{s4}^Λ. This can be traced back to the familiar behavior of the so-called backscattering coupling $g_{1\perp}^\Lambda = \frac{1}{2}\,(g_{s2}^\Lambda - g_t^\Lambda)$, that is, the amplitude for the exchange of two particles

with opposite spin at opposite Fermi points. Backscattering is known to vanish logarithmically in the low-energy limit for spin-rotation invariant spin-$\frac{1}{2}$ Luttinger liquids [Voit 1995]. We emphasize that this logarithmic behavior is not promoted to a power law by higher order terms beyond our approximation. By contrast, the linear combination of couplings which determines the Luttinger-liquid parameter K_ρ converges very quickly to a finite fixed-point value.

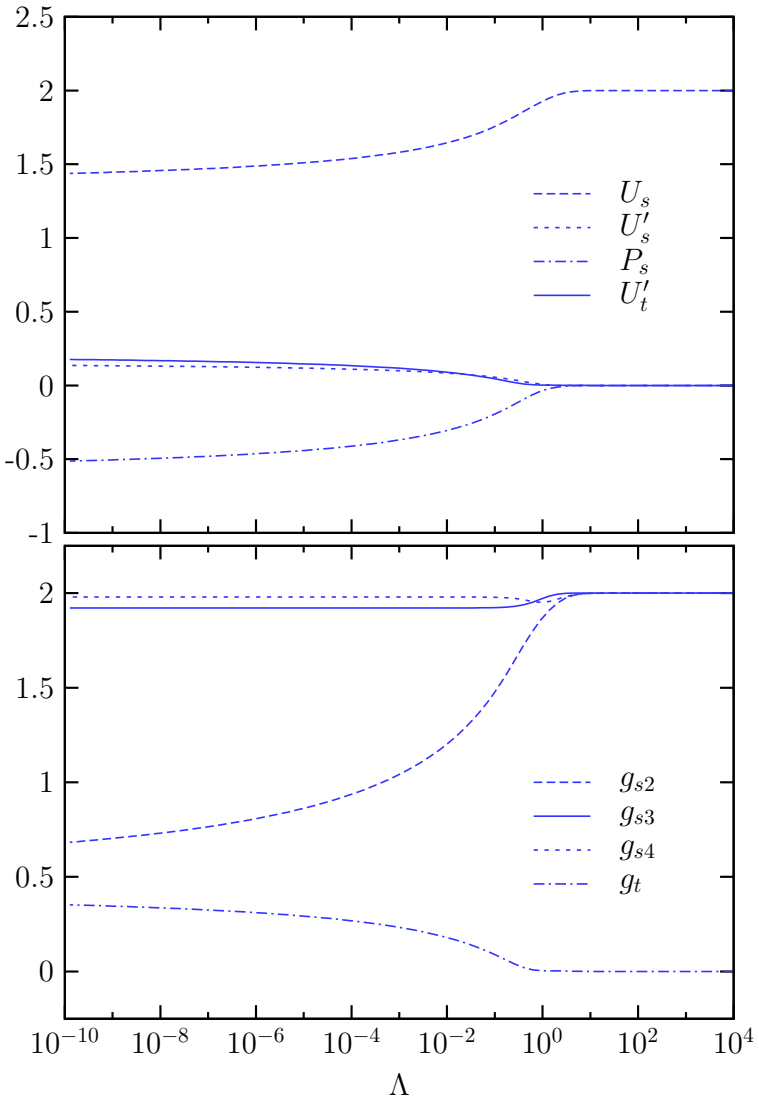

Figure 4.4: *Vertex flow for the Hubbard model at quarter filling ($n = 1/2$) and $U = 1$;* upper panel*: flow of the renormalized real space interactions,* lower panel*: flow of the momentum space couplings.*

Due to the above parametrization of the vertex by real space interactions which do not extend beyond nearest neighbors on the lattice, the self-energy generated by the flow equations is frequency independent and tridiagonal in real space. Inserting the spin and real space structure of Γ^Λ into the general flow equation for the self-energy (4.17), one obtains

$$\begin{aligned}\frac{\partial}{\partial\Lambda}\,\Sigma^\Lambda_{j,j} &= -\frac{1}{4\pi}\sum_{\omega=\pm\Lambda}\Big[\,U_s^\Lambda\,\tilde G^\Lambda_{j,j}(i\omega) + (U_s'^\Lambda + 3U_t'^\Lambda)\sum_{r=\pm1}\tilde G^\Lambda_{j+r,j+r}(i\omega)\,\Big]\\ \frac{\partial}{\partial\Lambda}\,\Sigma^\Lambda_{j,j\pm1} &= -\frac{1}{4\pi}\sum_{\omega=\pm\Lambda}\Big[\,(U_s'^\Lambda - 3U_t'^\Lambda)\,\tilde G^\Lambda_{j,j\pm1}(i\omega) + P_s^\Lambda\,\tilde G^\Lambda_{j\pm1,j}(i\omega)\,\Big]\;, \qquad (4.55)\end{aligned}$$

where $\tilde G^\Lambda = (G_0^{-1} - \Sigma^\Lambda)^{-1}$.

Due to the slow decay of G at large frequencies, the integration of the flow equation for Σ from $\Lambda = \infty$ to $\Lambda = \Lambda_0$ yields a contribution which remains finite even in the limit $\Lambda_0 \to \infty$, as described in Sec. 4.2.2. For the extended Hubbard model this contribution is given by $\Sigma^{\Lambda_0}_{j,j} = U/2 + 2U'$ for $j = 2,\ldots,L-1$ and $\Sigma^{\Lambda_0}_{1,1} = \Sigma^{\Lambda_0}_{L,L} = U/2 + U'$. The numerical integration of the flow is started at a sufficiently large Λ_0 with Σ^{Λ_0} as initial condition.

4.2.5 Extension to finite temperature

At finite temperatures the Matsubara frequencies ω_n are discrete. The sum over ω_n of a function f can be written as an integral over a continuous variable ω by introducing the distribution function P with a normalization $\int_{|\omega-\omega_n|\le\pi T} d\omega\, P(\omega) = 1$ for all n,

$$\sum_{\omega_n} f(\omega_n) = \sum_{\omega_n}\int_{|\omega-\omega_n|\le\pi T} d\omega\, P(\omega)\, f(\omega_n) = \int d\omega\, P(\omega) f(\omega_{n,\omega})\;, \qquad (4.56)$$

where $\omega_{n,\omega}$ denotes the discrete Matsubara frequency closest to ω. Introducing a sharp frequency cutoff in the continuous variable ω, the extension of the flow equations to finite temperatures is fairly simple, as pointed out by T. Enss [Andergassen et al. 2005b]. The general form of the flow equation for the generating functional for the 1PI vertex functions Υ at $T = 0$,

$$\frac{\partial}{\partial\Lambda}\Upsilon^\Lambda = \int d\omega\,\delta(|\omega|-\Lambda)\,\mathcal{F}\big[\Theta(|\omega|-\Lambda), \Upsilon^\Lambda(\omega)\big]\;, \qquad (4.57)$$

is modified to

$$\frac{\partial}{\partial\Lambda}\Upsilon^\Lambda = T\int d\omega\, P(\omega)\,\delta(|\omega|-\Lambda)\,\mathcal{F}\big[\Theta(|\omega|-\Lambda),\Upsilon^\Lambda(\omega_{n,\omega})\big] \tag{4.58}$$

at $T>0$. Applying the lemma (4.16) the integral over ω can be carried out analytically

$$\begin{aligned}\frac{\partial}{\partial\Lambda}\Upsilon^\Lambda &= T\int d\omega\, P(\omega)\,\delta(|\omega|-\Lambda)\int_0^1 dt\,\mathcal{F}\big[t,\Upsilon^\Lambda(\omega_{n,\omega})\big]\\ &= T\sum_{\omega=\pm\Lambda} P(\omega)\,F\big[\Upsilon^\Lambda(\omega_{n,\omega})\big]\,,\end{aligned} \tag{4.59}$$

where $F(\cdot)=\int_0^1 dt\,\mathcal{F}(t,\cdot)$. The contribution to the flow on the interval $\omega_{n,\Lambda}-\pi T\le\Lambda<\omega_{n,\Lambda}+\pi T$ is described by an autonomous differential equation, as the only explicit Λ dependence appears in P. As a consequence the result is independent of the particular choice of the distribution function P; for simplicity we choose the constant

$$P(\omega)=\frac{1}{2\pi T}\,. \tag{4.60}$$

This leads to the final form of the flow equation

$$\frac{\partial}{\partial\Lambda}\Upsilon^\Lambda = \frac{1}{2\pi}\sum_{\omega=\pm\omega_{n,\Lambda}} F\big[\Upsilon^\Lambda(\omega)\big] \tag{4.61}$$

for Υ. Hence, in the flow equations for the self-energy and the two-particle vertex, Eqs. (4.17) and (4.23) respectively, the expression $\omega=\pm\Lambda$ at $T=0$ is replaced by $\omega=\pm\omega_{n,\Lambda}$ at finite temperature, the functional dependence on ω remains the same.

Note that for $P(\omega)=\delta(\omega-\omega_{n,\omega})$ the flow equation cannot be simplified by (4.16) and a smooth frequency cutoff has to be chosen [Enss et al. 2005; Enss 2005].

4.3 Calculation of K_ρ

The Luttinger-liquid parameter K_ρ, which determines the critical exponents of Luttinger liquids, can be computed from the fixed-point couplings as obtained from the fRG. A relation between the fixed-point couplings and K_ρ can be established via the exact solution of the fixed-point Hamiltonian of Luttinger liquids, the Luttinger model. A comparison of the fRG result for K_ρ with the exact Bethe-ansatz result

for the bulk model (without impurity) serves also as a check for the accuracy of our vertex renormalization. Since the above simplified flow equations yield not only the correct low-energy asymptotics to second order in the renormalized interaction, but contain also all *nonuniversal* second-order corrections at $\pm k_F$ from higher energy scales, the resulting K_ρ is obtained correctly to second order in the interaction.

4.3.1 Spinless fermions

For spinless fermions, K_ρ is determined by the Luttinger model parameters g and v_F as

$$K_\rho = \sqrt{\frac{1 - g/(2\pi v_F)}{1 + g/(2\pi v_F)}}\,, \tag{4.62}$$

where g is the interaction between left and right movers and v_F the effective Fermi velocity of the model, that is, the slope of the (linear) dispersion relation, with a possible shift due to interactions between particles moving in the same direction (g_4-coupling) already included [Voit 1995]. We therefore need to extract g and v_F from the fRG flow in the limit $\Lambda \to 0$. In order to obtain K_ρ correctly to order U^2, it is sufficient to obtain v_F correctly to linear order in U.

The Luttinger model interaction g and the fixed-point coupling $g^* = \Gamma^{\Lambda\to 0}_{k_F,-k_F;k_F,-k_F}$ from the fRG are not simply identical, in contrast to what one might naively expect. To find the true relation between g and g^*, one has to take into account that the forward scattering limit of the dynamical two-particle vertex is generally not unique (in the absence of cutoffs), and depends on whether momentum or frequency transfers tend to zero first. This ambiguity is well-known in Fermi-liquid theory, where it leads to the distinction between quasi-particle interactions and scattering amplitudes [Negele and Orland 1987], but is equally present in Luttinger liquids, for the same reason in all cases: the ambiguity of the small momentum, small frequency limit of particle-hole propagators contributing to the vertex function. In the *dynamical limit*, where the momentum transfer q vanishes first, the singular particle-hole propagators do not contribute. In Fermi liquids this limit yields the quasi-particle interaction. In the opposite *static limit* the frequency transfer ν vanishes first and particle-hole propagators yield a finite contribution. In the presence of an infrared cutoff $\Lambda > 0$ the forward scattering limit of the vertex function is unique, since the ambiguity in the particle-hole propagator is due to the infrared pole of the single-particle propagator. Hence $\Gamma^{\Lambda}_{k_F,-k_F;k_F,-k_F}$ is well defined. However, $\Gamma^{\Lambda}_{k_F,-k_F;k_F,-k_F}$

and also its limit for $\Lambda \to 0$ depend on the choice for the cutoff function. For a momentum cutoff, which excludes states with excitation energies below Λ around the Fermi points, particle-hole excitations with small momentum transfers q are impossible. Hence particle-hole propagators with infinitesimal q do not contribute to the vertex at any $\Lambda > 0$, such that $\Gamma^{\Lambda}_{k_F,-k_F;k_F,-k_F}$ converges to the dynamical forward scattering limit, which is simply given by the bare coupling constant g in the Luttinger model. For a frequency cutoff the particle-hole propagators with vanishing momentum and frequency transfer yield a finite contribution at $\Lambda > 0$, which tends to the static limit for $\Lambda \to 0$. This can be seen directly by integrating $\sum_{\omega=\pm\Lambda} \int dp\, [G^0_p(i\omega)]^2$ over Λ from infinity to zero. Hence the vertex $\Gamma^{\Lambda}_{k_F,-k_F;k_F,-k_F}$ obtained from our frequency cutoff fRG tends to the static forward scattering limit.

For the Luttinger model the static forward scattering limit of the vertex can be obtained from the dynamical effective interaction between left and right movers $D(q, i\nu)$, which is defined as the sum of particle-hole chains

$$D(q,i\nu) = g + g\,\Pi^0_-(q,i\nu)\,g\,\Pi^0_+(q,i\nu)\,g + \cdots = \frac{g}{1 - g^2\,\Pi^0_-(q,i\nu)\,\Pi^0_+(q,i\nu)}\ , \quad (4.63)$$

where

$$\Pi^0_\pm(q,i\nu) = \pm\frac{1}{2\pi}\,\frac{q}{i\nu \mp v_F q} \quad (4.64)$$

is the bare particle-hole bubble for right (+) and left (−) movers. Note that only odd powers of g contribute to the effective interaction between left and right movers. This effective interaction appears naturally in the exact solution of the Luttinger model via Ward identities [Dzyaloshinskii and Larkin 1973; Metzner and Di Castro 1993]. For the static limit one obtains

$$\lim_{q\to 0} D(q,0) = \frac{g}{1 - [g/(2\pi v_F)]^2} \quad (4.65)$$

which we identify with our fixed-point coupling g^* as obtained from the fRG with frequency cutoff. Inverting this relation between g and g^* we obtain

$$g = \frac{2\pi v_F}{g^*}\,\left[-\pi v_F + \sqrt{(\pi v_F)^2 + (g^*)^2}\right]\ . \quad (4.66)$$

For spinless fermions the difference between g and g^* appears only at third order in the coupling, but for models with spin the distinction becomes important already at second order.

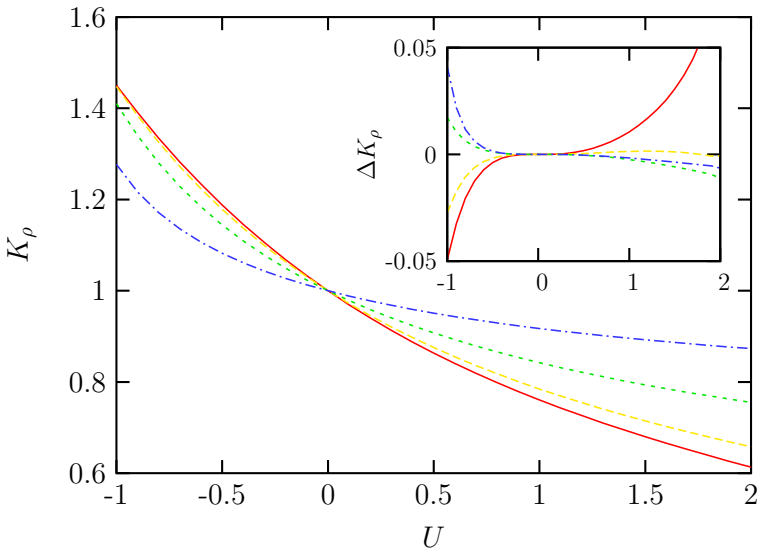

Figure 4.5: *Luttinger-liquid parameter K_ρ as a function of U at various densities (as in Fig. 4.3) for the spinless fermion model; the inset shows the difference between the fRG result and the exact Bethe ansatz result for K_ρ.*

The Fermi velocity v_F can be computed from the (frequency-independent) self-energy in momentum space as

$$v_F = v_F^0 + \partial_k \Sigma_k|_{k_F} \ , \tag{4.67}$$

where $v_F^0 = \partial_k \epsilon_k|_{k_F}$ is the bare Fermi velocity. The self-energy is computed from the flow equation (4.38), which can be rewritten in momentum space as

$$\frac{\partial}{\partial \Lambda} \Sigma_k^\Lambda = -\frac{U^\Lambda}{\pi} \sum_{\omega=\pm\Lambda} \int \frac{dp}{2\pi} \frac{1-\cos(k-p)}{i\omega - \xi_p - \Sigma_p^\Lambda} \ , \tag{4.68}$$

where $\xi_p = \epsilon_p - \mu$. The chemical potential μ has to be fixed by the final condition $\xi_{k_F} + \Sigma_{k_F} = 0$, where $k_F = \pi n$ depends only on the density, not the interaction. From the tridiagonal structure of Σ in real space, but also from the above expression it follows that Σ_k^Λ has the form $\Sigma_k^\Lambda = a^\Lambda + b^\Lambda \cos k$. The functional flow equation for Σ_k^Λ yields a coupled set of ordinary flow equations for the coefficients a^Λ and b^Λ, with initial conditions $a^{\Lambda_0} = U$ and $b^{\Lambda_0} = 0$. The momentum integrals can be evaluated analytically via the residue theorem, such that the remaining set of two coupled differential equations (with U^Λ as input) can be easily solved numerically. The result for v_F is correct at least to first order in U, but not necessarily to second

order, since our simplified parametrization captures the two-particle vertex correctly to second order only at the Fermi points.

Inserting g and v_F into the Luttinger model formula (4.62) we can now compute K_ρ as a function of U and density for the microscopic spinless fermion model. In Fig. 4.5 we show results for $K_\rho(U)$ for various fixed densities. A comparison with exact results from the Bethe ansatz solution of the spinless fermion model [Haldane 1980] in the inset shows that the fRG results are correct to second order in U and the vertex renormalization scheme described above is very accurate.

4.3.2 Spin-$\frac{1}{2}$ fermions

The Luttinger-liquid parameter K_ρ for spin-$\frac{1}{2}$ fermions is given by

$$K_\rho = \sqrt{\frac{1 + (g_{\rho 4} - g_{\rho 2})/(\pi v_F)}{1 + (g_{\rho 4} + g_{\rho 2})/(\pi v_F)}} \,. \tag{4.69}$$

The coupling constants $g_{\rho 2}$ and $g_{\rho 4}$ parametrize forward scattering interactions in the charge channel (that is, spin symmetrized) between opposite and equal Fermi points respectively. They are related to the bare singlet and triplet vertices of the Luttinger model by

$$\begin{aligned} g_{\rho 2} &= \frac{1}{4} \left(\gamma_{s|\, k_F,-k_F;k_F,-k_F} + 3\gamma_{t|\, k_F,-k_F;k_F,-k_F} \right) \\ g_{\rho 4} &= \frac{1}{4} \gamma_{s|\, k_F,k_F;k_F,k_F} \,. \end{aligned} \tag{4.70}$$

These bare vertices are identical to the *dynamical* forward scattering limits of the full vertex Γ^Λ. On the other hand, the vertex Γ^Λ obtained from the fRG with a frequency cutoff yields the *static* forward scattering limit for $\Lambda \to 0$ (cf. Sec. 4.3.1). For the Luttinger model, the static forward scattering limit for the vertex can be computed from the effective interactions $D_{\rho 2}(q, i\nu)$ and $D_{\rho 4}(q, i\nu)$, which are defined as the sum over all particle-hole chains with the bare interactions $g_{\rho 2}$ and $g_{\rho 4}$ [Sólyom 1979]. The summation becomes a simple geometric series if one introduces symmetric and antisymmetric combinations $g_{\rho\pm} = g_{\rho 4} \pm g_{\rho 2}$ and $D_{\rho\pm}(q, i\nu) = D_{\rho 4}(q, i\nu) \pm D_{\rho 2}(q, i\nu)$. The static limit of the effective interaction $D_{\rho\pm}(q, i\nu)$ yields the relation

$$g^*_{\rho\pm} = \frac{g_{\rho\pm}}{1 - g_{\rho\pm}/(\pi v_F)} \tag{4.71}$$

between the Luttinger model couplings $g_{\rho\pm}$ and the fixed-point couplings

$$g^*_{\rho\pm} = \frac{1}{4}\left[\, g^*_{s4} \pm \left(\, g^*_{s2} + 3g^*_t \,\right)\right] \tag{4.72}$$

from the fRG with frequency cutoff. Inverting (4.71) one obtains

$$K_\rho = \sqrt{\frac{1 - g^*_{\rho+}/(\pi v_F)}{1 - g^*_{\rho-}/(\pi v_F)}}\,. \tag{4.73}$$

The Fermi velocity v_F can be computed from the self-energy for the translation-invariant pure system as in the spinless case, using the momentum representation of the flow equations (4.55).

The results for K_ρ from the above procedure are correct to second order in the bare interaction for the Hubbard model and also for the extended Hubbard model. While the flowing couplings g^Λ_{s2} and g^Λ_t converge only logarithmically to their fixed-point values for $\Lambda \to 0$, the linear combination $g^\Lambda_{s2} + 3g^\Lambda_t$ which enters K_ρ converges much faster.

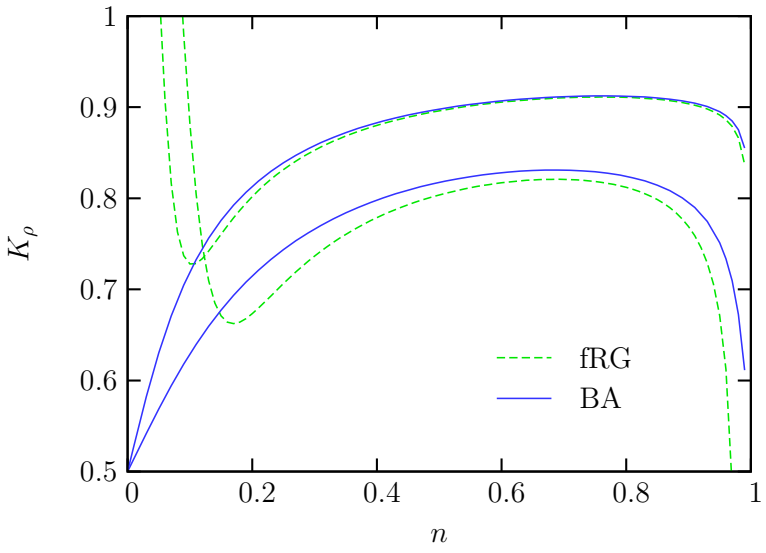

Figure 4.6: *Luttinger-liquid parameter K_ρ for the Hubbard model as a function of electron density; results from the fRG are compared to exact results from the Bethe ansatz; the upper curves are for $U = 1$ and the lower ones for $U = 2$.*

In Fig. 4.6 we show results for K_ρ for the Hubbard model as obtained from the fRG and, for comparison, from the exact Bethe ansatz solution [Frahm and Korepin 1990; Kawakami and Yang 1990; Schulz 1990]. Details on the solution

of the corresponding integral equations are reported in App. B. The truncated fRG yields accurate results at weak coupling except for low densities and close to half filling. In the latter case this failure is expected since umklapp scattering interactions renormalize toward strong coupling, even if the bare coupling is weak. At low densities already the bare dimensionless coupling U/v_F is large for fixed finite U, simply because v_F is proportional to n for small n, such that neglected higher order terms become important. Note, for comparison, that for spinless fermions with a fixed nearest-neighbor interaction the bare dimensionless coupling at the Fermi level vanishes in the low-density limit.

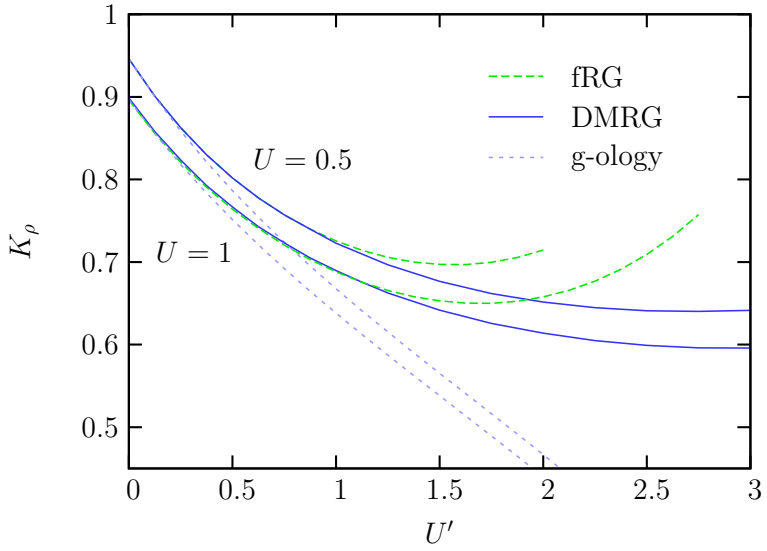

Figure 4.7: *Luttinger-liquid parameter K_ρ for the quarter-filled extended Hubbard model as a function of U' for $U = 0.5$ and 1; results from the fRG are compared to DMRG data and to results from a one-loop g-ology calculation.*

For the extended Hubbard model Fig. 4.7 shows a comparison of fRG results for K_ρ to DMRG data [Ejima et al. 2005]. The fRG results are exact to second order in the interaction and are thus very accurate for weak U and U'. Results from a standard one-loop g-ology calculation as described in Sec. A.2 deviate quite strongly already for $U' > 0.5$. In the g-ology approach interaction processes are classified into backward scattering ($g_{1\perp}$), forward scattering involving electrons from opposite Fermi points ($g_{2\perp}$), from the same Fermi points ($g_{4\perp}$), and umklapp scattering ($g_{3\perp}$). All further momentum dependences of the vertex are discarded. This is justified by the irrelevance of these momentum dependences in the low-energy limit, but leads to

deviations from the exact flow at finite scales, and therefore to less accurate results for the fixed-point couplings.

The flow of $g_{i\perp}^{\Lambda}$, $i = 1, ..., 4$, is plotted in Fig. 4.8, in the upper panel for the quarter-filled Hubbard model with bare interaction $U = 1$, and for the extended Hubbard model with $U' = U/\sqrt{2}$ in the lower. The fRG result is compared to the result from a one-loop g-ology calculation. The backscattering coupling $g_{1\perp}$ vanishes logarithmically in both cases, as expected for the Luttinger-liquid fixed point [Voit 1995]. For the pure Hubbard model the good agreement with g-ology results stems from the purely local interaction in real space, since in that case pronounced momentum dependences of the vertex develop only in the low-energy regime where the g-ology parametrization is a good approximation. By contrast, for the extended Hubbard model momentum dependences of the vertex which are not captured by the g-ology classification (except for small Λ) are obviously more important. A generalization of the g-ology parametrization of the vertex to higher dimensions, which amounts to neglecting the momentum dependence normal to the Fermi surface, is frequently used in one-loop fRG calculations in two dimensions [Halboth and Metzner 2000; Zanchi and Schulz 2000; Honerkamp et al. 2001; Kampf and Katanin 2003]. The above comparison indicates that this parametrization works well for the pure Hubbard model, but could be improved for models with nonlocal interactions. The parametrization of the vertex by an effective short-range interaction used here could be easily extended to higher dimensions, where it will probably yield more accurate results, too. The relevance of an improved parametrization of the vertex beyond the conventional g-ology classification has also been demonstrated in a recent fRG analysis of the phase diagram of the half-filled extended Hubbard model [Tam et al. 2005].

The inclusion of the momentum dependence due to the nearest-neighbor interaction component in real space on the right-hand side of the flow equation for the two-particle vertex modifies the flow of the couplings at intermediate scales, before reaching the regime where a g-ology description at weak coupling applies. A small repulsive initial backscattering amplitude may renormalize to an effective *attractive* one. For negative $g_{1\perp}$ the renormalization group scales to strong coupling, indicating an instability of the model towards a different ground state characterized by a gap in the spin excitation spectrum [Voit 1995]. In Fig. 4.9 the phase boundary for the Luttinger liquid and spin gap is shown as a function of n and U', as obtained from the fRG together with the result from a one-loop g-ology calculation. The fRG

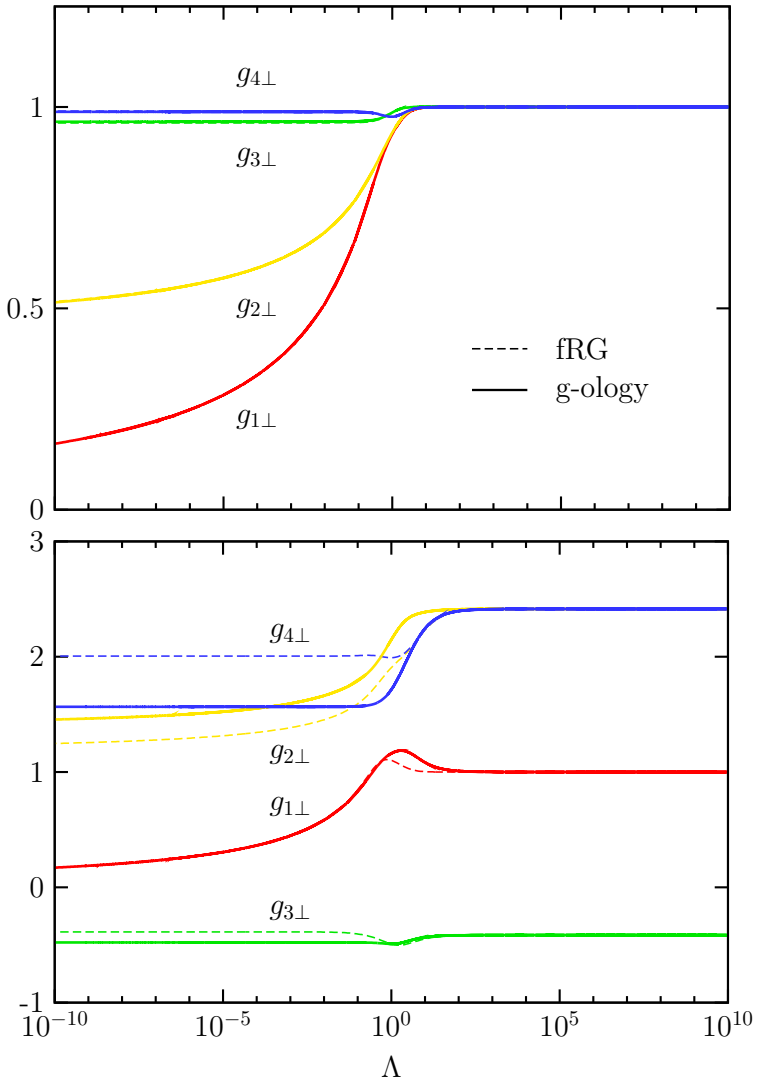

Figure 4.8: *Flow of vertex on the Fermi points (in g-ology notation) at quarter filling and* $U = 1$*;* upper panel*: Hubbard model,* lower panel*: extended Hubbard model with* $U' = U/\sqrt{2}$*; the fRG flow is compared to the one-loop g-ology flow; note that in the upper panel fRG and g-ology results almost coincide.*

results confirm the spin gap phase at low densities found with numerical Quantum Monte Carlo methods [Clay et al. 1999], where the spin gap develops with increasing U' from $U' = 0$. At low densities and close to half filling the truncated fRG results are not meaningful, since renormalization towards strong coupling occurs in these limits and neglected higher order terms become important, see also Fig. 4.6.

Close to half filling the spin gap opens with increasing U' from $U' = U/2$, as for the one-loop g-ology calculation. A full functional implementation of the momentum dependence of the two-particle vertex would allow a more detailed analysis of the phase diagram.

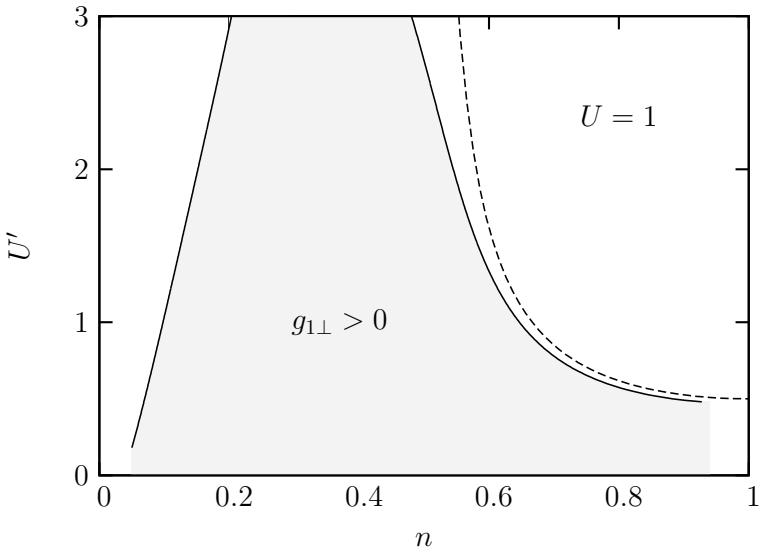

Figure 4.9: *Phase boundary between the Luttinger liquid ($g_{1\perp} > 0$) and spin gap phase ($g_{1\perp} < 0$) for the extended Hubbard model as a function of n and U' for $U = 1$; results from the fRG (solid lines) are compared to results from a one-loop g-ology calculation (dashed line).*

4.4 Observables

In the next section we will present results for spectral properties of single-particle excitations near an impurity or boundary, the density profile and the linear conductance. Here we describe how the relevant observables are computed from the solution of the flow equations.

4.4.1 Single-particle excitations

Integrating the flow equation for the self-energy Σ^Λ down to $\Lambda = 0$ yields the physical (cutoff-free) self-energy Σ and the single-particle propagator $G = (G_0^{-1} - \Sigma)^{-1}$. From the latter spectral properties of single-particle excitations can be extracted. We focus

on local spectral properties, which are described by the *local spectral function*

$$\rho_j(\omega) = -\frac{1}{\pi} \operatorname{Im} G_{jj}(\omega + i0^+) \;, \tag{4.74}$$

where $G_{jj}(\omega + i0^+)$ is the local propagator, analytically continued to the real frequency axis from above.

In our approximation the self-energy is frequency independent and can therefore be viewed as an effective single-particle potential. The propagator G is thus the Green function of an effective single-particle Hamiltonian. In real space representation this Hamiltonian is given by the tridiagonal matrix $h_{\text{eff}} = h_0 + \Sigma$, where the matrix elements of h_0 are the hopping amplitudes in H_0, Eq. (4.2). For a lattice with L sites this matrix has L (including possible multiplicities) eigenvalues ϵ_λ and an orthonormal set of corresponding eigenvectors ψ_λ. For the spectral function $\rho_j(\omega)$ one thus obtains a sum of δ peaks

$$\rho_j(\omega) = \sum_\lambda w_{\lambda j}\, \delta(\omega - \xi_\lambda) \;, \tag{4.75}$$

where $\xi_\lambda = \epsilon_\lambda - \mu$, and the *spectral weight* $w_{\lambda j}$ is the squared modulus of the amplitude of ψ_λ on site j. For large L the level spacing between neighboring eigenvalues is usually of order L^{-1}, except for one or a few levels outside the band edges which correspond to bound states.

Due to even-odd effects etc. the spectral weight $w_{\lambda j}$ generally varies quickly from one eigenvalue to the next one. A smooth function of ω which suppresses these usually irrelevant finite-size details can be obtained by averaging over neighboring eigenvalues. In addition, dividing the spectral weight $w_{\lambda j}$ by the level spacing between eigenvalues yields the local *density of states*, which we denote by $D_j(\omega)$.

4.4.2 Density profile

Boundaries or impurities induce a density profile with long-range Friedel oscillations, which are expected to decay with a power law at long distances [Egger and Grabert 1995]. The expectation value of the local density n_j could be computed from the local one-particle propagator G_{jj}, if G was known exactly. However, the approximate flow equations for Σ can be expected to describe the asymptotic behavior of G correctly only at long distances between creation and annihilation operator in time and/or space, while in the local density operator time and space variables coincide. In the

standard renormalization-group terminology n_j is a *composite* operator, which has to be renormalized separately [Zinn-Justin 2002].

The flow equation for n_j^Λ can be derived by computing the shift of the grand canonical potential Ω^Λ generated by a small field ϕ_j coupled to the local density. Alternatively to the numerical differentiation one may carry out the ϕ_j derivative analytically in the flow equations, which yields a flow equation for the density in terms of the density response vertex. The general structure at $T = 0$ is described in Refs. [Andergassen et al. 2004; Enss 2005]; the final form of the flow equation for the density is

$$\frac{\partial}{\partial\Lambda} n_j^\Lambda = -\frac{1}{2\pi} \sum_{\omega=\pm\Lambda} \mathrm{tr}\left[e^{i\omega 0^+} \tilde{G}^\Lambda(i\omega)\, R_j^\Lambda(i\omega) \right] , \tag{4.76}$$

with the density response vertex given by

$$\frac{\partial}{\partial\Lambda} R^\Lambda_{j;1',1} = -\frac{1}{2\pi} \sum_{\omega=\pm\Lambda} \sum_{2,2'} \sum_{3,3'} \tilde{G}^\Lambda_{2,3}(i\omega)\, R^\Lambda_{j;3,3'}\, \tilde{G}^\Lambda_{3',2'}(i\omega)\, \Gamma^\Lambda_{1',2';1,2} . \tag{4.77}$$

Note that within the approximate treatment of the two-particle vertex described in Sec. 4.2.2, the density-response vertex is frequency independent.

For Γ^Λ parametrized by local and nearest-neighbor interactions in real space, the matrix R_j^Λ is tridiagonal, that is, only the components $R^\Lambda_{j;3,3}$ and $R^\Lambda_{j;3,3\pm1}$ are nonzero. The initial condition for the density is $n_j^{\Lambda_0} = \frac{1}{2}$ for any filling, due to the slow convergence of the flow equation (4.76) at large frequencies, which yields a finite contribution to the integrated flow from $\Lambda = \infty$ to Λ_0 for arbitrarily large finite Λ_0, as in the case of the self-energy discussed in more detail in Sec. 4.2.2. The initial condition for the response vertex is $R^{\Lambda_0}_{j;l,l'} = \delta_{jl}\delta_{ll'}$.

To avoid the interference of Friedel oscillations emerging from the impurity or one boundary with those coming from the (other) boundaries of our systems we suppress the influence of the latter by coupling the finite chain to semi-infinite noninteracting leads, with a smooth decay of the interaction at the contacts, as described in detail in the next section.

4.4.3 Conductance

For the calculation of the conductance G a finite interacting chain (with sites $1, \ldots, L$) is coupled to noninteracting leads at both ends, corresponding to an experimental setup where the Luttinger-liquid wires are connected to (higher dimensional) Fermi-liquid leads. Using a projection method the system with leads can

be reduced to an effective L-site problem [Taylor 1972]. The leads are modeled by a one-dimensional tight-binding lattice with nearest-neighbor hopping amplitude t. The influence of the leads on the interacting chain can be taken into account by an additional dynamical boundary potential

$$V_j^{\mathrm{lead}}(i\omega_n) = \frac{i\omega_n + \mu_0}{2}\left(1 - \sqrt{1 - \frac{4}{(i\omega_n + \mu_0)^2}}\right)(\delta_{1,j} + \delta_{L,j}) \tag{4.78}$$

in the bare propagator G_0 of the interacting chain [Enss et al. 2005]. The parameter μ_0 is the chemical potential, which is related to the density n in the leads by $\mu_0 = -2\cos k_F$. Uncontrolled conductance drops due to scattering at the contacts between leads and the interacting part of the chain can be avoided by switching off the interaction potential smoothly near the contacts. As long as the switching on of the interaction is smooth enough and the bulk part of the wire is large compared to the switching region, the results are independent of the microscopic details of this procedure. In addition, interaction-induced bulk shifts of the density have to be compensated by a suitable bulk potential [Enss et al. 2005].

In linear response the conductance is computed via the Kubo formula from the current-current correlation function [Mahan 2000]. Within our approximation scheme the self-energy has no imaginary part, which implies that there are no vertex corrections [Oguri 2001]. In this approximation the Kubo formula reduces to the Landauer-Büttiker formula [Datta 1995], relating the transmission probability directly to the linear conductance $G(T, L)$ of noninteracting fermions. For a detailed derivation we refer to Refs. [Enss et al. 2005; Enss 2005]; the final expression for the conductance is given by

$$G(T, L) = -z\,\frac{e^2}{h}\int_{-2-\mu_0}^{2-\mu_0} |t(\varepsilon, T, L)|^2\, f'(\varepsilon)\, d\varepsilon\ , \tag{4.79}$$

with $|t(\varepsilon, T, L)|^2 = [4 - (\mu_0 + \varepsilon)^2]|G_{1,L}(\varepsilon, T)|^2$, and f the Fermi function; z is the number of spin components.

5 Solution of fRG equations and results

In this section we present results for the local density of states near boundaries and impurities, the density profile, and the linear conductance for the spinless fermion model and the extended Hubbard model, as obtained from the solution of the fRG flow equations. A comparison with exact DMRG data is made for those observables and system sizes for which such data could be obtained. The asymptotic low-energy behavior for weak and intermediate impurity strengths is approached only at rather low energy scales, accessible only for very large systems. For spin-$\frac{1}{2}$ systems two-particle backscattering leads to striking effects, which are not captured if the bulk system is approximated by its low-energy fixed point, the Luttinger model. In particular, the expected decrease of spectral weight near the impurity and of the conductance at low energy scales is often preceded by a pronounced increase, and the asymptotic power laws are modified by logarithmic corrections.

5.1 Spinless fermions

5.1.1 Effective impurity potential

The typical shape of the self-energy representing the effective impurity potential can be seen in Fig. 5.1, where we plot the diagonal elements $\Sigma_{j,j}$ and the off-diagonal elements $\Sigma_{j,j+1}$ near a site impurity of strength $V = 1.5$ added to the spinless fermion model with interaction strength $U = 1$ at quarter filling. Recall that the self-energy is tridiagonal in real space and frequency independent within our treatment. The diagonal elements can be interpreted as a local effective potential, the off-diagonal elements as a nonlocal effective potential which renormalizes the hopping

amplitudes. At long distances from the impurity both $\Sigma_{j,j}$ and $\Sigma_{j,j+1}$ tend to a constant. The former describes just a bulk shift of the chemical potential, the latter a bulk renormalization of the hopping amplitude toward larger values. The oscillations around the bulk shifts are generated by the impurity. The wave number of the oscillations is $2k_F = \pi/2$, where k_F is the Fermi wave vector of the bulk system at quarter filling. Fig. 5.2 shows $\Sigma^{\Lambda}_{j_0,j_0}$ for a site impurity of strength $V = 1.5$ as a function of Λ for different system sizes L. For finite L the flow is effectively cut off on a scale $\sim 1/L$, a sequence of L provides an extrapolation to the thermodynamic limit. The renormalized potential at the impurity site remains *finite* in the limit $L \to \infty$, while the Fourier transform $\Sigma^{\Lambda}_{k,k'}$ for momenta with $k - k' = \pm 2k_F$ diverges. Similarly for a hopping impurity the effective amplitude does not scale to zero in the limit $L \to \infty$, and the weak-link behavior is associated to the long-range oscillations in real space. The straight line in a log-log plot of the difference between the asymptotic value $\Sigma^0_{j_0,j_0}(L = \infty)$ and $\Sigma^0_{j_0,j_0}(L)$ shown in the inset indicates a power law dependence.

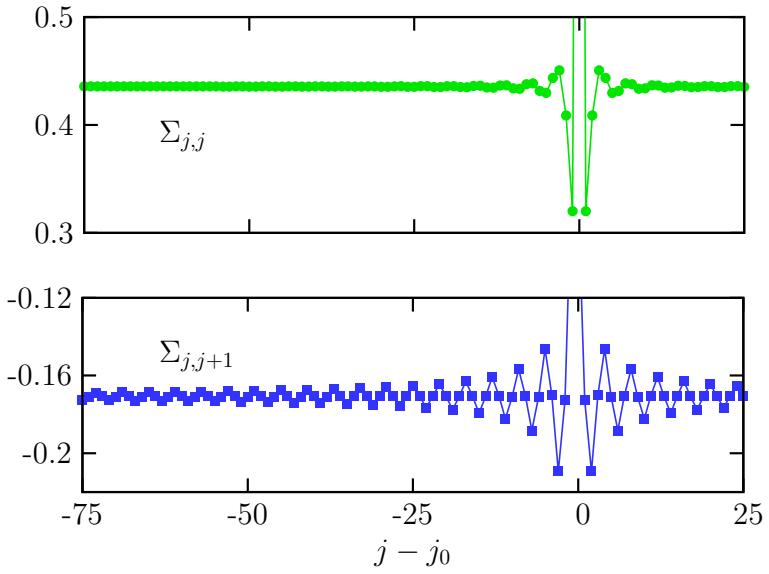

Figure 5.1: *Self-energy near a site impurity of strength* $V = 1.5$ *for the spinless fermion model at quarter filling and interaction strength* $U = 1$*; the impurity is situated at the center of a chain with* $L = 1025$ *sites.*

The amplitude of the oscillations generated by an impurity in Σ decays slower than the inverse distance from the impurity at intermediate length scales, but approaches a decay proportional to $1/|j - j_0|$ for $|j - j_0| \to \infty$. This can be seen most

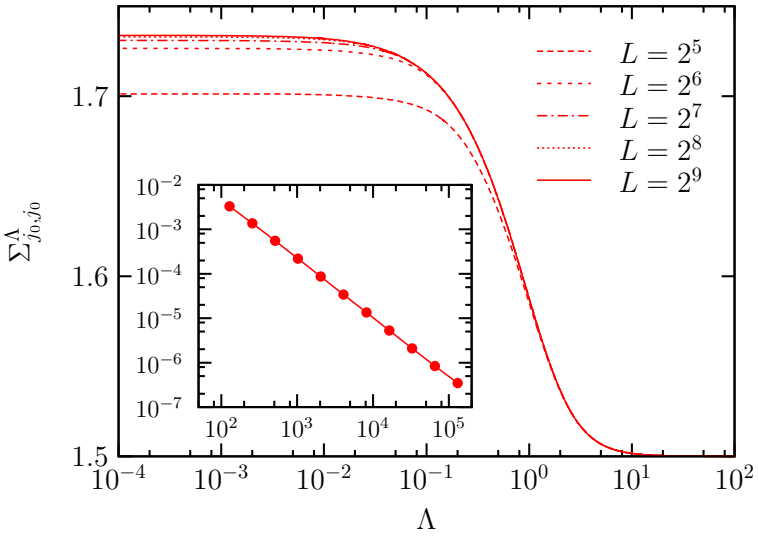

Figure 5.2: $\Sigma^{\Lambda}_{j_0,j_0}$ *as a function of* Λ *for a site impurity of strength* $V = 1.5$ *for spinless fermions at half filling and* $U = 1$*; the impurity is situated at the center of a chain of length* L*; the inset shows the difference from the asymptotic value* $\Sigma^{0}_{j_0,j_0}(\infty) - \Sigma^{0}_{j_0,j_0}(L)$ *as a function of* L*.*

clearly by plotting an effective exponent β_j for the decay of the oscillations, defined as the negative logarithmic derivative of the oscillation amplitude with respect to the distance $|j - j_0|$. In Fig. 5.3 we show the effective exponent resulting from the oscillations of $\Sigma_{j,j}$ as a function of the distance from a site impurity, for $U = 1$ and half filling. The impurity is situated at the center of a long chain with $L = 2^{18} + 1$ sites. To avoid interferences with oscillations from the boundaries we have attached semi-infinite noninteracting leads to the ends of the interacting chain, as described in Sec. 4.4.3. Only for relatively large impurity strengths the asymptotic regime corresponding to $\beta_j = 1$ is reached before finite-size effects set in. For small V one can see that β_j increases from values below one, but the asymptotic long-distance behavior is cut off by the boundaries of the interacting region. For very small V (for example $V = 0.01$ in Fig. 5.3) we observe a plateau in β_j for intermediate distances from the impurity site. In this regime β_j is close to K_ρ which can be understood by analytically solving the flow equations for small V [Meden et al. 2002a,b].

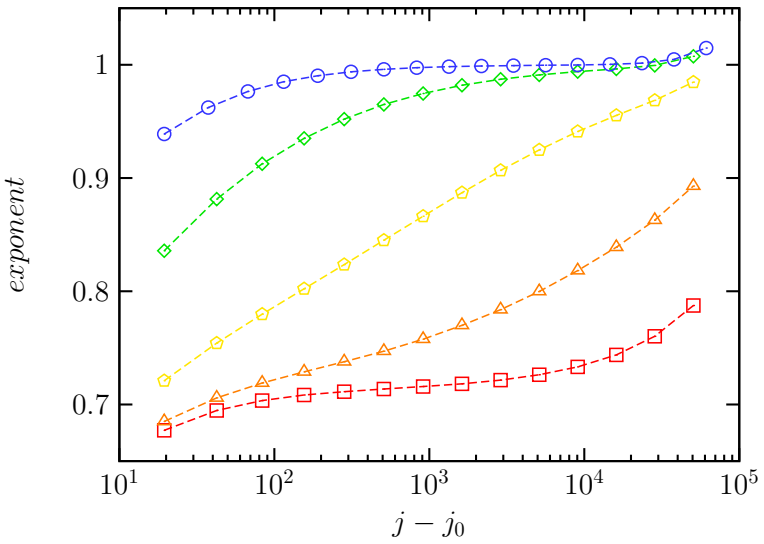

Figure 5.3: *Effective exponent for the decay of oscillations of* $\Sigma_{j,j}$ *as a function of the distance from a site impurity of strengths* $V = 0.01$, 0.1, 0.3, 1, 10 *(from bottom to top), for the spinless fermion model at half filling and interaction strength* $U = 1$*; the impurity is situated at the center of a chain with* $L = 2^{18} + 1$ *sites.*

5.1.2 Local density of states

The long-range $2k_F$-oscillations of the self-energy lead to a marked suppression of the spectral weight for single-particle excitations at the Fermi level, that is, at $\omega = 0$. In Fig. 5.4 we show the local density of states $D_j(\omega)$ on the site next to a site impurity of strength $V = 1.5$ for the spinless fermion model at half filling. The result for the interacting system at $U = 1$ is compared to the noninteracting case. Even-odd effects have been eliminated by averaging over neighboring eigenvalues (cf. Sec. 4.4.1). δ peaks outside the band edges corresponding to bound states are not plotted. The interaction leads to a global broadening of the band, which is due to an enhancement of the bulk hopping amplitude, and also to a strong suppression of $D_j(\omega)$ at low frequencies which is not present in the noninteracting system. For a finite system (here $L = 1025$) the spectral weight at the Fermi level remains finite, but tends to zero with increasing system size. In Fig. 5.5 we show results for the density of states choosing the same parameters as in Fig. 5.4, but now for densities away from half filling: $n = 1/4$ and $n = 3/4$. In addition to the dip near $\omega = 0$ a second singularity appears at a finite frequency. This effect is due to the fact that a long-range potential with a wave number $2k_F$ does not only strongly

scatter states with momenta near k_F, but also those with momenta close to $\pi - k_F$. Indeed the singularity is situated at $\omega = \epsilon_{\pi-k_F} - \mu$, where ϵ_k is the renormalized (bulk) dispersion. In the half-filled case only one singularity is seen simply because $\pi - k_F = k_F$ for $k_F = \pi/2$.

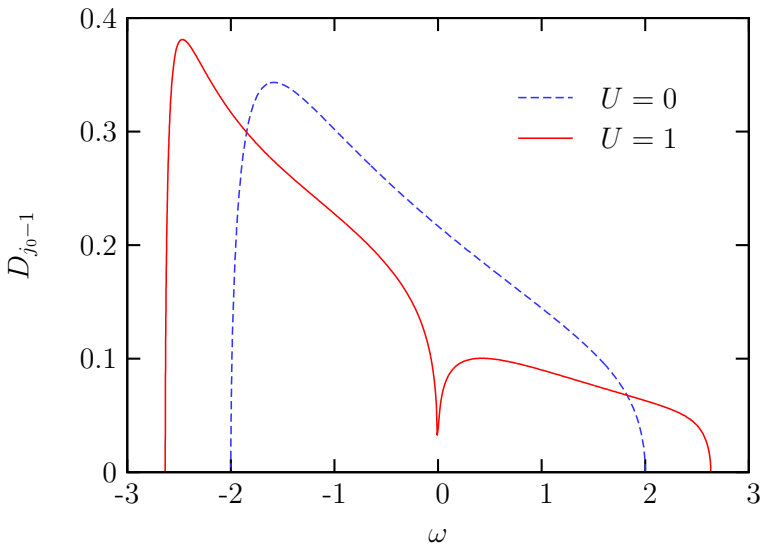

Figure 5.4: *Local density of states on the site next to a site impurity of strength* $V = 1.5$ *for spinless fermions at half filling and* $U = 1$*; the impurity is situated at the center of a chain with* 1025 *sites; the noninteracting case* $U = 0$ *is shown for comparison.*

Similar results are found for a hopping impurity, shown in Fig. 5.6. For an attractive interaction the density of states is strongly enhanced at the Fermi level. For comparison, typical results for the local density of states at a boundary are presented in Fig. 5.7.

The spectral weight at the Fermi level is expected to vanish asymptotically as a power law $|\omega|^{\alpha_B}$, where

$$\alpha_B = \frac{1}{K_\rho} - 1 \tag{5.1}$$

is the *boundary exponent* describing the power-law suppression of the density of states at the boundary of a semi-infinite chain with repulsive interactions [Kane and Fisher 1992b]. That exponent depends only on the bulk parameters of the model, not on the impurity strength. For the spinless fermion model it can be computed exactly from the Bethe ansatz solution [Haldane 1980].

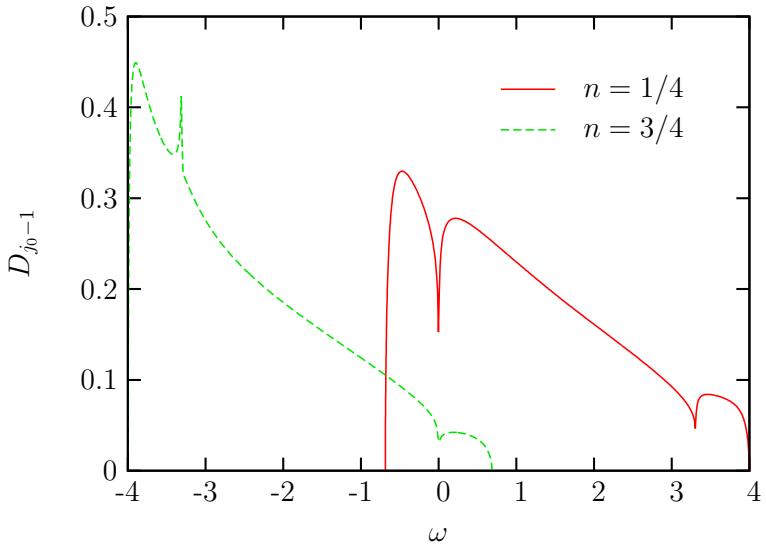

Figure 5.5: *Local density of states on the site next to a site impurity as in Fig. 5.4 (same parameters), but now for densities* $n = 1/4$ *and* $3/4$.

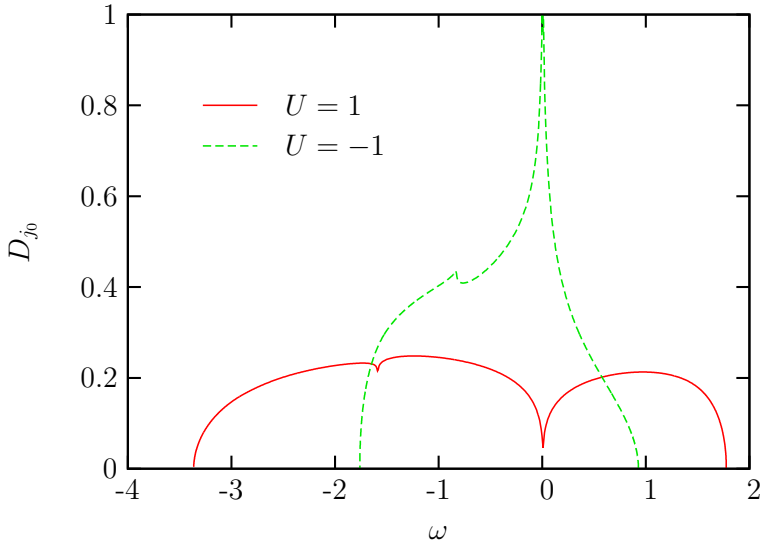

Figure 5.6: *Local density of states on the site next to a hopping impurity* $t' = 0.25$ *for spinless fermions at density* $n = 0.6$ *and* $U = 1$*; the impurity is situated at the center of a chain with* 1024 *sites; the attractive case* $U = -1$ *is shown for comparison.*

In the above figures the envelope of the δ peaks of weight w characterizing the spectral function of a finite system size introduced in Sec. 4.4.1 is shown. As a consequence the energy range over which a power-law suppression is observed is

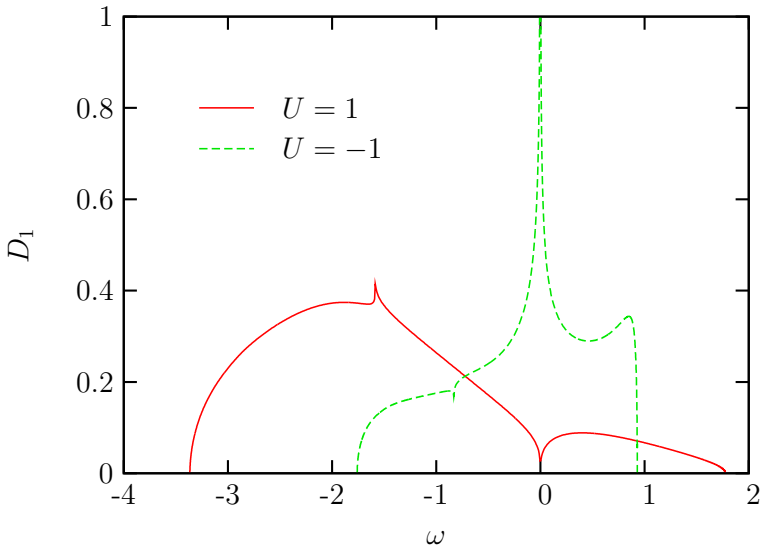

Figure 5.7: *Local density of states at the boundary, for the same parameters as in Fig. 5.6.*

cut off by the finite size of the system at low energies. For a reliable analysis of the exponential behavior it is more convenient to consider the finite-size scaling of the spectral weight at the chemical potential. The large L dependence of the spectral weight is expected to exhibit a power law with the same exponent, and the scale where the power-law behavior sets in is given by $L \sim \omega/\pi v_F$. In Fig. 5.8 the spectral weight at a boundary of a half-filled chain of length $L = 10^6$ and different interaction strengths U is shown as a function of ω. The straight line in a log-log plot corresponds to a power law. Results for the same density and interaction parameters, but now as a function of system size L are presented in Fig. 5.9. Within the extension to finite temperatures (cf. Sec. 4.2.5), the same power-law behavior is found as a function of temperature, a detailed analysis in the context of transport phenomena follows below.

We now analyze the asymptotic behavior of the spectral weight at the Fermi level by defining an effective exponent $\alpha(L)$ as the negative logarithmic derivative of the spectral weight with respect to the system size, such that $\alpha(L)$ tends to a (positive) constant in case of a power law suppression. In Fig. 5.10 we show results for $\alpha(L)$ as obtained from the fRG for the spinless fermion model at quarter filling with up to about 10^6 sites, for a weak ($U = 0.5$) and an intermediate ($U = 1.5$) interaction parameter. The spectral weight has been computed either at a bound-

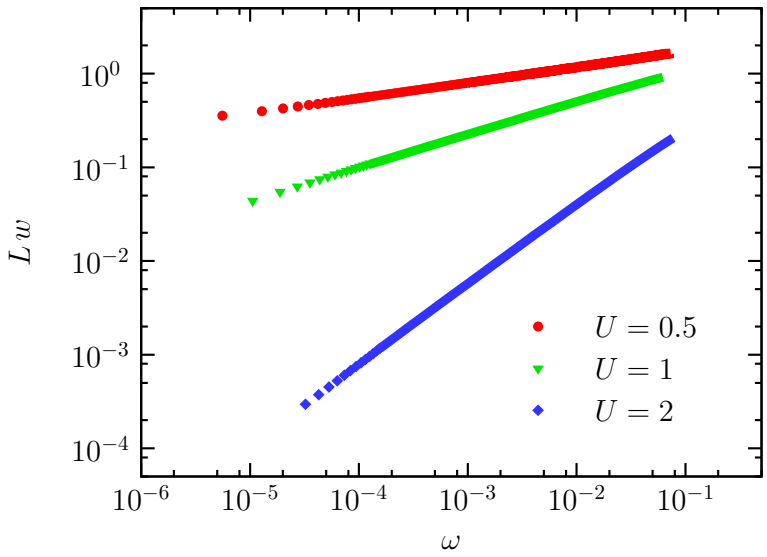

Figure 5.8: *Spectral weight at a boundary as a function of ω for the spinless fermion model at half filling, $L = 10^6$ and different interaction strengths U.*

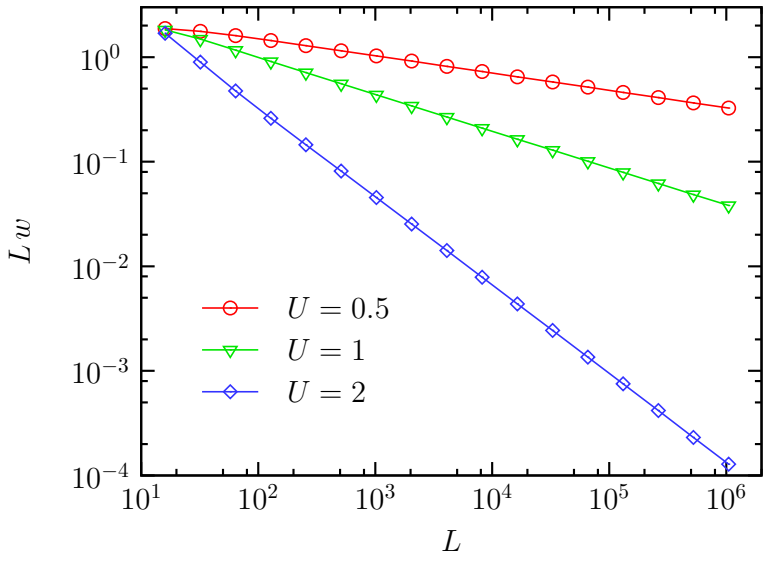

Figure 5.9: *Spectral weight at the Fermi level as a function of system size L, for the same parameters as in Fig. 5.8.*

ary, or near a hopping impurity of strength $t' = 0.5$. Results obtained from the fRG without (upper panel) and with (lower panel) vertex renormalization, corresponding to Scheme I and Scheme II introduced in Sec. 4.2.2, are compared to exact numerical DMRG results (for up to 512 sites) and the exact boundary exponents

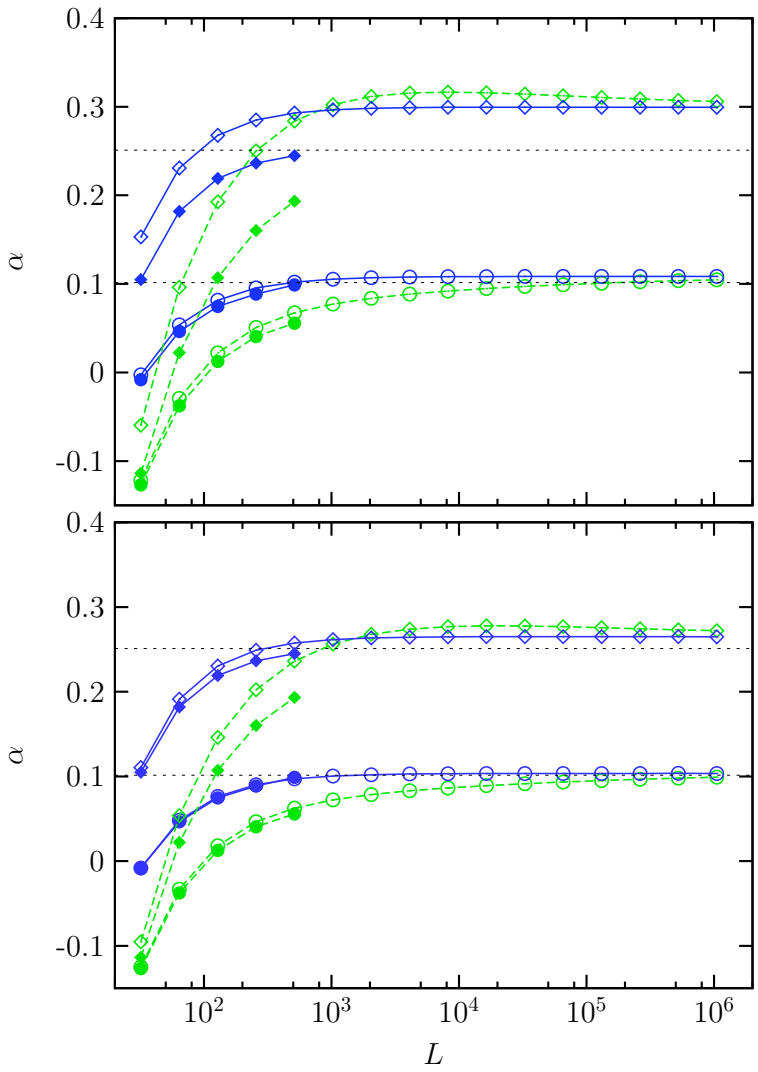

Figure 5.10: *Logarithmic derivative of the spectral weight at the Fermi level near a boundary (solid lines) or hopping impurity (dashed lines) as a function of system size L, for spinless fermions at quarter filling and interaction strength $U = 0.5$ (circles) or $U = 1.5$ (squares);* upper panel*: without vertex renormalization,* lower panel*: with vertex renormalization; the open symbols are fRG, the filled symbols DMRG results; the horizontal lines represent the exact boundary exponents for $U = 0.5$ and 1.5.; in the boundary case (solid lines) the spectral weight has been taken on the first site of a homogeneous chain, in the impurity case (dashed lines) on one of the two sites next to a hopping impurity $t' = 0.5$ in the center of the chain.*

α_B, plotted as horizontal lines. The fRG results follow a power law for large L, with the same asymptotic exponent for the boundary and impurity case, confirming thus the expected universality. However, the asymptotic regime is reached only for fairly large systems, even for the intermediate interaction strength $U = 1.5$. For the fRG Scheme I developed previously for impurities in spinless Luttinger liquids the effects of a single static impurity in a spinless Luttinger liquid are fully captured qualitatively, and in the weak-coupling limit also quantitatively. Originally developed for the analysis of spectral densities of single-particle excitations, this scheme has been applied recently also to transport problems, such as persistent currents in mesoscopic rings and the conductance of interacting wires connected to noninteracting leads [Meden et al. 2003; Meden and Schollwöck 2003a,b]. The comparison with the exact DMRG results and exact exponents shows that the fRG Scheme II is also quantitatively rather accurate, and that the inclusion of vertex renormalization leads to a substantial improvement at intermediate coupling strength.

A quantitative estimate of the accuracy of the exponents can be obtained from a comparison to exact results from the Bethe ansatz solution of the spinless fermion model [Haldane 1980] shown in Fig. 5.11. The results obtained without vertex renormalization (Scheme I) are represented with open symbols. The fRG results are correct to first order in the interaction U. In the approximate treatment of the two-particle vertex (cf. Sec. 4.2.2) terms of order U^2 are only partially included, and an agreement to higher order can not be expected. Nevertheless the quantitative accuracy is improved considerably. The n dependence of the accuracy is related to the different importance of the vertex renormalization for different densities, as can be seen in Fig. 4.3. For half filling the vertex renormalization leads to a pronounced increase of the renormalized interaction, whereas for smaller fillings the effect is smaller, eventually leading to a decrease for $n \lesssim 1/3$.

Results for the effective exponent α in the case of a site impurity are shown in Fig. 5.12, at quarter filling and for an interaction strength $U = 1$. The comparison of the different curves obtained for different impurity strengths confirms once again the expected asymptotic universality, and also how the asymptotic regime shifts rapidly toward larger systems as the bare impurity strength decreases. The crossover scale depends on the bare impurity strength V as [Kane and Fisher 1992a,c; Fendley et al. 1995]

$$\frac{1}{L_c} \sim \left(\frac{V}{\pi v_F}\right)^{\frac{1}{1-K_\rho}} , \tag{5.2}$$

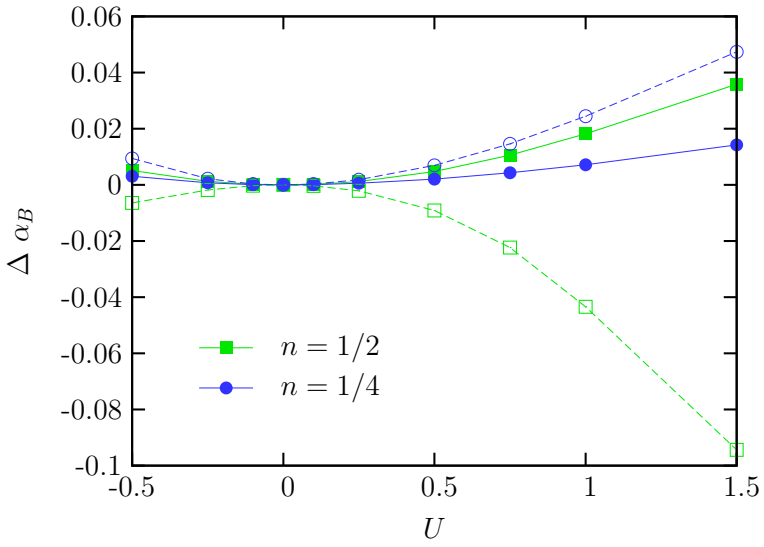

Figure 5.11: *Difference between the fRG result and the exact Bethe ansatz result for the boundary exponent α_B as a function of U, at densities $n = 1/2$ and $1/4$ for the spinless fermion model as obtained from the power-law suppression of the spectral weight at the boundary; the open symbols are results without vertex renormalization, the filled symbols results with vertex renormalization.*

in agreement with our findings. The scale on which the impurity flows to strong coupling depends on the initial strength V and the "flow velocity" given by $1 - K_\rho$. The effective flowing impurity strength can be estimated by

$$V_{\text{eff}} \sim V L^{1-K_\rho} \,, \tag{5.3}$$

where the crossover scale L_c in Eq. (5.2) corresponds to $V_{\text{eff}} \sim \pi v_F$. Note that for weak impurities and intermediate system sizes the spectral weight follows a power law corresponding to the bulk behavior, and approaches the boundary exponent only at large distances. The bulk suppression of the spectral weight described by the anomalous dimension $\alpha = (K_\rho + K_\rho^{-1} - 2)/2$ is not captured within the present scheme, since the self-energy is frequency independent. In the 1PI version of the fRG the frequency dependence is generated by the two-particle vertex. The anomalous dimension could be included in an improved scheme by an iterative solution of the fRG flow inserting the two-particle vertex into the flow equation for the self-energy without neglecting its frequency dependence. This gives a two-loop diagram including the full two-particle vertex functions at scale Λ. The right-hand side of the differential equation for the self-energy is then nonlocal in Λ: the change of

the two-particle vertex and self-energy at scale Λ involves two-particle vertices and self-energies at scales $\Lambda \geq \Lambda'$. In presence of sufficiently strong effective impurity potentials however, the boundary behavior prevails over the bulk suppression of the spectral weight, as $\alpha_B \sim U$ and $\alpha \sim U^2$.

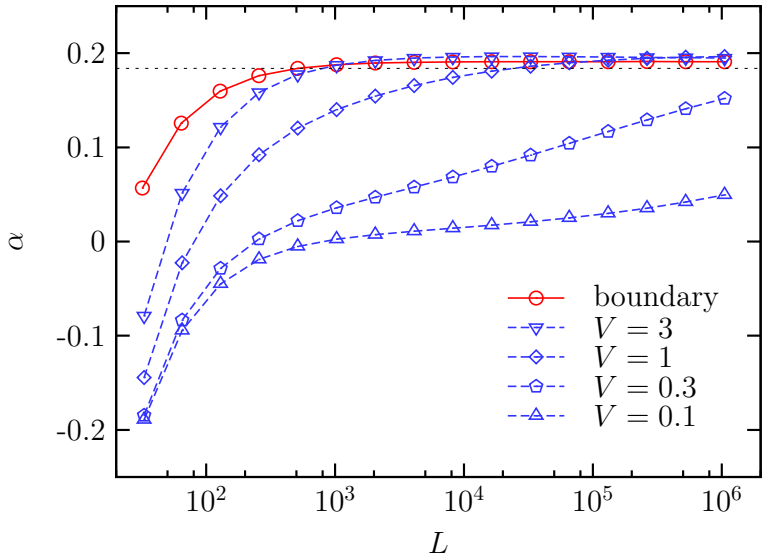

Figure 5.12: *Logarithmic derivative of the spectral weight at the Fermi level near a boundary (solid line) or site impurity (dashed lines) as a function of system size L, for spinless fermions at quarter filling and interaction strength $U = 1$; in the boundary case the spectral weight has been taken on the first site of a homogeneous chain, in the impurity case on the site next to a site impurity of strength V in the center of the chain; the horizontal line represents the exact boundary exponent for $U = 1$.*

5.1.3 Friedel oscillations

We now discuss results for the density profile n_j. Boundaries and impurities induce Friedel oscillations of the local density with a wave vector $2k_F$. In a noninteracting system these oscillations decay proportionally to the inverse distance from the boundary or impurity. In an interacting Luttinger liquid the Friedel oscillations are expected to decay as $|j - j_0|^{-K_\rho}$ at long distances $|j - j_0|$. For a very weak impurity one expects a slower decay proportional to $|j - j_0|^{1-2K_\rho}$ at intermediate distances, and a crossover to the asymptotic power law with exponent K_ρ at very long distances [Egger and Grabert 1995]. At intermediate distances the response of

the density to a weak impurity can be treated in linear response theory, such that the density modulation is determined by the density-density response function at $2k_F$, which leads to the power-law decay with exponent $2K_\rho - 1$.

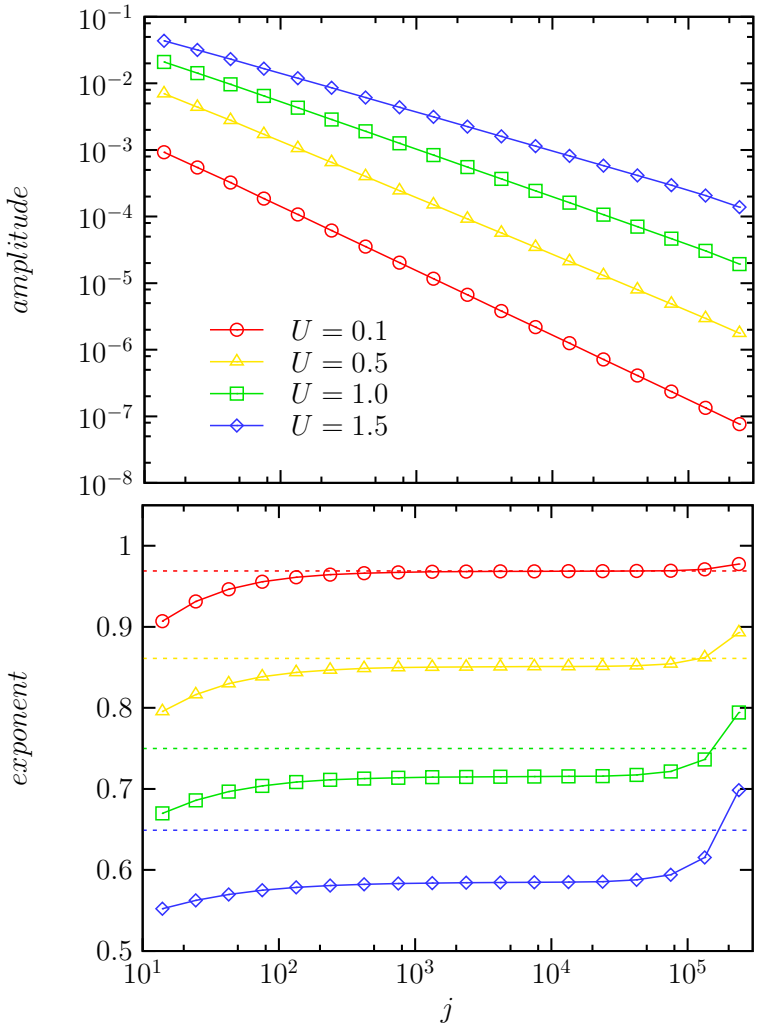

Figure 5.13: *Amplitude (envelope) of oscillations of the density profile n_j induced by a boundary as a function of the distance from the boundary, for spinless fermions with various interaction strengths U at half filling; the interacting chain with $2^{19}+1$ sites is coupled to a semi-infinite noninteracting lead at the end opposite to the boundary;* upper panel*: log-log plot of the amplitude,* lower panel*: effective exponents for the decay, and the exact asymptotic exponents as horizontal lines.*

We analyze the long-distance behavior of the amplitudes more closely for the half-filled case, and compare to exact results for the asymptotic exponents. For

incommensurate filling factors the density profile looks more complicated, but at long distances from the boundary the oscillation amplitude has a well-defined envelope which exhibits a power law as a function of j. In Fig. 5.13 we show fRG results for the amplitude of density oscillations emerging from an open boundary, for a very long spinless fermion chain with $2^{19}+1$ sites and various interaction strengths U. The end opposite to the open boundary is smoothly connected to a noninteracting lead. In a log-log plot (upper panel of Fig. 5.13) the amplitude follows a straight line for almost all j, corresponding to a power-law dependence. Deviations from a perfect power law can be seen more neatly by plotting the effective exponent α_j, defined as the negative logarithmic derivative of the amplitude with respect to j (see the lower panel of Fig. 5.13). The effective exponent is almost constant except at very short distances or when j approaches the opposite end of the interacting chain, which is not surprising. From a comparison with the exact exponent (horizontal lines in the figure) one can assess the quantitative accuracy of the fRG results.

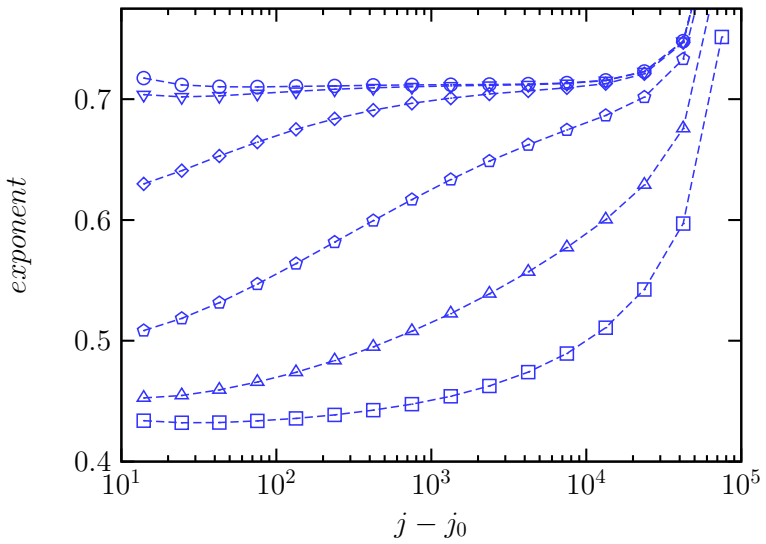

Figure 5.14: *Effective exponent for the decay of density oscillations as a function of the distance from a site impurity of strengths* $V = 0.01, 0.1, 0.3, 1, 3, 10$ *(from bottom to top); the impurity is situated at the center of a spinless fermion chain with* $2^{18}+1$ *sites and interaction strength* $U = 1$ *at half filling; the interacting chain is coupled to semi-infinite noninteracting leads at both ends.*

Effective exponents describing the decay of Friedel oscillations generated by site impurities of various strengths are shown in Fig. 5.14, for a half-filled spinless fermion

chain with $2^{18}+1$ sites and interaction $U = 1$. Both ends of the interacting chains are coupled to noninteracting leads to suppress oscillations coming from the boundaries. For strong impurities the results are close to the boundary result (cf. Fig. 5.13), as expected. For weaker impurities the oscillations decay more slowly, that is, with a smaller exponent, and approach the boundary behavior only asymptotically at large distances (beyond the range of our chain for $V < 1$). For very weak impurities ($V = 0.01$ in Fig. 5.14) the oscillation amplitude follows a power law corresponding to the linear response behavior with exponent $2K_\rho - 1$ at intermediate distances. Similar results are obtained for attractive interactions [Andergassen et al. 2004].

A comparison with the exact exponents from the Bethe ansatz solution of the spinless fermion model [Haldane 1980] is shown in Fig. 5.15, where the difference ΔK_ρ is reported as a function of the interaction U at densities $n = 1/2$ and $n = 1/4$. The open symbols represent the accuracy for the weak-impurity behavior in the linear response regime and the filled ones for the asymptotic exponent for strong impurities at long distances. Deviations from the exact result are quadratic in the interaction U.

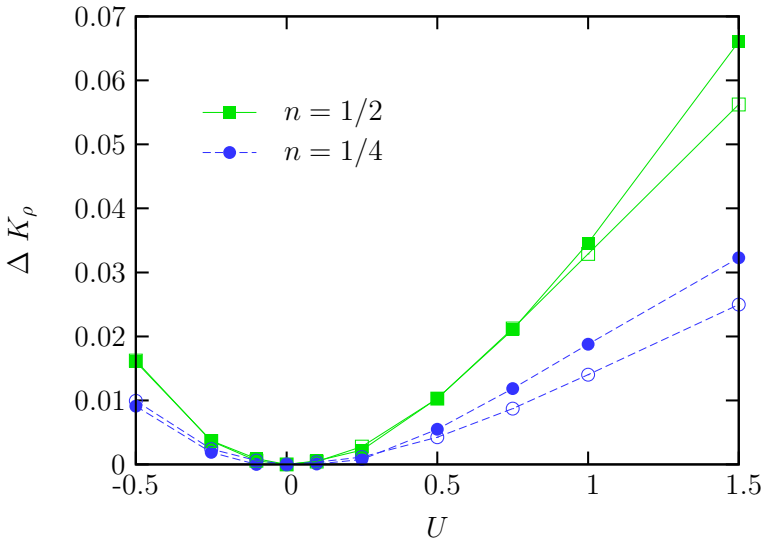

Figure 5.15: *Difference between the fRG result and the exact Bethe ansatz result for the Luttinger-liquid parameter K_ρ as a function of U at densities $n = 1/2$ and $1/4$ for the spinless fermion model, as obtained from the power-law decay of Friedel oscillations generated by a strong impurity at long distances (filled symbols), and by a weak impurity at intermediate distances (open symbols).*

5.1.4 Scaling of the conductance

In this section we study the transport through an interacting wire with a single impurity connected to semi-infinite noninteracting leads. The conductance exhibits the same asymptotic scaling behavior as a function of temperature T for an infinite wire as at $T = 0$ as a function of L. For more than one impurity the T dependence is richer, showing nonmonotonic behavior and distinctive power-laws with different universal exponents in various regimes; an extensive analysis is reported in Ref. [Enss et al. 2005; Enss 2005]. Although this difference does not appear for a single impurity, we will mainly focus on the more physical temperature dependence of the conductance.

Before analyzing the scaling behavior we present in Fig. 5.16 a comparison of fRG results to numerical DMRG data for the conductance for a short wire at $T = 0$, determined from the persistent current observed in the presence of a magnetic flux piercing a noninteracting ring in which the interacting wire is embedded [Meden et al. 2003; Meden and Schollwöck 2003a,b]. The excellent agreement proves the reliability of the approximate fRG scheme for interactions in the range $1/2 \leq K_\rho \leq 1$.

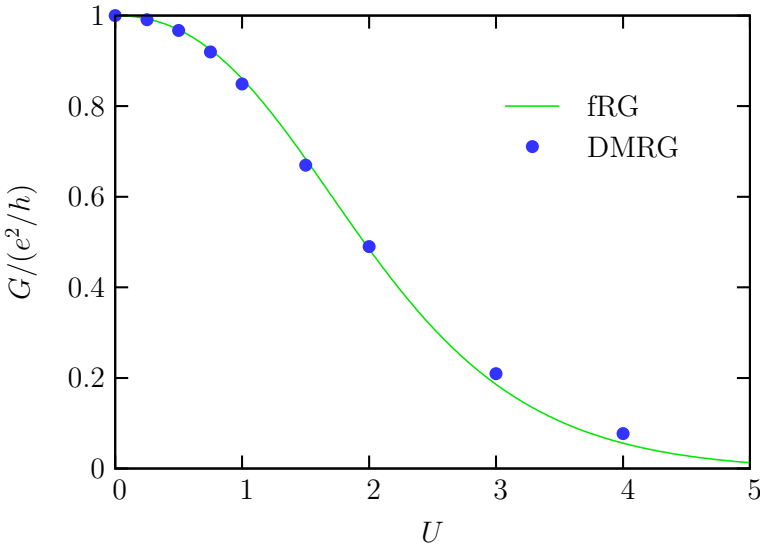

Figure 5.16: *Conductance as a function of the interaction U for a homogeneous spinless fermion chain at half filling, with $L = 12$ sites; the interaction is turned on sharply at the contacts.*

Fig. 5.17 shows typical fRG results for the T dependence of the conductance through a single site impurity of strength V. The $1/T$ scaling observed for high

temperatures (of the order of the bandwidth) results from the $1/T$ behavior of the derivative of the Fermi function in Eq. (4.79), together with the weak temperature dependence of $|t(\varepsilon, T, L)|^2$ at high T. For a strong impurity $V = 10$, $G(T)$ follows a power law with exponent $2\alpha_B$ as indicated by the dashed line in Fig. 5.17, until saturation sets in for $T \sim \pi v_F/L$. For an intermediate impurity the slope of the data tends towards the asymptotic exponent, but is still significantly away from it when finite-size saturation sets in. This slow change of the slope is a general feature of intermediate V. For a weak impurity $G(T)$ approaches e^2/h. Similar behavior is found for the scaling of $1-G(T)/(e^2/h)$ in the limit of a weak impurity predicted to follow $T^{2(K_\rho-1)}$, which holds as long as the correction to perfect conductance stays small [Kane and Fisher 1992a,c; Fendley et al. 1995].

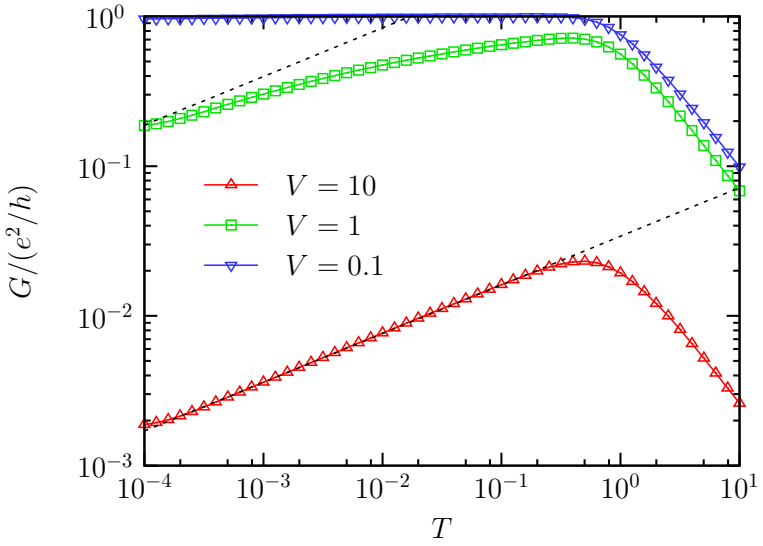

Figure 5.17: *Temperature dependence of the conductance for a half-filled spinless fermion wire of length $L = 10^4$, interaction $U = 0.5$ and a single site impurity of strengths V at the center of the wire; the dotted lines highlight power-law behavior.*

The above results are generic as long as the impurity is placed sufficiently away from the contact regions. The scale $\delta_{j_0} = \pi v_F/j_0$, where j_0 is the impurity position, sets a lower bound for the power-law scaling with the exponents discussed above [Furusaki and Nagaosa 1996]. For $T \simeq \delta_{j_0}$ a crossover to a power-law scaling with different exponents is found. For impurity positions in the contact region the exponent α_B describes the tunneling between the noninteracting and the interacting Luttinger liquids [Enss et al. 2005]. Restrictions on the temperature range where

universal scaling behavior might be detected arise from the bandwidth from above and the finite wire length from below. For an interacting wire of L lattice sites the energy scale $\delta_L = \pi v_F/L$ represents a lower bound for any temperature scaling. Depending on the impurity and interaction strength an asymptotic low-energy regime might not be reachable in experiments on finite wires. For finite temperatures systems of 10^4 lattice sites are considered, comparable for typical lattice constants to quantum wires in the micrometer range accessible to transport experiments.

Considering the conductance as a function of temperature and impurity strength, for a fixed K_ρ the renormalization-group flow from weak to strong impurity strength determines a scaling function $\tilde{G}_{K_\rho}(x)$ on which the data for different T and V collapse [Kane and Fisher 1992a,c; Moon et al. 1993; Fendley et al. 1995]. Using a one-parameter scaling ansatz

$$G = \frac{e^2}{h}\tilde{G}_{K_\rho}(x) \;, \qquad \text{with} \qquad x = [T/T_0(U,n,V)]^{K_\rho - 1} \;, \tag{5.4}$$

the curves for $G(T)$ and different V can be collapsed onto the K_ρ-dependent scaling function $\tilde{G}_{K_\rho}(x)$ for an appropriate nonuniversal scale $T_0(U,n,V)$. It has the limiting behavior $\tilde{G}_{K_\rho}(x) \sim 1 - x^2$ for $x \to 0$, and $\tilde{G}_{K_\rho}(x) \sim x^{-2/K_\rho}$ for $x \to \infty$; for $K_\rho = 1/2$ and $K_\rho = 1/3$ the functional form of $\tilde{G}_{K_\rho}$ was determined explicitly [Kane and Fisher 1992c; Moon et al. 1993; Fendley et al. 1995]. An example is shown in Fig. 5.18 for $U = 0.5$, the different colors stand for different impurity strengths V. As a consequence of the extended crossover region between weak and strong-impurity behavior, even for the fairly large system size of $L = 10^4$ sites and the large range of temperatures we can treat, it is impossible to directly demonstrate the full crossover for a single set of parameters. A power-law behavior in both limits is found, with exponents which can be expressed consistently in terms of a single approximate Luttinger-liquid parameter K_ρ. Data for the same K_ρ but different interaction and filling parameters collapse on the results for half filling, since the scaling function depends on U and n only via the Luttinger-liquid parameter K_ρ. Considering different types of impurity potentials extending over more than one site or bond does not modify $\tilde{G}_{K_\rho}$.

A previous analysis of the zero temperature scaling behavior in the wire length L, replacing T in the above ansatz by $\pi v_F/L$, showed that one-parameter scaling is not affected by the presence of leads if the interaction is turned on very smoothly at the contacts and no one-particle scattering terms at the contacts are considered [Meden et al. 2003]. In addition, fRG data are found to collapse onto the $K = 1/2$ local sine-

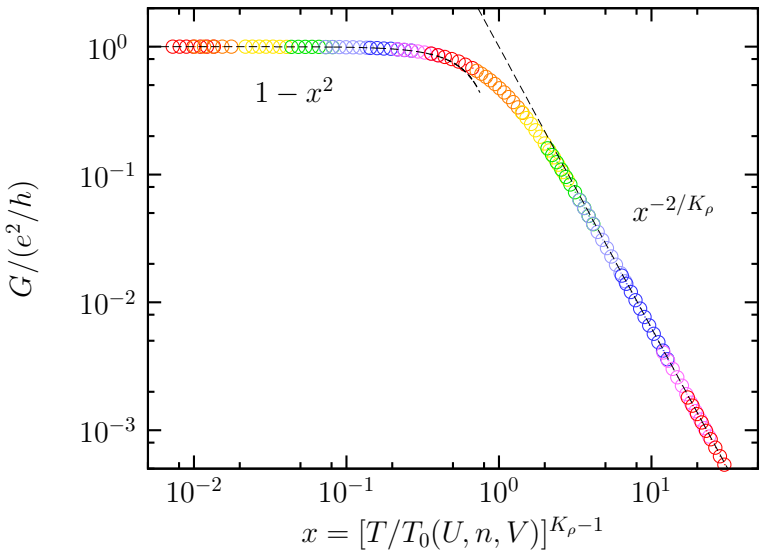

Figure 5.18: *One-parameter scaling plot of the conductance for the spinless fermion model at half filling with $U = 0.5$; the colors represent results obtained for different impurity strengths; the dashed lines indicate the asymptotic behavior for small and large x.*

Gordon scaling function known analytically [Meden et al. 2003; Enss et al. 2005]. We finally remark that one-parameter scaling represents an excellent example for the power of the fRG technique capturing complex crossover phenomena at intermediate scales.

There is an interesting correspondence between the transport through impurities in a Luttinger liquid and the quantum Brownian motion in a cosine potential examined in Ref. [Weiss 1999]. The duality symmetry of the latter maps a weak impurity (small V) exactly to a strong impurity (large V) under the substitution $K_\rho \to 1/K_\rho$. For $K_\rho < 1$ the system becomes localized, whereas the effective barrier height vanishes for $K_\rho > 1$. This symmetry can be extended also to finite temperatures by a frequency-dependent transformation [Weiss 1999]. The equivalence between the mobility of the Brownian particle and the conductance through an impurity in a Luttinger liquid relates the behavior for a strong impurity to the one for an appropriate weak impurity by

$$G_{\text{strong}}(T, K_\rho)/(e^2/h) = 1 - G_{\text{weak}}(T, 1/K_\rho)/(e^2/h)\ . \tag{5.5}$$

In particular, the above relation holds for expansions around $V \ll 1$ and $V \gg 1$. The respective convergence radius defines the crossover scale between the two dual

descriptions by $T_c^{\text{strong}}(K_\rho) = T_c^{\text{weak}}(1/K_\rho)$. For $K_\rho > 1$ high and low temperatures are exchanged. Similar scaling behavior is found for the nonlinear conductance, where the bias assumes the role of the temperature [Weiss 1999].

As a consequence of this symmetry and the knowledge of the analytic form for a particular value of $K_\rho \neq 1$ the explicit scaling function can be derived, as well as an expression for the crossover scale [Weiss 1999]. The solution reproduces the result from the thermodynamic Bethe ansatz [Fendley et al. 1995].

5.2 Spin-$\frac{1}{2}$ fermions

5.2.1 Single-particle excitations

For $\omega \to 0$ the spectral weights and the local density of states near a boundary or impurity are ultimately suppressed according to a power law with the boundary exponent

$$\alpha_B = \frac{1}{2K_\rho} + \frac{1}{2K_\sigma} - 1 \,, \tag{5.6}$$

with $K_\sigma = 1$ for spin-rotation invariant systems [Giamarchi 2004]. However, due to the slow logarithmic decrease of the two-particle backscattering amplitude, the fixed point value of K_σ is reached only logarithmically from above. Hence, we can expect that the asymptotic value of α_B is usually reached only very slowly from below.

The local density of states at the boundary of a quarter-filled Hubbard chain, computed by the fRG, is shown in Fig. 5.19 for various values of the local interaction U. Contrary to the expected asymptotic power-law suppression the spectral weight near the chemical potential is strongly *enhanced*. The predicted suppression occurs only at very small energies for sufficiently large systems. In the main panel of Fig. 5.19 the crossover to the asymptotic behavior cannot be observed, as the finite-size cutoff $\sim \pi v_F/L$ is too large. Results for a larger system with $L = 10^6$ sites at $U = 2$ in the inset show the crossover to the asymptotic suppression, albeit only at very small energies. The dependence of the boundary spectral weight at the Fermi level on the system size L is plotted in Fig. 5.20. The L dependence of the spectral weight at zero energy is expected to display the same asymptotic power-law behavior for large L as the ω dependence discussed above. Instead of decreasing with increasing L, the spectral weight increases even for rather large systems for small and moderate values of U. For $U > 2$ the crossover to a suppression is visible

in Fig. 5.20. For $U = 0.5$ only an increase is obtained up to the largest systems studied. The crossover depends sensitively on the interaction strength U, for small U it is exponentially large in $\pi v_F/U$.

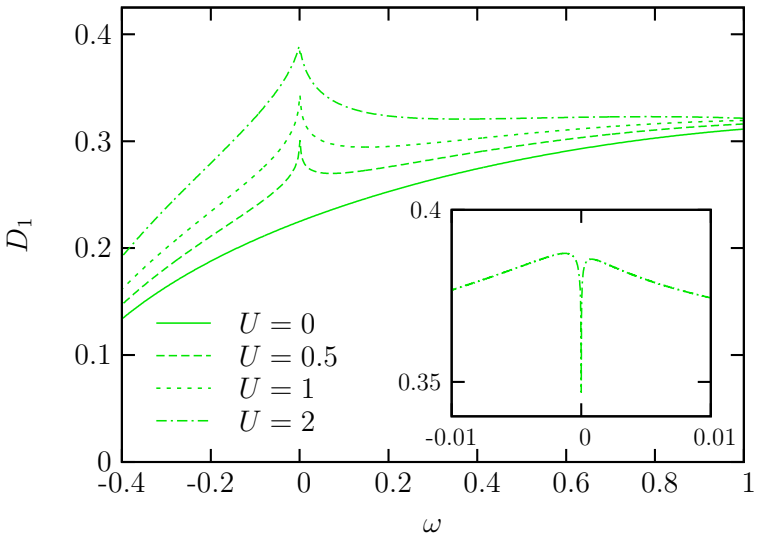

Figure 5.19: *Local density of states at the boundary of a Hubbard chain of length $L = 4096$ at quarter filling and various interaction strengths U; the inset shows results for $U = 2$ and $L = 10^6$ at very low ω.*

The above behavior of the spectral weight and the density of states near a boundary of the Hubbard chain, that is, a pronounced increase preceding the asymptotic power-law suppression, is captured qualitatively already by the Hartree-Fock approximation [Meden et al. 2000; Schönhammer et al. 2000]. This is at first sight surprising, as the Hartree-Fock theory does not capture any Luttinger-liquid features in the bulk of a translational invariant system. In particular, a self-consistent Hartree-Fock calculation leads to the unphysical result of a charge-density-wave ground state for all $U > 0$ [Cohen et al. 1998], since a single impurity can not modify bulk properties of the system. The initial increase of $D_j(\omega)$ near a boundary is actually obtained already within perturbation theory at first order in the interaction [Meden et al. 2000],

$$D_j(\omega) = D_j^0(\omega) \left[1 + \frac{\tilde{V}(0) - z\tilde{V}(2k_F)}{2\pi v_F} \ln|\omega/\epsilon_F| + \mathcal{O}(\tilde{V}^2) \right] \tag{5.7}$$

where $D_j(\omega)^0$ is the noninteracting density of states, $\tilde{V}(q)$ the Fourier transform of the real space interaction, and z the number of spin components. For spinless

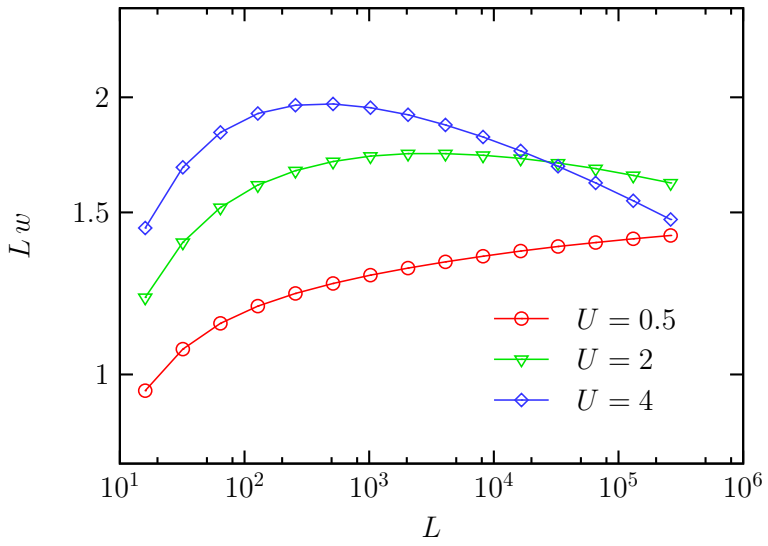

Figure 5.20: *Spectral weight at the Fermi level at the boundary of a quarter-filled Hubbard chain as a function of system size L, for various different interaction strengths.*

fermions ($z = 1$) with repulsive interactions the coefficient in front of the logarithm is always positive such that the first-order term leads to a suppression of $D_j(\omega)$. For the Hubbard model, one has $z = 2$ and $\tilde{V}(0) - 2\tilde{V}(2k_F) = -U$ is negative for repulsive U. Hence, at least for weak U the density of states increases for decreasing ω until terms beyond first oder become important. For the extended Hubbard model, $\tilde{V}(0) - 2\tilde{V}(2k_F) = 2U'[1 - 2\cos(2k_F)] - U$, which can be positive or negative for $U, U' > 0$, depending on the density and the relative strength of the two interaction parameters. At quarter filling $\tilde{V}(0) - 2\tilde{V}(2k_F)$ is negative and therefore leads to an enhanced density of states for $U' < U/2$.

Using g-ology notation (cf. Sec. A.2), one can write $\tilde{V}(0) - 2\tilde{V}(2k_F) = g_{2\perp} - 2g_{1\perp}$, which reveals that substantial two-particle backscattering ($g_{1\perp} > g_{2\perp}/2$) is necessary to obtain an enhancement of $D_j(\omega)$ for repulsive interactions. Backscattering vanishes at the Luttinger-liquid fixed point, but only very slowly. In case of a negative $\tilde{V}(0) - 2\tilde{V}(2k_F)$ the crossover to a suppression of $D_j(\omega)$ is due to higher order terms, which are expected to become important when the first-order correction is of order one, that is, for energies below the scale

$$\omega_c = \epsilon_F \exp\Big(\frac{2\pi v_F}{\tilde{V}(0) - 2\tilde{V}(2k_F)}\Big) \tag{5.8}$$

corresponding to a system size $L_c = \pi v_F/\omega_c$. The scale ω_c is exponentially small

for weak interactions. A more accurate analytical estimate of the crossover scale from enhancement to suppression has been derived for the Hubbard model within Hartree-Fock approximation in Ref. [Meden et al. 2000]. In a renormalization-group treatment ω_c is somewhat enhanced by the downward renormalization of backscattering.

A comparison of fRG results with DMRG data for the spectral weight at the Fermi level is shown in Fig. 5.21, for a boundary site in the upper panel, and near a hopping impurity of strength $t' = 0.5$ in the lower. The agreement improves at weaker coupling, as expected, and is generally better for the impurity case, compared to the boundary case. The deviations in the boundary case are probably due to our approximate translation-invariant parametrization of the two-particle vertex. Boundaries and to a minor extent impurities spoil the translation invariance of the two-particle vertex. Although the deviations from translation invariance of the vertex become irrelevant in the low-energy or long-distance limit, and therefore do not affect the asymptotic behavior, they are nevertheless present at intermediate scales. This feedback of impurities into the vertex increases of course with the impurity strength and is thus particularly important near a boundary. The scale for the crossover from enhancement to suppression of spectral weight discussed above depends sensitively on effective interactions at intermediate scales and can therefore be shifted considerably even by relatively small errors in that regime.

With the additional nearest-neighbor interaction in the extended Hubbard model it is possible to tune parameters such that the two-particle backscattering amplitude becomes negligible. In that case the asymptotic power-law suppression of spectral weight should be free from logarithmic corrections and accessible already for smaller systems and at higher energy scales. The bare backscattering interaction in the extended Hubbard model is given by $g_{1\perp} = U + 2U' \cos(2k_F)$ and therefore vanishes for $U' = -U/[2\cos(2k_F)]$, which is repulsive for $U > 0$ if $n > 1/2$. In a one-loop calculation a slightly different value of U' has to be chosen to obtain a negligible renormalized $g_{1\perp}^{\Lambda}$ for small finite Λ, since the flow generates backscattering terms at intermediate scales even if the bare $g_{1\perp}$ vanishes. In Fig. 5.22 we show fRG and DMRG results

for the spectral weight of the extended Hubbard model at the Fermi level near a hopping impurity. In the upper panel a generic case with sizeable backscattering is shown, while the parameters leading to the curves in the lower panel have been chosen such that the two-particle backscattering amplitude is negligible at low en-

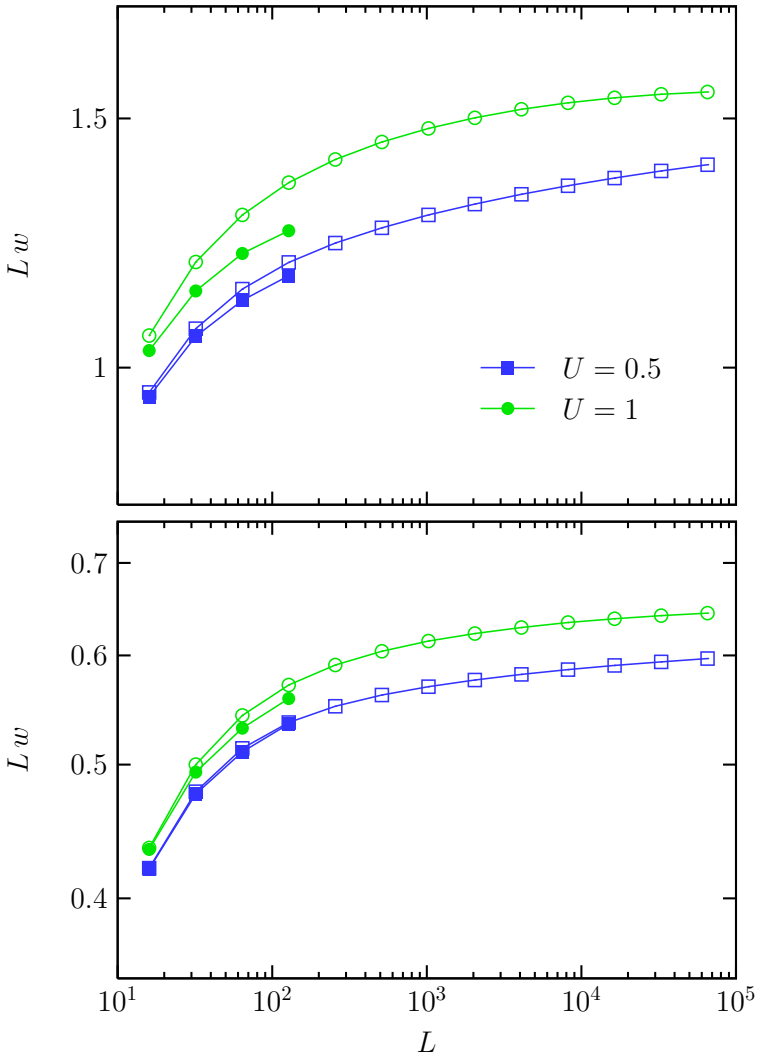

Figure 5.21: *Spectral weight at the Fermi level near a boundary (*upper panel*) and a hopping impurity $t' = 0.5$ (*lower panel*) as a function of system size L for the Hubbard model at quarter filling and different interaction strengths U; results from the fRG (open symbols) are compared to DMRG data (filled symbols).*

ergy. Only in the latter case a pronounced suppression of spectral weight is reached already for intermediate system size, similar to the behavior obtained previously for spinless fermions with nearest-neighbor interaction [Andergassen et al. 2004; Meden et al. 2002a,b]. This is also reflected in the energy dependence of the local density of states near the impurity. For parameters leading to negligible two-particle back-scattering as in Fig. 5.23 the suppression of the density of states sets in already at

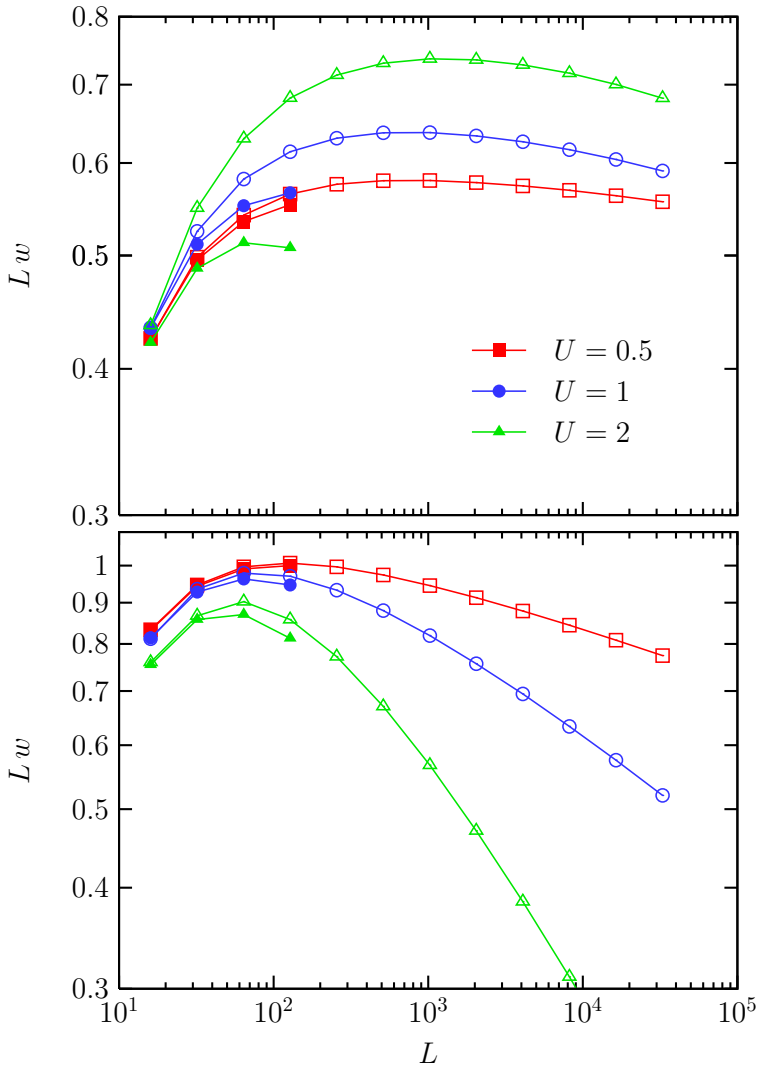

Figure 5.22: *Spectral weight at the Fermi level near a hopping impurity* $t' = 0.5$ *as a function of system size* L *for the extended Hubbard model with* $U' = U/\sqrt{2}$*, for various choices of* U*;* upper panel*:* $n = 1/2$ *(leading to sizeable backscattering),* lower panel*:* $n = 3/4$ *(leading to small backscattering); results from the fRG (open symbols) are compared to DMRG data (filled symbols).*

relatively high energies and is not preceded by any interaction-induced increase; the slight increase for small system sizes is a finite-size effect present also in the non-interacting case. Note also that the fRG results are much more accurate for small backscattering, as can be seen by comparing the agreement with DMRG data in the upper and lower panel of Fig. 5.22 especially for larger U. This indicates that

the influence of the impurity on the vertex flow, which we have neglected, is more important in the presence of a sizable backscattering interaction.

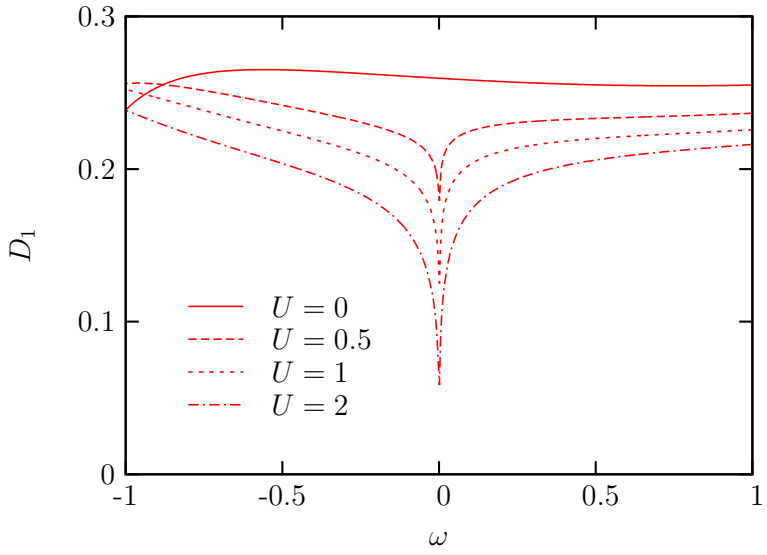

Figure 5.23: *Local density of states near a hopping impurity* $t' = 0.5$ *in an extended Hubbard model with density* $n = 3/4$ *and interaction* $U' = U/\sqrt{2}$ *(leading to a small backscattering interaction) for various choices of* U*; the size of the chain is* $L = 4096$*.*

In the case of a negligible backscattering amplitude, the spectral weight at the Fermi level approaches a power law without logarithmic corrections for accessible system sizes if the impurity is sufficiently strong. The power law is seen most clearly by plotting the effective exponent $\alpha(L)$, that is, the negative logarithmic derivative of the spectral weight with respect to the system size. Fig. 5.24 shows $\alpha(L)$ on the site next to a site impurity of strength V for the extended Hubbard model with $U = 1$, $U' = 0.65$ and $n = 3/4$. The backscattering amplitude is very small for these parameters. The fRG results approach the expected universal V-independent power law for large L, but only very slowly for small V. For weak bare impurity potential V, the crossover to a strong effective impurity occurs only on a large length scale of order $V^{2/(K_\rho - 1)}$ [Kane and Fisher 1992a,c]. For $V = 0.1$ this scale is obviously well above the largest system size reached in Fig. 5.24. The Hartree-Fock approximation also yields power laws for large L, but the exponents depend on the impurity parameters. This failure of Hartree-Fock theory was already observed earlier for spinless fermions [Meden et al. 2002a,b].

The effective exponent obtained from the fRG calculation agrees with the exact

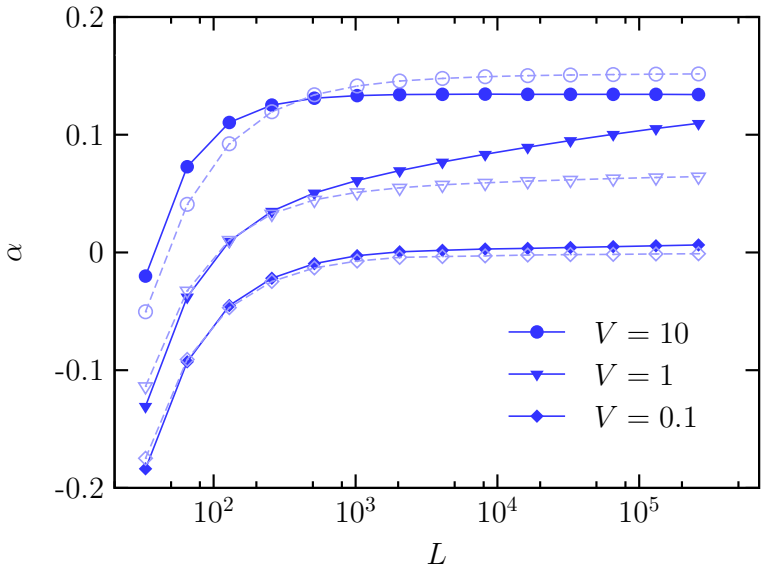

Figure 5.24: *Logarithmic derivative of the spectral weight at the Fermi level on the site next to a site impurity of strength V in the center of the chain as a function of system size L, for the extended Hubbard model with interaction parameters $U = 1$, $U' = 0.65$ and density $n = 3/4$; here the filled symbols are fRG, the open symbols Hartree-Fock results.*

boundary exponent to linear order in the bare interaction, but not to quadratic order. A quantitative estimate of the accuracy is obtained from a comparison to exact DMRG results [Ejima et al. 2005] shown in Fig. 5.25, for the extended Hubbard model at $n = 3/4$ and with $U' = U/\sqrt{2}$ leading to a negligible backscattering amplitude. To improve this, the frequency dependence of the two-particle vertex, has to be taken into account. This is also necessary to describe inelastic processes and to capture the anomalous dimension of the bulk system (see also Sec. 5.1.2).

5.2.2 Density profile

Boundaries and impurities induce a density profile with long-range Friedel oscillations, which are expected to decay with a power law with exponent $(K_\rho + K_\sigma)/2$ at long distances, where $K_\sigma = 1$ for spin-rotation invariant systems [Egger and Grabert 1995]. For weak impurities linear response theory predicts a decay as $|j - j_0|^{1-K_\rho-K_\sigma}$ at intermediate distances.

As an additional benchmark for the fRG technique, we compare in Fig. 5.26 fRG and DMRG results for the density profile n_j for a quarter-filled Hubbard chain

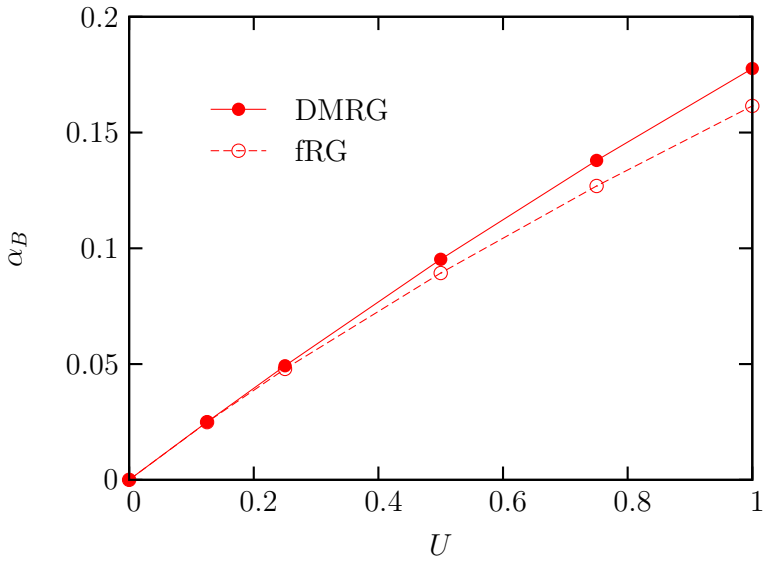

Figure 5.25: *Boundary exponent α_B as a function of U at densities $n = 3/4$, with $U' = U/\sqrt{2}$ (small backscattering interaction) as obtained from the power-law suppression of the spectral weight at the boundary; fRG results are compared to DMRG data.*

with $L = 128$ lattice sites and open boundaries. Friedel oscillations emerge from both boundaries and interfere in the center of the chain. The fRG results have been shifted by a small constant amount to allow for a better comparison of the oscillations. Note that the mean value of n_j in the tails of the oscillations deviates from the average density by a finite-size correction of order $1/L$, which is related to the asymmetry of the oscillations near the boundaries.

The long-distance behavior of the density oscillations as obtained within the fRG scheme has been analyzed in detail for spinless fermions in Sec. 5.1.3. For fermions with spin, asymptotic power laws can be identified only for special parameters leading to negligible two-particle backscattering. In general, the asymptotic behavior of Friedel oscillations is realized only at very long distances, and the power laws are modified by logarithmic corrections. We finally remark the presence of a $4k_F$-component of the Friedel oscillations for spin-$\frac{1}{2}$ fermions, which decays as $|j - j_0|^{-2K_\rho}$. In the present weak-coupling treatment this contribution is negligible, since the $2k_F$ component dominates for $K_\rho > 1/3$ [Egger and Grabert 1995].

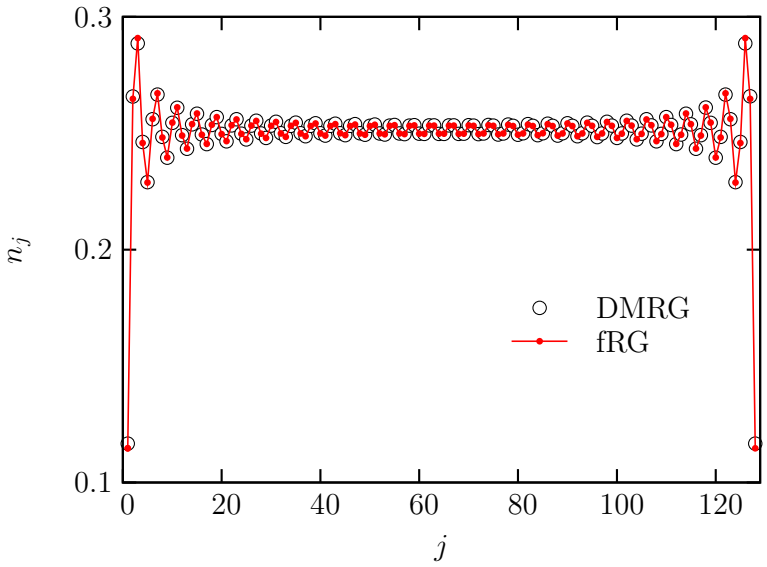

Figure 5.26: *Density profile n_j for the Hubbard model with* 128 *sites and interaction strength $U = 1$ at quarter filling; fRG results are compared to DMRG data.*

5.2.3 Conductance

Single impurity

For a system of spinless fermions with a single impurity it was already shown that the conductance obtained from the truncated fRG obeys the expected power laws, in particular $G(T) \propto T^{2\alpha_B}$ at low T, and one-parameter scaling behavior [Meden et al. 2003; Enss et al. 2005]. The corresponding scaling function agrees remarkably well with an exact result for $K_\rho = 1/2$, although the interaction required to obtain such a small K_ρ is quite strong. The more complex temperature dependence of the conductance in the case of a double barrier at or near a resonance is also fully captured by the fRG [Enss et al. 2005; Meden et al. 2005].

Fig. 5.27 shows typical fRG results for the temperature dependence of the conductance for the extended Hubbard model with a single strong site impurity ($V = 10$). Similar results were obtained for a hopping impurity. The considered size $L = 10^4$ corresponds to interacting wires in the micrometer range, which is the typical size of quantum wires available for transport experiments. For $U' = 0$ the conductance *increases* as a function of decreasing T down to the lowest temperatures in the plot. For increasing nearest-neighbor interactions U' a suppression of $G(T)$ at low T becomes visible, but in all the data obtained at quarter-filling

the suppression is much less pronounced than what one expects from the asymptotic power law with exponent $2\alpha_B$. By contrast, the suppression is much stronger and follows the expected power law more closely if parameters are chosen such that two-particle backscattering becomes negligible at low T, as can be seen from the conductance curve for $n = 3/4$ and $U' = 0.65$ in Fig. 5.27. The value of K_ρ for these parameters almost coincides with the one for another parameter set in the plot, $n = 1/2$ and $U' = 0.75$, but the behavior of $G(T)$ is completely different. Note that at $T \sim \pi v_F/L$ finite-size effects set in, as can be seen at the low T end of some of the curves in the figure. An enhancement of the conductance due to backscattering has been found already earlier in a renormalization-group study of impurity scattering in the g-ology model [Matveev et al. 1993; Yue et al. 1994].

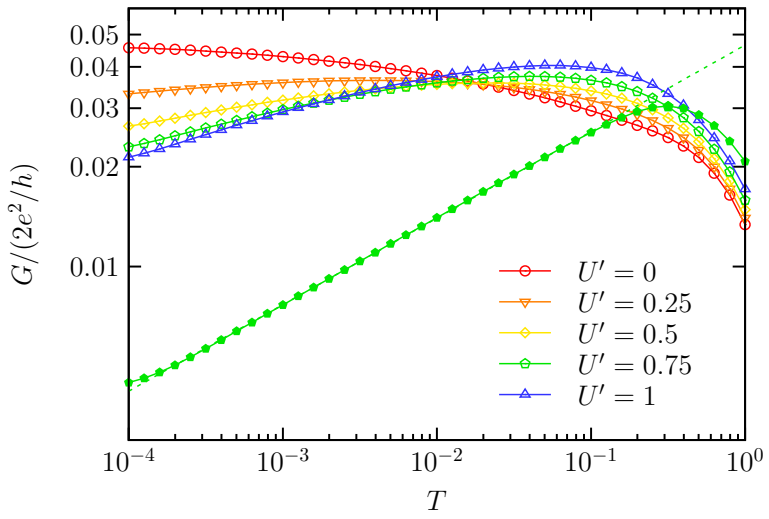

Figure 5.27: *Temperature dependence of the conductance for the extended Hubbard model with $L = 10^4$ sites and a single site impurity of strength $V = 10$, for a Hubbard interaction $U = 1$ and various choices of U'; the density is $n = 1/2$, except for the lowest curve, which has been obtained for $n = 3/4$ and $U' = 0.65$ (leading to a very small backscattering interaction); the dashed line is a power-law fit for the latter parameter set.*

Results for the conductance of the extended Hubbard model with a hopping impurity with various amplitudes t' are shown in Fig. 5.28. The bulk parameters have been chosen such that the two-particle backscattering is practically zero at low T. From the plot of the logarithmic derivative of $G(T)$ in the upper panel one can see that for a strong impurity (small t') the conductance follows a well-defined power law $G(T) \propto T^{2\alpha_B}$ over a large temperature range. For intermediate t' the curves

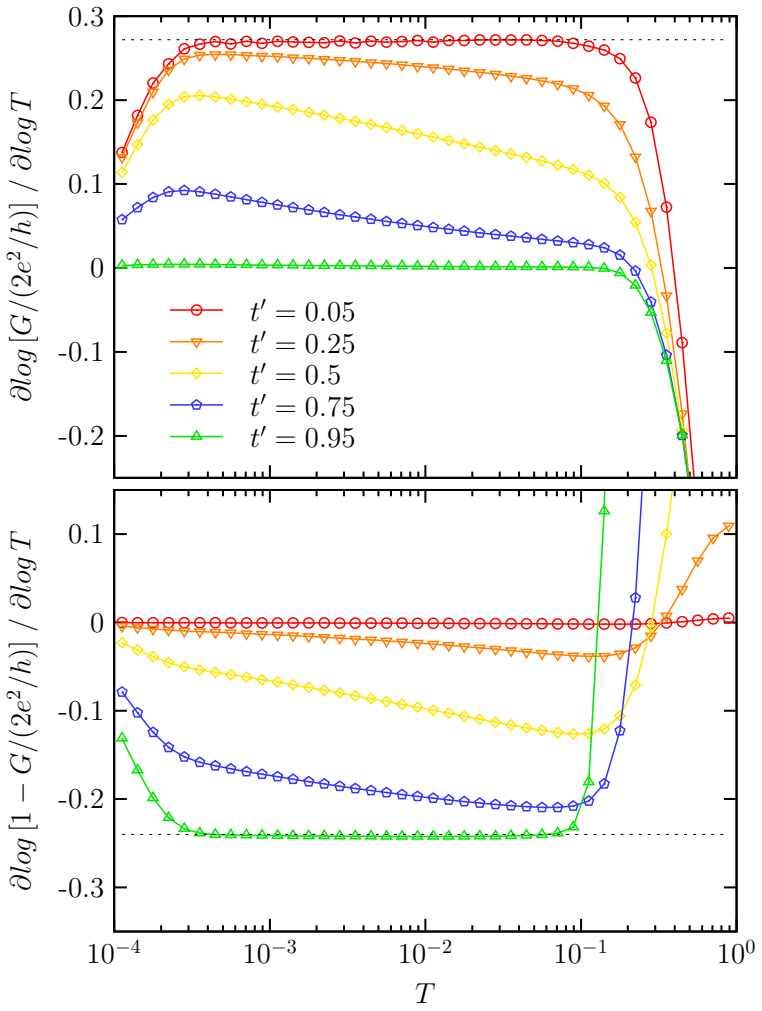

Figure 5.28: *Logarithmic temperature derivative of the conductance (upper panel) and of its deviation from the unitarity limit (lower panel) for the extended Hubbard model with $L = 10^4$ sites and various hopping impurities. The density is $n = 3/4$, interaction parameters are $U = 1$ and $U' = 0.65$. The dashed horizontal lines highlight power-law behavior.*

approach the asymptotic exponent at low T from below, but do not reach it before finite-size effects lead to a saturation of $G(T)$ for $T < \pi v_F/L$. For the weakest impurity in the plot, $t' = 0.95$, the conductance remains very close to the unitarity limit. However, the plot of the logarithmic derivative of $1 - G/(2e^2/h)$ in the lower panel of Fig. 5.28 shows that $1 - G/(2e^2/h)$ increases as $T^{K_\rho - 1}$ for decreasing T, as expected for a weak impurity in the perturbative regime [Kane and Fisher 1992a,c].

The effective exponents indicated by the two horizontal lines in the figure deviate from the exact values (determined from the DMRG result [Ejima et al. 2005] for K_ρ) by about 20% in the case of $2\alpha_B$ and only by 5% for $K_\rho - 1$ (cf. Sec. 5.1.4).

Depending on the bare impurity and interaction parameters, nonuniversal behavior dominates at intermediate energy and length scales. Moreover, in the presence of backscattering the asymptotic power laws are modified by logarithmic corrections.

Double impurity

We finally present results for the conductance of a wire with a double-barrier impurity [Andergassen et al. 2005a]. The setup modeling a quantum dot is shown in Fig. 5.29. Applying a gate voltage V_g on the dot sites $j \in [j_l, j_r]$ by

$$H_{\text{gate}} = V_g \sum_{j,\sigma} n_{j,\sigma} \tag{5.9}$$

the conductance can be tuned to resonance. $L_D = j_r - j_l + 1$ is sufficiently far away from the contacts at sites 1 and L the position of the dot does not play a role.

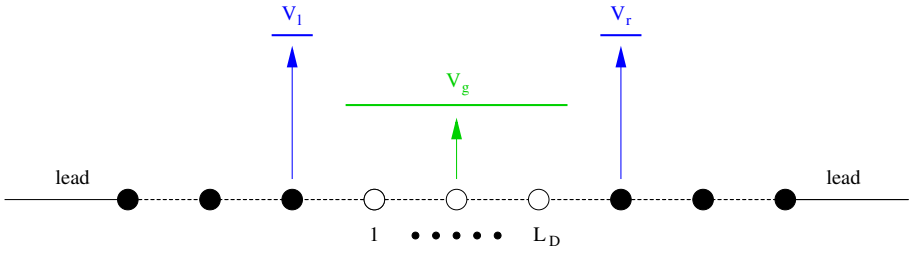

Figure 5.29: *Quantum dot schematization.*

Earlier studies of tunneling through a quantum dot embedded in a spinless Luttinger liquid showed that at $T = 0$ and for finite L the resonances in the linear conductance $G(V_g)$ are characterized by an almost Lorentzian shape with unitary height for symmetric barriers and a width w vanishing as a power law with a K_ρ-dependent exponent in the limit $L \to \infty$. For asymmetric barriers the resonances disappear for increasing L [Kane and Fisher 1992a,c]. At $T > 0$ the peak value of the conductance shows distinctive power-law behavior as a function of temperature [Enss et al. 2005; Meden et al. 2005]. Including the spin degree of freedom the physics becomes more complex due to the appearance of the Kondo effect. For

noninteracting leads ($L = 1$) the Kondo physics was investigated theoretically for the single-impurity Anderson model [Glazman and Raikh 1988; Ng and Lee 1988]. At low temperatures and for sufficiently high tunnel barriers the Kondo effect leads to a *broad plateau-like line* shape of the resonance replacing the Lorentzian. On resonance the number of electrons on the dot is odd implying a local spin-$\frac{1}{2}$ degree of freedom responsible for the Kondo effect [Hewson 1993]. For the single-impurity Anderson model the conductance is proportional to the one-particle spectral weight of the dot at the chemical potential [Meir and Wingreen 1992]. Varying V_g within an energy range of order U the Kondo resonance of the spectral function is pinned at μ_0 at height $2e^2/h$ explaining the broad plateau-like resonance in $G(V_g)$ [Hewson 1993; Gerland et al. 2000]. The problem of a single spin-$\frac{1}{2}$ coupled to a Luttinger liquid was investigated generalizing the Kondo model [Furusaki 2005]. The fRG approach allows for a direct computation of the electron transport through a quantum dot embedded in a Luttinger liquid in the presence of the Kondo effect. Here we address the question of the resonance line shape and the power-law scaling of $G(T)$ resulting from the *competition* between the two correlation effects.

For this purpose we first consider the situation $L = L_D = 1$ at $T = 0$ corresponding to the single-impurity Anderson model. Unless otherwise stated we consider symmetric dot-lead couplings. In Fig. 5.30 the conductance G as a function of gate voltage V_g for the single-impurity Anderson model is shown for different tunnel barriers t' in the upper panel, together with the occupation of the dot in the lower. For $t' \ll U$ the resonance has a plateau-like shape [Gerland et al. 2000]. In this region the occupation is close to 1 while it sharply raises/drops to 2/0 to the left/right of the plateau. Also for asymmetric barriers we reproduce the exact resonance height $4\Delta_L\Delta_R(\Delta_L + \Delta_R)^2\,(2e^2/h)$, where $\Delta = \Delta_L + \Delta_R$ measures the hybridization of the dot and the (left and right) lead states [Hewson 1993; Gerland et al. 2000]. Here we are interested in the interplay of Kondo and Luttinger-liquid physics and thus focus on small t', that is, on tunnel barriers with small transmission.

The pinning of the spectral function and the subsequent plateau-like resonance can be derived within the fRG Scheme I (cf. Sec. 4.2.2). For $L = 1$ the chemical potential only shifts the position of the resonance. For half filling $G(V_g)$ is symmetric around 0 and the flow equation for the effective onsite energy $V = V_g + \Sigma^\Lambda_{j_D,j_D}$ on the dot site j_D reduces to

$$\frac{\partial}{\partial\Lambda}V^\Lambda = -\frac{U}{\pi}\,\mathrm{Re}\,\mathcal{G}^\Lambda_{j_D,j_D}(i\Lambda) = \frac{UV^\Lambda/\pi}{(\Lambda+\Delta)^2 + (V^\Lambda)^2} \tag{5.10}$$

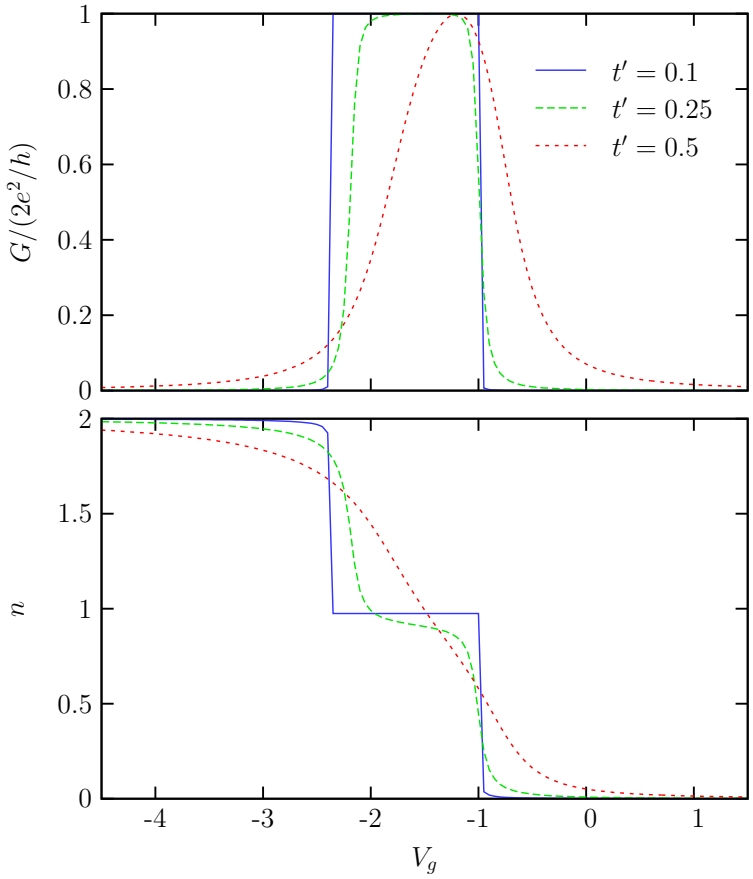

Figure 5.30: Upper panel: *conductance as a function of gate voltage for the Hubbard model at quarter filling, with* $U = 1$*, for* $L = L_D = 1$ *and different* t' *;* lower panel: *average number of electrons on the dot.*

in the limit of $\Delta \ll U$. Here $\Delta = 2\pi t'^2 \rho$ is the hybridization, and ρ denotes the spectral weight at the end of the leads in the infinite band width limit [Hewson 1993]. The initial condition is $V^{\Lambda_0} = V_g$. In this scheme the self-energy is frequency independent leading to a Lorentzian spectral function of width 2Δ and height $1/(\pi\Delta)$ centered around $V = V^{\Lambda=0}$. This implies that the spectral weight at μ_0 and thus $G(V_g)$ is determined by V [Meir and Wingreen 1992]. The solution of the differential equation (5.10) at $\Lambda = 0$ is obtained in implicit form

$$\frac{vJ_1(v) - \delta J_0(v)}{vY_1(v) - \delta Y_0(v)} = \frac{J_0(v_g)}{Y_0(v_g)} \,, \tag{5.11}$$

with $v = V\pi/U$, $v_g = V_g\pi/U$, $\delta = \Delta\pi/U$, and Bessel functions J_n, Y_n. For $|V_g| < V_c$ this equation has a solution with a small $|V|$, where $v_c = V_c\pi/U$ is the first zero of

J_0 corresponding to $V_c \simeq 0.77U$. For $U \gg \Delta$ the crossover to a solution with $|V|$ being of order U (for $|V_g| > V_c$) is fairly sharp. Expanding both sides of Eq. (5.11) for small $|v|$ and $|v_g|$ gives

$$V = V_g \exp\left(\frac{U}{\pi\Delta}\right). \tag{5.12}$$

The exponential pinning of the spectral weight at $\mu_0 = 0$ for small $|V_g|$ and the sharp crossover to a V of order U when $|V_g| > V_c$ leads to the observed resonance line shape. For $U \gg \Delta$ the width of the plateau is $2V_c \simeq 1.5U$, which is larger than the width U found with the numerical renormalization-group method [Gerland et al. 2000]. Our approximation furthermore slightly overestimates the sharpness of the box-shaped resonance. We expect the agreement is improved with the more accurate fRG Scheme II (cf. Sec. 4.2.2).

In the complementary case of Luttinger-liquid leads and in the absence of Kondo effect, suppressed by turning off the interaction on the dot, similar results as for spinless fermions are obtained. Luttinger-liquid behavior leads to *infinitely sharp* resonances in the limit $L \to \infty$, in strong contrast to the broad resonances induced by the Kondo effect [Enss et al. 2005]. To clearly observe Luttinger-liquid behavior for spin-$\frac{1}{2}$ fermions at experimentally accessible scales one has to consider a situation in which the backscattering process yielding logarithmic corrections to the power-laws is small by tuning the nearest-neighbor interaction U', see Sec. 5.2.1. In Fig. 5.31 the L dependence of $G(V_g)$ for a single-site dot computed for a small backscattering amplitude and lead length $L = 10^4$ typical for experiments is shown. At $T = 0$ the width of the resonance in $G(V_g)$ tends to zero for $L \to \infty$. The extracted width w as a function of L reported in the lower panel with open symbols follows a power law $L^{(K_\rho - 1)/2}$ with an fRG approximation to the Luttinger-liquid parameter that is, correct to leading order in the interaction. Off resonance G asymptotically vanishes as $L^{-2\alpha_B}$ [Kane and Fisher 1992a,c; Enss et al. 2005]. For V_g close to resonance and $1 - G/(2e^2/h) \ll 1$, the deviation from the unitary limit increases as L^{1-K_ρ} characteristic of the scaling of a weak single impurity. Further increasing L the behavior eventually crosses over to the off-resonance power-law suppression of G mentioned above. Due to an exponentially large crossover scale, even for the very large system sizes accessible with our method the complete crossover from one to the other power law can not be seen for a single fixed V_g but follows from one-parameter scaling [Kane and Fisher 1992a,c; Enss et al. 2005]. For a sizeable backscattering amplitude the off-resonance conductance and thus the width first slightly increase

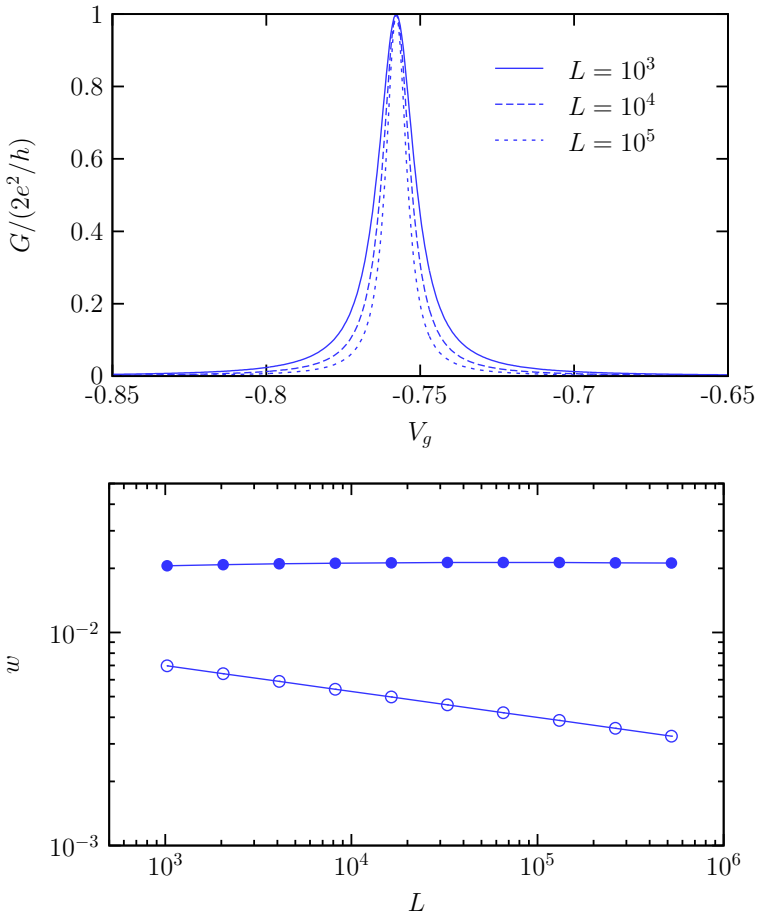

Figure 5.31: Upper panel: *conductance as a function of gate voltage for the extended Hubbard model at* $n = 3/4$, *with* $U = 1$, *and* $U' = 0.65$, *for a noninteracting dot with* $L_D = 1$, $t' = 0.1$ *and different* L; lower panel: *scaling of the resonance width for the same parameters as in the upper panel corresponding to a small backscattering interaction (open symbols), and for* $n = 1/4$, $U = 1$, $U' = 0$ *corresponding to a large backscattering interaction (filled symbols).*

for increasing L - becoming larger than for the noninteracting dot - followed by a crossover to a decrease for exponentially large L, as indicated by the filled symbols in the lower panel. Due to the logarithmic vanishing of the backscattering process this behavior can in general not be observed on experimentally accessible scales, confirming the important role of two-particle backscattering on intermediate length scales. An upper bound of the length of quasi one-dimensional wires realized in experiments is of the order of μm, roughly corresponding to 10^4 lattice sites [Bockrath

et al. 1999; Yao et al. 1999; Auslaender and Fishman 2000; Picciotto et al. 2001].

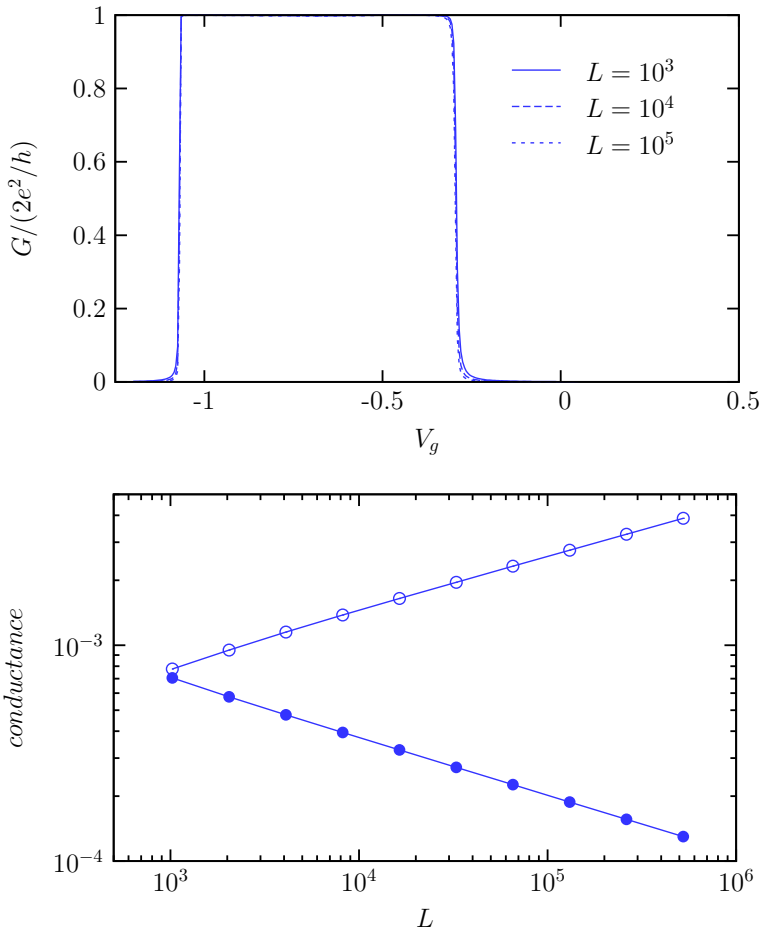

Figure 5.32: Upper panel: *conductance $G(V_g)$ as in Fig. 5.31 (same parameters), but now with interaction on the dot;* lower panel: *scaling of $G/(2e^2/h)$ at $V_g = 0$ outside the plateau (filled symbols), and of $1 - G/(2e^2/h)$ on the plateau at $V_g = -0.685$ (open symbols).*

We now analyze the linear conductance through a quantum dot in the presence of both Kondo effect as well as Luttinger-liquid leads. The upper panel of Fig. 5.32 shows the L dependence of $G(V_g)$ for the same parameters as in Fig. 5.31, but now including the interaction on the dot. Note the different scales on the x-axis. For interactions large compared to the hybridization the broad plateau-like resonance induced by the Kondo effect is also present at least for *finite* Luttinger-liquid leads. The same holds for $L_D > 1$. The width of the plateaus is proportional to the ratio of the local component of the effective interaction at the end of the fRG flow and L_D. The differences between the curves for different L are barely visible, in

particular the changes of the resonance width are marginal. For generic parameters with sizeable backscattering, the difference between curves computed for different L are even smaller. We note that the plateaus vanish if U, U', and n are chosen such that at the end of the fRG flow the local part of the interaction is small, and the resonance peaks are sharp. To analyze the L dependence at small backscattering in more detail in the lower panel of Fig. 5.32 the scaling of $G/(2e^2/h)$ for a gate voltage outside the plateau (filled symbols) and of $1 - G/(2e^2/h)$ for a gate voltage on the resonance plateau (open symbols) are shown. Off resonance G follows a power-law with the exponent $2\alpha_B$ and G vanishes for $L \to \infty$. Within every plateau there a value of $V_g = V_g^r$ where $G = 2e^2/h$ independently of L. For $V_g \neq V_g^r$ still within the plateau the deviation of G from the unitary limit scales as L^{1-K_ρ}, that is, with the weak single-impurity exponent. This shows that any deviation from V_g^r acts as an impurity. By analogy with the single-impurity behavior discussed in the previous sections we conclude that in the asymptotic low-energy limit the impurity will effectively grow and in the limit $L \to \infty$ the plateaus will vanish. For infinitely long Luttinger-liquid leads the resonances are infinitely sharp even in the presence of Kondo physics. However, for tunnel barriers with small transmission the plateaus at finite L are well developed and the length scale on which the plateaus start to deteriorate is extremely large. For sizeable two-particle backscattering this scale is enhanced and the plateaus are more pronounced.

Also for asymmetric barriers we find (almost) plateau-like resonances. To discuss this in more detail we focus on typical parameters with $N = 10^4$ and an asymmetry $\Delta_l/\Delta_R \sim 2$. Then the width is almost unaffected by the asymmetry. For the interaction and filling as in Fig. 5.32 the height within the plateaus varies by a few percent (with maxima at the left and right boundaries) and has average value $\sim 0.85\,(2e^2/h)$. With increasing L the variation of the conductance on the plateaus increases while the average value decreases. We expect that for $L \to \infty$ the resonance disappears.

Concerning the power-law scaling of the conductance as a function of temperature, $G(T)$, the resonant tunneling behavior in general extends over a range of gate voltages defined by the width of the resonance plateau, since for all experimentally accessible length scales and for typical asymmetries of the dot-lead hybridizations the plateau-like resonances characteristic for Kondo physics will also be present if the leads are Luttinger liquids. The vanishing of the resonance plateau in the limit of infinite system size is beyond the infrared cutoff scale set by the system size

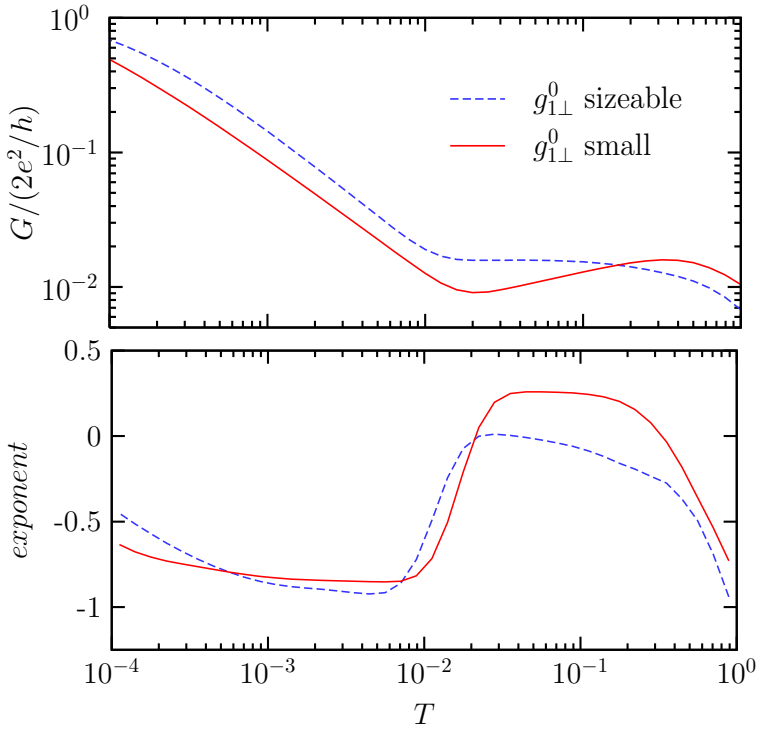

Figure 5.33: *Temperature dependence of the conductance for the extended Hubbard model with $L = 10^4$ sites, Hubbard interaction $U = 1$, for $U' = 0.65$ and $n = 3/4$ (leading to a small backscattering interaction), and for $U' = 0.75$ and $n = 1/4$ (leading to a sizable backscattering interaction); dot parameters: $t' = 0.1$, $L_D = 100$;* upper panel*: log-log plot of the conductance,* lower panel*: effective exponents; the gate potential is chosen at the center of the resonance plateau closest to $V_g = 0$.*

$T \sim \pi v_F/L$ for the appearance of power-law scaling with interaction-dependent exponents characteristic for Luttinger-liquid behavior. Hence the behavior of $G(T)$ is similar to the one found for spinless fermions [Enss et al. 2005; Meden et al. 2005]. In Fig. 5.33 the temperature dependence of the conductance for a large dot with $L_D = 100$ and for V_g placed at the center of the resonance plateau closest to $V_g = 0$ is shown. We distinguish the case of sizable and small backscattering processes $g^0_{1\perp}$. For a small backscattering amplitude we identify temperature regimes in which $G(T)$ follows distinctive power-law behavior with universal exponents. For T larger than the level spacing of the dot given by $\pi v_F/L_D$ a power law with the single-impurity exponent $2\alpha_B$ is found, arising from two independent single barriers acting as resistors in series. It follows a sequential tunneling regime characterized by

the power-law exponent $\alpha_B - 1$, until saturation sets in at $T \sim \pi v_F/L$. Small dots with L_D of order 1 exhibit only the latter. Similar results are obtained for other V_g within the resonance plateau, outside the plateaus the conductance follows the on-resonance behavior down to a scale set by the deviation from resonance. For smaller T we find a crossover to $T^{2\alpha_B}$. By contrast, for a sizable backscattering amplitude no clear power law can be distinguished, as can be seen from the conductance curve for $n = 1/4$ and $U' = 0.75$ in Fig. 5.33. The value of K_ρ for these parameters almost coincides with the one for another parameter set in the plot, $n = 3/4$ and $U' = 0.65$, but the behavior of $G(T)$ is completely different. For weak barriers analogous power-laws are detected in $1 - G/(2e^2/h)$, described by the single-impurity exponent $K_\rho - 1$ at high temperatures and by $K_\rho + 1$ in the sequential tunneling regime, similarly to the spinless case investigated in detailed in Ref. [Enss et al. 2005].

For systems with long-range interactions backscattering is strongly reduced compared to forward scattering. This seems to be the case in carbon nanotubes [Egger and Gogolin 1997; Kane et al. 1997]. Hence, the conductance can be expected to follow the asymptotic power law at accessible temperature scales for sufficiently strong impurities in these systems, as is indicated also by experiments [Yao et al. 1999]. However, the effects due to two-particle backscattering should be observable in systems with a screened Coulomb interaction. Whether Luttinger-liquid behavior has convincingly been demonstrated experimentally is still a matter of debate. Nonetheless, the above scenario has to be taken into consideration in the discussion of the influence of boundaries or impurities in quasi one-dimensional conductors.

6 Conclusions and outlook

The fRG provides a powerful tool to compute the intriguing properties of Luttinger liquids with static impurities. It captures the physics at all energy scales from the Fermi energy to the ultimate low-energy limit. The presented computation scheme extends previous work for spinless fermions [Meden et al. 2002a,b] to spin-$\frac{1}{2}$ fermions, including the vertex renormalization in addition to the renormalization of the effective impurity potential. The underlying approximations are devised for weak short-range interactions and arbitrary impurity potentials. The results agree remarkably well with exact asymptotic results up to intermediate interaction strength, and cover the universal low-energy asymptotics, as well as nonuniversal behavior and crossover phenomena at higher scales.

Various observables have been computed for different fermion lattice models: spectral properties of single-particle excitations, the oscillations in the density profile induced by impurities or boundaries, and the temperature dependence of the linear conductance. The comparison to DMRG results, for those observables and system sizes for which such data could be obtained, yields a good agreement at weak coupling. For intermediate interaction strengths with sizable two-particle backscattering and strong impurities the deviations are significantly larger for spin-$\frac{1}{2}$ than for spinless fermions. For the computation of the nonuniversal behavior at intermediate scales the neglected influence of impurities on vertex renormalization, in particular the interplay of impurities and the two-particle backscattering amplitude, is probably important for fermions with spin.

We confirm the universality of the open chain fixed point, but it turns out that very large systems are required to reach the fixed point for realistic choices of the impurity and interaction parameters. The spectral properties of single-particle excitations and the Friedel oscillations in the density profile induced by impurities or boundaries present the characteristic asymptotic power laws at low energy or large distance. For the linear conductance through a single impurity in Luttinger liquids connected to noninteracting leads the fRG captures the expected power-law scaling, as well as the complete crossover from the weak to the strong-impurity

limit determined by a one-parameter scaling function. For resonant tunneling in a Luttinger liquid with a double barrier enclosing a dot region, depending on the dot parameters several temperature regimes with distinctive power-law behavior of the resonance conductance as well as regimes characterized by non-universal behavior are identified [Enss et al. 2005; Meden et al. 2005].

Including the spin degree of freedom, two-particle backscattering of particles with opposite spin at opposite Fermi points leads to two important effects, not present in the case of spinless fermions. First, the expected decrease of spectral weight and of the conductance at low energy scales is often preceded by an increase, which can be particularly pronounced for the density of states near an impurity or boundary as a function of ω. For the density of states near a boundary this effect has been found already earlier within a Hartree-Fock and DMRG study of the Hubbard model [Meden et al. 2000; Schönhammer et al. 2000], and for the conductance by a renormalization-group analysis of the g-ology model [Matveev et al. 1993; Yue et al. 1994]. Second, the asymptotic low-energy power laws are usually modified by logarithmic corrections. In the extended Hubbard model the backscattering can be eliminated for a special fine-tuned choice of parameters. Then the results are very similar to those for spinless fermions. For weak and intermediate impurity strengths the asymptotic low-energy behavior is approached only at rather low scales, which are accessible only for very large systems. This slow convergence observed already for spinless fermions holds also in the absence of two-particle backscattering.

Interesting further extensions of the fRG for impurities in Luttinger liquids include the investigation of non-equilibrium phenomena and the analysis of disorder. For isolated impurities the influence of impurities on the vertex renormalization is irrelevant for the asymptotic low-energy or long-distance behavior, although it may contribute quantitatively at intermediate scales. For disordered systems with a finite impurity density the influence of the latter on the two-particle vertex is crucial and must be taken into account [Giamarchi 2004]. In principle this is possible by computing the vertex flow with full propagators, which contain the renormalized impurity potential via the self-energy. A further challenging extension concerns the inclusion of inelastic processes. They appear at second order in the interaction and can be included in the flow equations by inserting the two-particle vertex into the flow equation for the self-energy without neglecting its frequency dependence. Finally, a flexible microscopic modeling feasible with the fRG approach allows for a more realistic description of contacts and leads in experimental systems.

A Evaluation of vertex flow for spin-$\frac{1}{2}$ fermions

A.1 Functional RG

Here we present a detailed derivation of the flow equations for the two-particle vertex Γ^Λ. Starting from the flow equation (4.51) we insert on the right-hand side the parametrization (4.47) for Γ_t^Λ and (4.49) for Γ_s^Λ. The flow of the singlet vertex $\Gamma^\Lambda_{s|\,k_1',k_2';k_1,k_2}$ is computed for the three choices of (k_1', k_2', k_1, k_2) which yield the flow of g_{s2}^Λ, g_{s3}^Λ, g_{s4}^Λ corresponding to Eqs. (4.42) and (4.43), while the flow of the triplet vertex $\Gamma^\Lambda_{t|\,k_1',k_2';k_1,k_2}$ is evaluated only for $(k_1', k_2', k_1, k_2) = (k_F, -k_F, k_F, -k_F)$ as in (4.41), which yields the flow of g_t^Λ. For $\alpha = s2, s3, s4, t$ we obtain

$$\frac{\partial g_\alpha}{\partial \Lambda} = \frac{1}{4\pi^2} \sum_{\omega=\pm\Lambda} \int_0^{2\pi} \frac{dp}{2\pi}\, f_\alpha(p,\omega)\ , \tag{A.1}$$

with

$$\begin{aligned}
f_{s2}(p,\omega) =& \frac{(2P_s + U_s - 2\mu_0 U_s' \cos p)^2}{2(i\omega - \xi_p^0)(-i\omega - \xi_{-p}^0)} + \frac{(2U_s' + U_s - \mu_0(U_s' + P_s)\cos p)^2}{4(i\omega - \xi_p^0)^2} \\
&- \frac{(4-\mu_0^2)(U_s' - P_s)^2 \sin^2 p + 6(2+\mu_0\cos p) U_t'(2U_s' + U_s)}{4(i\omega - \xi_p^0)^2} \\
&+ \frac{6(2+\mu_0\cos p)\mu_0 U_t'(U_s' + P_s)\cos p - (4-\mu_0^2)(U_s' - P_s)\sin^2 p}{4(i\omega - \xi_p^0)^2} \\
&- \frac{3(2\cos p + \mu_0)^2 U_t'^2}{4(i\omega - \xi_p^0)^2} + \frac{((\mu_0^2-2)U_s' + U_s + 2(U_s' + P_s)\cos p)^2}{4(i\omega - \xi^0_{p-k_F})(i\omega - \xi^0_{p+k_F})} \\
&- \frac{6(\mu_0^2 - 2 - 2\cos p) U_t'((\mu_0^2-2)U_s' + U_s + 2(U_s' + P_s)\cos p)}{4(i\omega - \xi^0_{p-k_F})(i\omega - \xi^0_{p+k_F})} \\
&- \frac{3(\mu_0^2 - 2 - 2\cos p)^2 U_t'^2}{4(i\omega - \xi^0_{p-k_F})(i\omega - \xi^0_{p+k_F})}
\end{aligned} \tag{A.2}$$

$$
\begin{aligned}
f_{s3}(p,\omega) =& \frac{(2U_s' - U_s)^2 - 16U_s'^2 \sin^2 p}{2(i\omega - \xi^0_p)(-i\omega - \xi^0_{\pi-p})} - \frac{4(U_s' + P_s)^2 \sin^2 p - (2U_s' - U_s)^2}{2(i\omega - \xi^0_p)(i\omega - \xi^0_{\pi+p})} \\
& - \frac{6U_t'(2(U_s' + P_s)\sin^2 p - 2U_s' + U_s) + 6U_t'^2 \cos^2 p}{(i\omega - \xi^0_p)(i\omega - \xi^0_{\pi+p})}
\end{aligned} \tag{A.3}
$$

$$
\begin{aligned}
f_{s4}(p,\omega) =& \frac{(4U_s' \cos p + (\mu_0^2 - 2)P_s + U_s)^2}{2(i\omega - \xi^0_{p-k_F})(-i\omega - \xi^0_{p+k_F})} \\
& + \frac{(2U_s' + U_s - \mu_0(U_s' + P_s)\cos p + 2(U_s' - P_s)\sin p \sin k_F)^2}{2(i\omega - \xi^0_p)^2} \\
& - \frac{6(2 + \mu_0 \cos p - 2\sin p \sin k_F)(2U_s' + U_s - \mu_0(U_s' + P_s)\cos p)U_t'}{2(i\omega - \xi^0_p)^2} \\
& - \frac{12(2 + \mu_0 \cos p - 2\sin p \sin k_F)U_t'(U_s' - P_s)\sin p \sin k_F}{2(i\omega - \xi^0_p)^2} \\
& - \frac{3(2 + \mu_0 \cos p - 2\sin p \sin k_F)^2 U_t'^2}{2(i\omega - \xi^0_p)^2}
\end{aligned} \tag{A.4}
$$

$$
\begin{aligned}
f_t(p,\omega) =& \frac{2(4 - \mu_0^2)U_t'^2 \sin^2 p}{(i\omega - \xi^0_p)(-i\omega - \xi^0_{-p})} - \frac{(2U_s' + U_s - \mu_0(U_s' + P_s)\cos p)^2}{4(i\omega - \xi^0_p)^2} \\
& + \frac{(4 - \mu_0)(U_s' - P_s)^2 \sin^2 p - 2(2 + \mu_0 \cos p)(2U_s' + U_s)U_t'}{4(i\omega - \xi^0_p)^2} \\
& + \frac{2(\mu_0(2 + \mu_0 \cos p)(U_s' + P_s)\cos p - (4 - \mu_0^2)(U_s' - P_s)\sin^2 p)U_t'}{4(i\omega - \xi^0_p)^2} \\
& - \frac{5(\mu_0 + 2\cos p)^2}{4(i\omega - \xi^0_p)^2 U_t'^2} + \frac{((\mu_0^2 - 2)U_s' + U_s + 2(U_s' + P_s)\cos p)^2}{4(i\omega - \xi^0_{p-k_F})(i\omega - \xi^0_{p+k_F})} \\
& + \frac{2(\mu_0^2 - 2 - 2\cos p)((\mu_0^2 - 2)U_s' + U_s + 2(U_s' + P_s)\cos p)U_t'}{4(i\omega - \xi^0_{p-k_F})(i\omega - \xi^0_{p+k_F})} \\
& + \frac{5(\mu_0^2 - 2 - 2\cos p)^2 U_t'^2}{4(i\omega - \xi^0_{p-k_F})(i\omega - \xi^0_{p+k_F})} \,.
\end{aligned} \tag{A.5}
$$

Here $\xi_k^0 = -2\cos k - \mu_0$ with $\mu_0 = -2\cos k_F$ is the bare dispersion relation relative to the bare Fermi level. Since the functions $f_\alpha(p,\omega)$ can be written as rational functions of $\cos p$ and $\sin p$, the p-integral of Eq. (A.1) can be carried out analytically using the substitution $z = e^{ip}$ and the residue theorem, in analogy to the spinless case described in Sec. 4.2.3. The resulting differential equations for the momentum space couplings g_α^Λ read

$$\begin{aligned}
\frac{\partial g_{s2}}{\partial\Lambda} =& \frac{2({U'}_s^2 + P_s^2 - 3{U'}_t^2 + 6U'_sU'_t) + \mu_0^2(2{U'}_s^2 + U'_sP_s + 3P_sU'_t)}{4\pi} \\
&+ \mathrm{Re}\Big[\frac{\gamma(\Lambda)}{\pi(4-(\mu_0+i\Lambda)^2)}\Big(\frac{(2P_s+U_s+\mu_0(\mu_0+i\Lambda)U'_s)^2}{i\Lambda} \\
&+\frac{(\mu_0+i\Lambda)((2U'_s+U_s)^2+2\mu_0^2(U'_s+P_s)^2)+4\mu_0(2U'_s+U_s)(U'_s+P_s)}{2(4-(\mu_0+i\Lambda)^2)} \\
&-\frac{\mu_0^2(\mu_0+i\Lambda)^3(U'_s+P_s)^2+24(\mu_0+i\Lambda)(4U'_s+2U_s-\mu_0^2(U'_s+P_s))U'_t}{8(4-(\mu_0+i\Lambda)^2)} \\
&+\frac{12\mu_0(U_s-2P_s)U'_t-3((\mu_0+i\Lambda)(\mu_0^2+4)-8\mu_0){U'}_t^2}{2(4-(\mu_0+i\Lambda)^2)} \\
&-\frac{(\mu_0+i\Lambda)(((\mu_0^2-2)U'_s+U_s)^2+4(U'_s+P_s)^2)}{2((\mu_0+i\Lambda)^2-\mu_0^2)} \\
&-\frac{2\mu_0(U'_s+P_s)((\mu_0^2-2)U'_s+U_s)-6\mu_0((\mu_0^2-2)P_s-U_s)U'_t}{(\mu_0+i\Lambda)^2-\mu_0^2} \\
&+\frac{3(\mu_0+i\Lambda)((\mu_0^2-2)((\mu_0^2-2)U'_s+U_s)-4(U'_s+P_s))U'_t}{(\mu_0+i\Lambda)^2-\mu_0^2} \\
&+\frac{3((\mu_0+i\Lambda)((\mu_0^2-2)^2+4)-4\mu_0(\mu_0^2-2)){U'}_t^2}{2((\mu_0+i\Lambda)^2-\mu_0^2)}+(\mu_0+i\Lambda)({U'}_s^2+P_s^2) \\
&-\frac{(\mu_0+i\Lambda)(\mu_0^2(U'_s-P_s)^2-12\mu_0^2P_sU'_t-48U'_sU'_t+24{U'}_t^2)}{8}\Big)\Big]
\end{aligned} \tag{A.6}$$

$$\begin{aligned}
\frac{\partial g_{s3}}{\partial\Lambda} =& -\frac{4{U'}_s^2+(U'_s+P_s)(U'_s+P_s+6U'_t)-3{U'}_t^2}{2\pi} \\
&+\mathrm{Re}\Big[\frac{\gamma(\Lambda)}{\pi}\Big(\frac{4{U'}_s^2}{\mu_0}+\frac{(U'_s+P_s)(U'_s+P_s+6U'_t)}{\mu_0+i\Lambda}
\end{aligned}$$

$$
\begin{aligned}
&- \frac{(2U_s' - U_s)(2U_s' - U_s - 12U_t')}{4(\mu_0 + i\Lambda)} + \frac{3(\mu_0 + i\Lambda)U_t'^2}{4 - (\mu_0 + i\Lambda)^2} \\
&- \frac{4(2P_s - U_s)^2 + \mu_0(\mu_0 + i\Lambda)(2U_s' - U_s)(2U_s' - U_s - 12U_t')}{4\mu_0(4 - (\mu_0 + i\Lambda)^2)} \Big) \Big] \qquad \text{(A.7)}
\end{aligned}
$$

$$
\begin{aligned}
\frac{\partial g_{s4}}{\partial \Lambda} =& \frac{8U_s'^2 + (\mu_0^2 - 2)(U_s'^2 + P_s^2 - 3U_t'^2 + 6U_s'U_t') + 4U_s'P_s + 12P_sU_t'}{4\pi} \\
&+ \mathrm{Re}\Big[\frac{\gamma(\Lambda)}{\pi(4 - (\mu_0 + i\Lambda)^2)} \Big(2(\mu_0 + i\Lambda)P_s(U_s' + 3U_t') \\
&+ \frac{(\mu_0 + i\Lambda)(\mu_0^2 - 2)(U_s'^2 + P_s^2 - 3U_t'^2 + 6U_t'U_s')}{2} \\
&- \frac{((\mu_0^2 - 2)P_s + U_s + ((\mu_0 + i\Lambda)\mu_0 - 4i\gamma(\Lambda)\sin k_F)U_s')^2}{\mu_0\Lambda^2} \big(\mu_0(\mu_0 + i\Lambda) \\
&+ 4i\gamma(\Lambda)\sin k_F - 4\big) + \frac{(\mu_0 + i\Lambda)((2U_s' + U_s)^2 + \mu_0^2(U_s' + P_s)^2)}{4 - (\mu_0 + i\Lambda)^2} \\
&+ \frac{4\mu_0(2U_s' + U_s)(U_s' + P_s) - 6(\mu_0 + i\Lambda)(4U_s' + 2U_s - \mu_0^2(U_s' + P_s))U_t'}{4 - (\mu_0 + i\Lambda)^2} \\
&+ \frac{12\mu_0(U_s - 2P_s)U_t' - 3((\mu_0 + i\Lambda)(4 + \mu_0^2) - 8\mu_0)U_t'^2}{4 - (\mu_0 + i\Lambda)^2} \Big) \Big] \qquad \text{(A.8)}
\end{aligned}
$$

$$
\begin{aligned}
\frac{\partial g_t}{\partial \Lambda} =& \frac{(4 - \mu_0^2)(U_s'P_s - P_sU_t' - 2U_t'^2)}{4\pi} \\
&+ \mathrm{Re}\Big[\frac{\gamma(\Lambda)}{\pi(4 - (\mu_0 + i\Lambda)^2)} \Big(\frac{(\mu_0 + i\Lambda)(4 - \mu_0^2)P_s(U_s' - U_t')}{2} \\
&+ \frac{(4 - \mu_0^2)(4 - (\mu_0 + i\Lambda)^2)U_t'^2}{i\Lambda} - \frac{2\mu_0(2U_s' + U_s)(U_s' + P_s)}{(4 - (\mu_0 + i\Lambda)^2)} \\
&- \frac{(\mu_0 + i\Lambda)((2U_s' + U_s)^2 + \mu_0^2(U_s' + P_s)^2)}{2(4 - (\mu_0 + i\Lambda)^2)} \\
&- \frac{((\mu_0 + i\Lambda)(4U_s' + 2U_s - \mu_0^2(U_s' + P_s)) - 2\mu_0(U_s - 2P_s))U_t'}{4 - (\mu_0 + i\Lambda)^2}
\end{aligned}
$$

$$
\begin{aligned}
&- \frac{5((\mu_0+i\Lambda)(\mu_0^2+4)-8\mu_0)U_t'^2}{2(4-(\mu_0+i\Lambda)^2)} - \frac{(\mu_0+i\Lambda)((\mu_0^2-2)U_s'+U_s)^2}{2((\mu_0+i\Lambda)^2-\mu_0^2)} \\
&- \frac{2(\mu_0+i\Lambda)(U_s'+P_s)^2+2\mu_0(U_s'+P_s)((\mu_0^2-2)U_s'+U_s)}{(\mu_0+i\Lambda)^2-\mu_0^2} \\
&- \frac{(\mu_0+i\Lambda)((\mu_0^2-2)((\mu_0^2-2)U_s'+U_s)-4(U_s'+P_s))U_t'}{(\mu_0+i\Lambda)^2-\mu_0^2} \\
&- \frac{2\mu_0((\mu_0^2-2)P_s-U_s)U_t'}{(\mu_0+i\Lambda)^2-\mu_0^2} - \frac{5(\mu_0+i\Lambda)((\mu_0^2-2)^2+4)U_t'^2}{2((\mu_0+i\Lambda)^2-\mu_0^2)} \\
&+ \frac{10\mu_0(\mu_0^2-2)U_t'^2}{(\mu_0+i\Lambda)^2-\mu_0^2}\Big)\Big] ,
\end{aligned}
\tag{A.9}
$$

with

$$
\gamma(\Lambda) = \frac{(\mu_0+i\Lambda)}{2}\sqrt{1-\frac{4}{(\mu_0+i\Lambda)^2}} \, . \tag{A.10}
$$

Using the linear equations (4.48) and (4.50) to replace g_α by the renormalized real space interactions on the left-hand side of the flow equations, we obtain a complete set of flow equations for the four renormalized interactions U_t', U_s, U_s', and P_s of the form (4.54).

A.2 One-loop g-ology calculation

In the low-energy limit the flow of the two-particle vertex Γ^Λ, as described in Sec. A.1, reduces to the one-loop flow of the g-ology model, the general effective low-energy model for one-dimensional fermions [Sólyom 1979]. In the g-ology approach interaction processes are classified into backward scattering ($g_{1\perp}$), forward scattering involving electrons from opposite Fermi points ($g_{2\perp}$), from the same Fermi points ($g_{4\perp}$), and umklapp scattering ($g_{3\perp}$). All further momentum dependences of the vertex are discarded.

The g-ology couplings are related to the momentum space couplings g_{s2}, g_{s3}, g_{s4} and g_t by

$$
g_{1\perp} = \frac{1}{2}(g_{s2} - g_t)
$$

$$
g_{2\perp} = \frac{1}{2}(g_{s2} + g_t)
$$

$$g_{3\perp} = \frac{g_{s3}}{2}$$
$$g_{4\perp} = \frac{g_{s4}}{2} \tag{A.11}$$

and to the real space couplings by

$$g_{1\perp} = \frac{1}{2}(\mu_0^2\Gamma_{s2} + 2\Gamma_{s3} + \Gamma_{s4} - (4-\mu_0^2)\Gamma_t)$$
$$g_{2\perp} = \frac{1}{2}(\mu_0^2\Gamma_{s2} + 2\Gamma_{s3} + \Gamma_{s4} + (4-\mu_0^2)\Gamma_t)$$
$$g_{3\perp} = \frac{1}{2}(-4\Gamma_{s2} - 2\Gamma_{s3} + \Gamma_{s4})$$
$$g_{4\perp} = \frac{1}{2}(4\Gamma_{s2} - (2-\mu_0^2)\Gamma_{s3} + \Gamma_{s4}) \tag{A.12}$$

respectively.

The flow equation for Γ^Λ (4.51) reduces to the standard one-loop g-ology calculation [Sólyom 1979], once the dependence on the internal momentum p on the right-hand side of the flow equation is neglected. Applying the above parametrization, we obtain a complete set of flow equations for $g_{i\perp}$ for $i = 1, \ldots, 4$ of the form

$$\frac{\partial g_{1\perp}}{\partial\Lambda} = \frac{1}{2\pi}\left[\, g_{1\perp}g_{2\perp}PP(0) + g_{1\perp}g_{4\perp}PH(0) + 2g_{1\perp}(g_{2\perp}-g_{1\perp})PH(2k_F)\,\right]$$
$$\frac{\partial g_{2\perp}}{\partial\Lambda} = \frac{1}{2\pi}\left[\, \frac{1}{2}(g_{1\perp}^2+g_{2\perp}^2)PP(0) + g_{4\perp}(g_{1\perp}-g_{2\perp})PH(0) + g_{2\perp}^2PH(2k_F)\,\right]$$
$$\frac{\partial g_{3\perp}}{\partial\Lambda} = \frac{1}{2\pi}\left[\, g_{3\perp}g_{4\perp}PP(\pi) + g_{3\perp}(2g_{2\perp}-g_{1\perp})PH(\pi)\,\right]$$
$$\frac{\partial g_{4\perp}}{\partial\Lambda} = \frac{1}{2\pi}\left[\, g_{4\perp}^2PP(2k_F) + \frac{1}{2}(g_{1\perp}^2+2g_{1\perp}g_{2\perp}-2g_{2\perp}^2+g_{4\perp}^2)PH(0)\,\right], \tag{A.13}$$

where

$$PP(q) = \frac{1}{2\pi}\sum_{\omega=\pm\Lambda}\int_0^{2\pi}\frac{dp}{2\pi}\,\frac{1}{i\omega-\xi_{p+q/2}}\,\frac{1}{-i\omega-\xi_{-p+q/2}}$$
$$PH(q) = \frac{1}{2\pi}\sum_{\omega=\pm\Lambda}\int_0^{2\pi}\frac{dp}{2\pi}\,\frac{1}{i\omega-\xi_{p+q/2}}\,\frac{1}{i\omega-\xi_{p-q/2}}\,. \tag{A.14}$$

The initial conditions are $g_{1\perp}^{\Lambda_0} = g_{3\perp}^{\Lambda_0} = U + (\mu_0^2-2)U'$ and $g_{2\perp}^{\Lambda_0} = g_{4\perp}^{\Lambda_0} = U + 2U'$. The integrals in Eq. (A.14) can be computed analytically using the residue theorem,

as discussed in Sec. A.1; for $q = 0$ and $q = 2k_F$ we obtain

$$\begin{aligned} PP(0) &= -\frac{4}{\Lambda}\,\mathrm{Re}\Big(\frac{i\gamma(\Lambda)}{4-(\mu_0+i\Lambda)^2}\Big) \\ PH(0) &= 4\,\mathrm{Re}\Big(\frac{(\mu_0+i\Lambda)\gamma(\Lambda)}{(4-(\mu_0+i\Lambda)^2)^2}\Big) \\ PP(2k_F) &= -\frac{4}{\mu_0}\,\mathrm{Re}\Big(\frac{\gamma(\Lambda)}{(4-(\mu_0+i\Lambda)^2)(4-\mu_0(\mu_0+i\Lambda)+4i\gamma(\Lambda)\sin k_F)}\Big) \\ PH(2k_F) &= 4\,\mathrm{Re}\Big(\frac{(\mu_0+i\Lambda)\gamma(\Lambda)}{(4-(\mu_0+i\Lambda)^2)(\mu_0^2-(\mu_0+i\Lambda)^2)}\Big)\,, \end{aligned} \tag{A.15}$$

where $\gamma(\Lambda)$ is defined by Eq. (A.10).

For $\mu \neq 0$ the above equations reduce to

$$\begin{aligned} PP(0) &= \frac{2}{\Lambda\sqrt{4-\mu_0^2}} \\ PH(0) &= -\frac{4(2+\mu_0^2)\Lambda}{(\sqrt{4-\mu_0^2})^5} \\ PP(2k_F) &= \frac{8\Lambda}{(\sqrt{4-\mu_0^2})^5} \\ PH(2k_F) &= -\frac{1}{\Lambda\sqrt{4-\mu_0^2}} \end{aligned} \tag{A.16}$$

in the limit $\Lambda \to 0$. The resulting flow equations in the low-energy limit are

$$\begin{aligned} \frac{\partial g_{1\perp}}{\partial\Lambda} &= \frac{g_{1\perp}^2}{\Lambda\pi\sqrt{4-\mu_0^2}} \\ \frac{\partial g_{2\perp}}{\partial\Lambda} &= \frac{g_{1\perp}^2}{2\Lambda\pi\sqrt{4-\mu_0^2}} \end{aligned} \tag{A.17}$$

for $g_{1\perp}$ and $g_{2\perp}$, whereas the flow for $g_{3\perp}$ and $g_{4\perp}$ vanishes. The solution reads

$$\begin{aligned} g_{1\perp}^{\Lambda} &= \frac{U+(\mu_0^2-2)U'}{1+\frac{U+(\mu_0^2-2)U'}{\pi\sqrt{4-\mu_0^2}}\ln\frac{\Lambda}{\Lambda_0}} \\ g_{2\perp}^{\Lambda} &= \frac{1}{2}\Big(\frac{U+(\mu_0^2-2)U'}{1+\frac{U+(\mu_0^2-2)U'}{\pi\sqrt{4-\mu_0^2}}\ln\frac{\Lambda}{\Lambda_0}} + U + (6-\mu_0^2)U'\Big)\,, \end{aligned} \tag{A.18}$$

yielding the fixed-point couplings $g_{1\perp} = 0$, $g_{2\perp} = \frac{1}{2}(U + (6-\mu_0^2)U')$, and $g_{3\perp} = U + (\mu_0^2-2)U'$, $g_{4\perp} = U + 2U'$.

B Bethe-ansatz calculation of K_ρ for the Hubbard model

The Luttinger-liquid parameter K_ρ can be evaluated exactly from the Bethe ansatz solution for the one-dimensional Hubbard model [Lieb and Wu 1968]. The Bethe ansatz provides the energies of the ground and excited states as solution of specific integral equations.

In the description of critical properties the "dressed charge matrix" is introduced [Frahm and Korepin 1990]. This 2×2 matrix contains the effective renormalized coupling constants within and between the low-energy charge and spin sectors of the Hilbert space of the Hubbard model, and therefore directly determines all critical exponents. It is defined as

$$Z = \begin{pmatrix} Z_{cc} & Z_{cs} \\ Z_{sc} & Z_{ss} \end{pmatrix} . \tag{B.1}$$

In the absence of a magnetic field, Z is completely determined by its first element Z_{cc} as

$$Z = \begin{pmatrix} \xi(k_0) & 0 \\ \frac{\xi(k_0)}{2} & \frac{1}{\sqrt{2}} \end{pmatrix} , \tag{B.2}$$

where k_0 is a cutoff determined by the particle density n [Frahm and Korepin 1990].

$\xi(k)$ obeys the integral equation

$$\xi(k) = 1 + \frac{4}{U} \int_{-k_0}^{k_0} \cos k' \, R\Big(\frac{4}{U} (\sin k - \sin k') \Big) \, \xi(k') \, dk' , \tag{B.3}$$

with the kernel

$$R(x) = \frac{1}{2\pi} \int_0^\infty \frac{\cos(\frac{xy}{2})}{1 + e^y} \, dy . \tag{B.4}$$

The cutoff momentum k_0 is defined by

$$\int_{-k_0}^{k_0} \rho(k') \, dk' = n , \tag{B.5}$$

where the integral equation for the ground-state charge distribution function $\rho(k)$ reads

$$\rho(k) = \frac{1}{2\pi} + \frac{4}{U}\cos k \int_{-k_0}^{k_0} R\left(\frac{4}{U}\left(\sin k - \sin k'\right)\right)\rho(k')\,dk' \tag{B.6}$$

in the limit $L \to \infty$.

The compressibility κ is related to the dressed charge matrix element $\xi(k_0)$ by $\xi^2(k_0) = \pi v_\rho \kappa$, where v_ρ is the charge velocity [Frahm and Korepin 1990]. On the other hand, the Luttinger-liquid parameter K_ρ is given by $K_\rho = \pi v_\rho \kappa/2$. Hence K_ρ is determined by

$$K_\rho = \frac{\xi^2(k_0)}{2} \; . \tag{B.7}$$

Solving the integral equation for $\xi(k_0)$ with k_0 determined from equations (B.5) and (B.6), yields the exact Luttinger-liquid parameter. For the numerical computation of the kernel $R(x)$ defined in Eq. (B.4), the following expression is more convenient

$$R(x) = \frac{1}{\pi}\sum_{l=1}^{\infty}(-1)^{l+1}\frac{2l}{x^2 + (2l)^2} \; . \tag{B.8}$$

Similarly the chemical potential μ is determined. A comparison of the fRG results with the exact results allows a quantitative estimate of the effect due to the neglected frequency dependence of the two-particle vertex. The chemical potential can be derived from the ground-state energy via

$$\mu = \frac{\partial \epsilon}{\partial n} = \frac{\partial \epsilon}{\partial k_0}\left(\frac{\partial n}{\partial k_0}\right)^{-1} , \tag{B.9}$$

where the energy per lattice site is given by

$$\epsilon(k) = -2\int_{-k_0}^{k_0} \cos k\, \rho(k)\, dk \; . \tag{B.10}$$

Using equations (B.5) and (B.6), the solution of the following integral equations

$$\begin{aligned} \frac{\partial \epsilon}{\partial k_0} &= -4\rho(k_0)\cos k_0 - 2\int_{-k_0}^{k_0} \cos k\, \frac{\partial \rho(k)}{\partial k_0}\, dk \\ \frac{\partial n}{\partial k_0} &= 2\rho(k_0) + \int_{-k_0}^{k_0} \frac{\partial \rho(k)}{\partial k_0}\, dk \; , \end{aligned} \tag{B.11}$$

with

$$\frac{\partial\rho(k)}{\partial k_0} = \frac{4}{U}\,\rho(k_0)\cos k\,\Big[\,R\Big(\frac{4}{U}\,(\sin k - \sin k_0)\Big) \;+\; R\Big(\frac{4}{U}\,(\sin k + \sin k_0)\Big)\,\Big]$$
$$+\,\frac{4}{U}\cos k\int_{-k_0}^{k_0} R\Big(\frac{4}{U}\,(\sin k - \sin k')\Big)\,\frac{\partial\rho(k')}{\partial k_0}\,dk' \qquad \text{(B.12)}$$

provides the exact chemical potential.

Analogous expressions can be derived for the spinless fermion model [Haldane 1980].

Bibliography

The electronic PDF file contains links to the online `arXiv` and journal references.

S. Andergassen, T. Enss, and V. Meden, *Kondo physics in transport through a quantum dot with Luttinger liquid leads*, `cond-mat/0509576`.

S. Andergassen, T. Enss, V. Meden, W. Metzner, U. Schollwöck, and K. Schönhammer, *Functional renormalization group for Luttinger liquids with impurities*, Phys. Rev. B **70**, 075102 (2004), `cond-mat/0403517`.

S. Andergassen, T. Enss, V. Meden, W. Metzner, U. Schollwöck, and K. Schönhammer, *Renormalization group analysis of the one-dimensional extended Hubbard model with a single impurity*, `cond-mat/0509021`.

W. Apel and T. M. Rice, *Combined effect of disorder and interaction on the conductance of a one-dimensional fermion system*, Phys. Rev. B **26**, R7063 (1982).

O. M. Auslaender and S. Fishman, *Correlations in the Adiabatic Response of Chaotic Systems*, Phys. Rev. Lett. **84**, 1886 (2000).

X. Barnabé-Thériault, A. Sedeki, V. Meden, and K. Schönhammer, *A junction of three quantum wires: restoring time-reversal symmetry by interaction*, Phys. Rev. Lett. **94**, 136405 (2005a), `cond-mat/0411612`.

X. Barnabé-Thériault, A. Sedeki, V. Meden, and K. Schönhammer, *Junctions of one-dimensional quantum wires - correlation effects in transport*, Phys. Rev. B **71**, 205327 (2005b), `cond-mat/0501742`.

G. Baym and L. P. Kadanoff, *Conservation Laws and Correlation Functions*, Phys. Rev. **124**, 287 (1961).

G. Benfatto and G. Gallavotti, *Perturbation Theory of the Fermi Surface in a Quantum Liquid. A General Quasiparticle Formalism and One-Dimensional Systems*, J. Stat. Phys. **59**, 541 (1990).

M. Bockrath, D. H. Cobden, J. Lu, A. G. Rinzler, R. Smalley, L. Balents, and P. L. Mceuen, *Luttinger-liquid behaviour in carbon nanotubes*, Nature **397**, 598 (1999).

R. T. Clay, A. W. Sandvik, and D. K. Campbell, *Possible exotic phases in the one-dimensional extended Hubbard model*, Phys. Rev. B **59**, 4665 (1999).

A. Cohen, K. Richter, and R. Berkovits, *Spin and interaction effects on charge distribution and currents in one-dimensional conductors and rings within the Hartree-Fock approximation*, Phys. Rev. B **57**, 6223 (1998), `cond-mat/9804018`.

S. Datta, *Electronic Transport in Mesoscopic Systems*, Cambridge University Press, Cambrigde, 1995.

I. E. Dzyaloshinskii and A. I. Larkin, *Correlation functions for a one-dimensional fermi system with long-range interaction (Tomonaga model)*, Zh. Eksp. Teor. Fiz. **65**, 411 (1973), [Sov. Phys. JETP 38, 202 (1974)].

R. Egger and A. O. Gogolin, *Effective Low-Energy Theory for Correlated Carbon Nanotubes*, Phys. Rev. Lett. **79**, 5082 (1997), `cond-mat/9708065`.

R. Egger and H. Grabert, *Friedel Oscillations for Interacting Fermions in One Dimension*, Phys. Rev. Lett. **75**, 3505 (1995), `cond-mat/9509100`.

S. Eggert and I. Affleck, *Magnetic impurities in half-integer-spin Heisenberg antiferromagnetic chains*, Phys. Rev. B **46**, 10866 (1992).

S. Ejima, F. Gebhard, and S. Nishimoto, *Tomonaga-Luttinger parameters for doped Mott insulators*, Europhys. Lett. **70**, 492 (2005), `cond-mat/0507508`, private communication.

T. Enss, *Renormalization, Conservation Laws and Transport in Correlated Electron Systems*, PhD thesis, University of Stuttgart, Germany, 2005, `cond-mat/0504703`.

T. Enss, V. Meden, S. Andergassen, X. Barnabé-Thériault, W. Metzner, and K. Schönhammer, *Impurity and correlation effects on transport in one-dimensional quantum wires*, Phys. Rev. B **71**, 155401 (2005), `cond-mat/0411310`.

J. Feldman and E. Trubowitz, *Perturbation Theory for Many Fermion Systems*, Helv. Phys. Acta **63**, 156 (1990).

P. Fendley, A. W. W. Ludwig, and H. Saleur, *Exact Conductance through Point Contacts in the $\nu = 1/3$ Fractional Quantum Hall Effect*, Phys. Rev. Lett. **74**, 3005 (1995), `cond-mat/9408068`.

H. Frahm and V. E. Korepin, *Critical exponents for the one-dimensional Hubbard model*, Phys. Rev. B **42**, 10553 (1990).

A. Furusaki, *Resonant tunneling through a quantum dot weakly coupled to quantum wires or quantum Hall edge states*, Phys. Rev. B **57**, 7141 (1998), `cond-mat/9712054`.

A. Furusaki, *Kondo Problems in Tomonaga-Luttinger liquids*, J. Phys. Soc. Jpn. **74**, 73 (2005), `cond-mat/0409016`.

A. Furusaki and N. Nagaosa, *Resonant tunneling in a Luttinger liquid*, Phys. Rev. B **47**, 3827 (1993a).

A. Furusaki and N. Nagaosa, *Single-barrier problem and Anderson localization in a one-dimensional interacting electron system*, Phys. Rev. B **47**, 4631 (1993b).

A. Furusaki and N. Nagaosa, *Tunneling through a barrier in a Tomonaga-Luttinger liquid connected to reservoirs*, Phys. Rev. B **54**, R5239 (1996), `cond-mat/9604193`.

U. Gerland, J. von Delft, T. A. Costi, and Y. Oreg, *Transmission Phase Shift of a Quantum Dot with Kondo Correlations*, Phys. Rev. Lett. **84**, 3710 (2000), `cond-mat/9909401`.

T. Giamarchi, *Quantum Physics in One Dimension*, Oxford University Press, New York, 2004.

T. Giamarchi and H. J. Schulz, *Anderson localization and interactions in one-dimensional metals*, Phys. Rev. B **37**, 325 (1988).

L. I. Glazman and M. É. Raikh, *Resonant Kondo transparency of a barrier with quasilocal impurity states*, JETP Lett. **47**, 452 (1988).

C. J. Halboth and W. Metzner, *Renormalization group analysis of the 2D Hubbard model*, Phys. Rev. B **61**, 7364 (2000), `cond-mat/9908471`.

F. D. M. Haldane, *General Relation of Correlation Exponents and Spectral Properties of One-Dimensional Fermi Systems: Application to the Anisotropic $S = 1/2$ Heisenberg Chain*, Phys. Rev. Lett. **45**, 1358 (1980).

F. D. M. Haldane, *Effective Harmonic-Fluid Approach to Low-Energy Properties of One-Dimensional Quantum Fluids*, Phys. Rev. Lett. **47**, 1840 (1981a).

F. D. M. Haldane, *'Luttinger liquid theory' of one-dimensional quantum fluids. I. Properties of the Luttinger model and their extension to the general 1D interacting spinless Fermi gas*, J. Phys. C **14**, 2585 (1981b).

A. Hewson, *The Kondo Problem to Heavy Fermions*, Cambridge University Press, Cambridge, 1993.

C. Honerkamp, D. Rohe, S. Andergassen, and T. Enss, *Interaction flow method for many-fermion systems*, Phys. Rev. B **70**, 235115 (2004), `cond-mat/0403633`.

C. Honerkamp and M. Salmhofer, *The temperature-flow renormalization group and the competition between superconductivity and ferromagnetism*, Phys. Rev. B **64**, 184516 (2001), `cond-mat/0105218`.

C. Honerkamp, M. Salmhofer, N. Furukawa, and T. M. Rice, *Breakdown of the Landau-Fermi liquid in Two Dimensions due to Umklapp Scattering*, Phys. Rev. B **63**, 035109 (2001), `cond-mat/9912358`.

A. P. Kampf and A. A. Katanin, *Competing phases in the extended U-V-J Hubbard model near the Van Hove fillings*, Phys. Rev. B **67**, 125104 (2003), `cond-mat/0212190`.

C. Kane, L. Balents, and M. P. A. Fisher, *Coulomb Interactions and Mesoscopic Effects in Carbon Nanotubes*, Phys. Rev. Lett. **79**, 5086 (1997), `cond-mat/9708054`.

C. L. Kane and M. P. A. Fisher, *Resonant tunneling in an interacting one-dimensional electron gas*, Phys. Rev. B **46**, 7268 (1992a).

C. L. Kane and M. P. A. Fisher, *Transmission through barriers and resonant tunneling in an interacting one-dimensional electron gas*, Phys. Rev. B **46**, 15233 (1992b).

C. L. Kane and M. P. A. Fisher, *Transport in a one-channel Luttinger liquid*, Phys. Rev. Lett. **68**, 1220 (1992c).

N. Kawakami and S.-K. Yang, *Luttinger anomaly exponent of momentum distribution in the Hubbard chain*, Phys. Lett. A **148**, 359 (1990).

G. Keller, C. Kopper, and M. Salmhofer, *Perturbative renormalization and effective Lagrangians in φ^4 in four dimensions*, Helv. Phys. Acta **65**, 32 (1992).

E. H. Lieb and F. Y. Wu, *Absence of Mott Transition in an Exact Solution of the Short-Range, One-Band Model in One Dimension*, Phys. Rev. Lett. **135**, A1505 (1968).

A. Luther and I. Peschel, *Single-particle states, Kohn anomaly, and pairing fluctuations in one dimension*, Phys. Rev. B **9**, 2911 (1974).

J. M. Luttinger, *An exactly soluble model of a many-fermion system*, J. Math. Phys. **4**, 1154 (1963).

G. D. Mahan, *Many-particle physics*, Kluwer Academic Publishers, New York, 3. edition, 2000.

D. C. Mattis, *New wave-operator identity applied to the study of persistent currents in 1D*, J. Math. Phys. **15**, 609 (1974).

D. C. Mattis and E. H. Lieb, *Exact solution of a many-fermion system and its associated boson field*, J. Math. Phys. **6**, 304 (1965).

K. A. Matveev, D. Yue, and L. I. Glazman, *Tunneling in one-dimensional non-Luttinger electron liquid*, Phys. Rev. Lett. **71**, 3351 (1993), `cond-mat/9306041`.

V. Meden, S. Andergassen, W. Metzner, U. Schollwöck, and K. Schönhammer, *Scaling of the conductance in a quantum wire*, Europhys. Lett. **64**, 769 (2003), `cond-mat/0303460`.

V. Meden, T. Enss, S. Andergassen, W. Metzner, and K. Schönhammer, *Correlation effects on resonant tunneling in one-dimensional quantum wires*, Phys. Rev. B **71**, 041302(R) (2005), `cond-mat/0403655`.

V. Meden, W. Metzner, U. Schollwöck, O. Schneider, T. Stauber, and K. Schönhammer, *Luttinger liquids with boundaries: Power-laws and energy scales*, Eur. Phys. J. B **16**, 631 (2000), `cond-mat/0002215`.

V. Meden, W. Metzner, U. Schollwöck, and K. Schönhammer, *Scaling behavior of impurities in mesoscopic Luttinger liquids*, Phys. Rev. B **65**, 045318 (2002a), `cond-mat/0104336`.

V. Meden, W. Metzner, U. Schollwöck, and K. Schönhammer, *A single impurity in a Luttinger liquid: How it "cuts" the chain*, J. Low Temp. Phys. **126**, 1147 (2002b), `cond-mat/0109013`.

V. Meden, P. Schmitteckert, and N. Shannon, *Orthogonality catastrophe in a one-dimensional system of correlated electrons*, Phys. Rev. B **57**, 8878 (1998), cond-mat/9707082.

V. Meden and U. Schollwöck, *The conductance of interacting nano-wires*, Phys. Rev. B **67**, 193303 (2003a), cond-mat/0210515.

V. Meden and U. Schollwöck, *Persistent currents in mesoscopic rings: A numerical and renormalization group study*, Phys. Rev. B **67**, 035106 (2003b), cond-mat/0209588.

Y. Meir and N. S. Wingreen, *Landauer formula for the current through an interacting electron region*, Phys. Rev. Lett. **68**, 2512 (1992).

W. Metzner, C. Castellani, and C. Di Castro, *Fermi Systems with Strong Forward Scattering*, Advances in Physics **47**, 317 (1998), cond-mat/9701012.

W. Metzner and C. Di Castro, *Conservation laws and correlation functions in the Luttinger liquid*, Phys. Rev. B **47**, 16107 (1993).

K. Moon, H. Yi, C. L. Kane, S. M. Girvin, and M. P. A. Fisher, *Resonant tunneling between quantum Hall edge states*, Phys. Rev. Lett. **71**, 4381 (1993), cond-mat/9304010.

T. R. Morris, *The Exact Renormalisation Group and Approximate Solutions*, Int. J. Mod. Phys. A **9**, 2411 (1994), hep-ph/9308265.

Y. V. Nazarov and L. I. Glazman, *Resonant Tunneling of Interacting Electrons in a One-Dimensional Wire*, Phys. Rev. Lett. **91**, 126804 (2003), cond-mat/0209090.

J. W. Negele and H. Orland, *Quantum Many-Particle Systems*, Addison-Wesley, Reading, 1987.

T. K. Ng and P. A. Lee, *On-site Coulomb repulsion and resonant tunneling*, Phys. Rev. Lett. **61**, 1768 (1988).

A. Oguri, *Transmission Probability for Interacting Electrons Connected to Reservoirs*, J. Phys. Soc. Jpn **70**, 2666 (2001), cond-mat/0106033.

R. D. Picciotto, H. L. Stormer, L. N. Pfeiffer, K. W. Baldwin, and K. W. West, *Four-terminal resistance of a ballistic quantum wire*, Nature **411**, 51 (2001).

J. Polchinski, *Renormalization and effective lagrangians*, Nucl. Phys. B **231**, 269 (1984).

D. G. Polyakov and I. V. Gornyi, *Transport of interacting electrons through a double barrier in quantum wires*, Phys. Rev. B **68**, 035421 (2003), `cond-mat/0212355`.

M. Salmhofer, *Continuous Renormalization for Fermions and Fermi Liquid Theory*, Commun. Math. Phys. **194**, 249 (1998), `cond-mat/9706188`.

M. Salmhofer, *Renormalization. An Introduction*, Springer, Berlin, 1999.

M. Salmhofer and C. Honerkamp, *Fermionic renormalization group flows: Technique and theory*, Prog. Theor. Phys. **105**, 1 (2001).

K. Schönhammer, *Luttinger liquids: the basic concepts*, In D. Baeriswyl and L. Degiorgi, editors, *Strong Interactions in Low Dimensions*, Kluwer Academic Publishers, 2004, `cond-mat/0305035`.

K. Schönhammer, V. Meden, W. Metzner, U. Scholl-wöck, and O. Gunnarsson, *Boundary effects on one-particle spectra of Luttinger liquids*, Phys. Rev. B **61**, 4393 (2000), `cond-mat/9903121`.

H. J. Schulz, *Correlation exponents and the metal-insulator transition in the one-dimensional Hubbard model*, Phys. Rev. Lett. **64**, 2831 (1990).

F. Schütz, L. Bartosch, and P. Kopietz, *Collective fields in the functional renormalization group for fermions, Ward identities, and the exact solution of the Tomonaga-Luttinger model*, Phys. Rev. B **72**, 035107 (2004), `cond-mat/0409404`.

R. Shankar, *Renormalization group for interacting fermions in d ¿ 1*, Physica A **177**, 530 (1991).

R. Shankar, *Renormalization-group approach to interacting fermions*, Reviews of Modern Physics **66**, 129 (1994), `cond-mat/9307009`.

J. Sólyom, *The Fermi gas model of one-dimensional conductors*, Adv. Phys. **28**, 201 (1979).

K. M. Tam, S. W. Tsai, and D. K. Campbell, *Functional Renormalization Group Analysis of the Half-filled One-dimensional Extended Hubbard Model*, `cond-mat/0505396`.

J. R. Taylor, *Scattering theory*, John Wiley and Sons, New York, 1972.

S. Tomonaga, *Remarks on Blochs method of sound waves applied to many-fermion problems*, Prog. Theor. Phys. **5**, 544 (1950).

J. Voit, *One-Dimensional Fermi liquids*, Rep. Prog. Phys. **58**, 977 (1995), `cond-mat/9510014`.

F. J. Wegner and A. Houghton, *Renormalization Group Equation for Critical Phenomena*, Phys. Rev. A **8**, 401 (1973).

S. Weinberg, *Critical phenomena for field theorists*, Erice Subnucl. Phys., 1 (1976).

U. Weiss, *Quantum Dissipative Systems*, World Scientific, Singapore, 2. edition, 1999, and references therein.

C. Wetterich, *Exact evolution equation for the effective potential*, Phys. Lett. B **301**, 90 (1993).

C. Wieczerkowski, *Symanzik improved actions from the viewpoint of the renormalization-group*, Commun. Math. Phys. **120**, 149 (1988).

K. J. Wiese, *The Functional Renormalization Group Treatment of Disordered Systems: a Review*, `cond-mat/0302322`.

K. G. Wilson, *Renormalization Group and Critical Phenomena. II. Phase-Space Cell Analysis of Critical Behavior*, Phys. Rev. B **4**, 3184 (1971).

K. G. Wilson and J. Kogut, *The renormalization group and the ϵ expansion*, Phys. Rep. **12**, 75 (1974).

C. N. Yang and C. P. Yang, *One-Dimensional Chain of Anisotropic Spin-Spin Interactions. I.+II.*, Phys. Rev. **150**, 321 (1966).

Z. Yao, H. W. C. Postma, L. Balents, and C. Dekker, *Carbon nanotube intramolecular junctions*, Nature **402**, 273 (1999).

D. Yue, L. I. Glazman, and K. A. Matveev, *Conduction of a weakly interacting one-dimensional electron gas through a single barrier*, Phys. Rev. B **49**, 1966 (1994).

D. Zanchi and H. J. Schulz, *Weakly correlated electrons on a square lattice: A renormalization group theory*, Europhys. Lett. **44**, 235 (1998), `cond-mat/9703189`.

D. Zanchi and H. J. Schulz, *Weakly correlated electrons on a square lattice: Renormalization-group theory*, Phys. Rev. B **61**, 13609 (2000), `cond-mat/9812303`.

J. Zinn-Justin, *Quantum Field Theory and Critical Phenomena*, Clarendon Press, Oxford, 4. edition, 2002.

Deutsche Zusammenfassung

Eindimensionale metallische Elektronensysteme zeichnen sich durch ausgeprägte Wechselwirkungseffekte aus. Im Unterschied zum üblichen Fermiflüssigkeitsverhalten wird das generische Niederenergieverhalten eindimensionaler Fermisysteme mit repulsiver Wechselwirkung durch die Luttingerflüssigkeitsphänomenologie beschrieben [Giamarchi 2004], die auf dem exakt lösbaren Luttingermodell beruht und durch ungewöhnliche Potenzgesetze in den Korrelationsfunktionen gekennzeichnet ist. Die Niederenergiephysik ist von einigen wenigen wechselwirkungsabhängigen Parametern, die in die Exponenten der Potenzgesetze eingehen, vollständig bestimmt, für spinrotationsinvariante Systeme einzig vom Luttingerflüssigkeitsparameter K_ρ.

Ein wichtiger Aspekt betrifft den Einfluß von Störstellen im Wechselspiel mit Wechselwirkungseffekten. Im Niederenergielimes teilt bereits eine einzelne schwache Störstelle das System effektiv in zwei, und die physikalischen Eigenschaften sind vom Randfixpunkt bestimmt [Kane and Fisher 1992a,c; Luther and Peschel 1974; Mattis 1974; Apel and Rice 1982; Giamarchi and Schulz 1988]. Das effektive Störstellenpotential weist langreichweitige Oszillationen auf, die zur charakteristischen Unterdrückung der lokalen Zustandsdichte an der Störstelle und des Leitwerts im Niederenergielimes führen. Das asymptotische Verhalten ist durch Potenzgesetze mit K_ρ-abhängigen Exponenten gekennzeichnet, die Details der Störstelle gehen nicht ein. Zwei-Teilchen-Rückstreuung führt im Allgemeinen zu logarithmischen Korrekturen der Potenzgesetze.

Die *asymptotischen* Eigenschaften von Luttingerflüssigkeiten mit einer einzelnen Störstelle sind weitgehend bekannt. Universelle Potenzgesetze und Skalenfunktionen wurden im Rahmen der Bosonisierung, konformer Feldtheorie und exakter Lösungen spezieller integrabler Systeme für die Niederenergieasymptotik bestimmt [Giamarchi 2004]. Numerische Methoden wie exakte Diagonalisierung und die Dichtematrixrenormierungsgruppe (DMRG) bestätigen die feldtheoretischen Vorhersagen und die Gültigkeit der diesen zugrunde liegenden Annahmen für mikroskopische Fermisysteme mit Luttingerflüssigkeitsverhalten. Die Begrenzung numerischer Methoden in der Systemgröße ermöglicht allerdings ausschließlich eine Untersuchung der perturbativ

zugänglichen Regimes schwacher und starker Störstellenpotentiale. Die Frage nach der *Skala*, auf der die Asymptotik einsetzt, und dem Gültigkeitsbereich asymptotischer Potenzgesetze kann damit nicht vollständig beantwortet werden. Diese Skala kann erstaunlich klein sein, und die Eigenschaften darüber sehr unterschiedlich vom asymptotischen Verhalten.

In den letzten Jahren wurde die funktionale Renormierungsgruppenmethode (fRG) zur direkten Untersuchung *mikroskopischer* Modelle von wechselwirkenden Fermionen eingeführt, die neben der korrekten Beschreibung der universellen Niederenergieasymptotik die Berechnung von Observablen auf sämtlichen Energieskalen ermöglicht. Dies erlaubt die Untersuchung *nichtuniverseller* Eigenschaften und einen möglichen Schlüssel zum Verständnis des Verhaltens auf mittleren Skalen, die in Experimenten zugänglich sind. Einige der nichtuniversellen Eigenschaften können numerisch mit der DMRG bestimmt werden, diese Methode ist jedoch auf Systemgrößen mit bis zu 1000 Gitterplätzen beschränkt und nur eine beschränkte Auswahl an Observablen kann zuverlässig berechnet werden.

Die fRG bietet einen effizienten Ansatz zur Untersuchung wechselwirkender Fermisysteme, insbesondere für niederdimensionale Systeme mit konkurrierenden Instabilitäten und verschränkten Infrarotsingularitäten. Ausgangspunkt ist eine exakte Hierarchie gekoppelter Differentialgleichungen für die Green oder Vertexfunktionen des Systems, die die graduelle Entwicklung vom mikroskopischen Modell zur effektiven Niederenergiewirkung als Funktion der Energie beschreiben [Salmhofer 1998]. Näherungen entstehen durch das Abschneiden der Hierarchie und der Parametrisierung der Vertexfunktionen mit einer überschaubaren Anzahl von Variablen oder Funktionen. Die fRG erfaßt sowohl universelle Potenzgesetze im Niederenergiebereich, als auch relevante Energieskalen und nichtuniverselle Crossoverphänomene auf mittleren Skalen, wie zum Beispiel für die Temperaturabhängigkeit des Leitwerts einer Doppelbarriere [Enss et al. 2005; Meden et al. 2005].

Der fRG Ansatz für Luttingerflüssigkeiten früherer Anwendungen auf spinlose Fermionen [Meden et al. 2002a,b] wird in dieser Arbeit auf Spin-$\frac{1}{2}$ Fermionen erweitert, ferner wird zur Renormierung des Störstellenpotentials die des Zwei-Teilchen-Vertex einbezogen. Für spinlose Fermionen wird die quantitative Übereinstimmung der Ergebnisse dadurch erheblich verbessert, während für Spin-$\frac{1}{2}$-Systeme die Vertexrenormierung notwendig ist, um die Rückstreuung von Elektronen mit entgegengesetztem Spin und unterschiedlichen Fermipunkten im Niederenergielimes korrekt zu erfassen. Die zugrundeliegenden Näherungen sind a priori für schwache Wech-

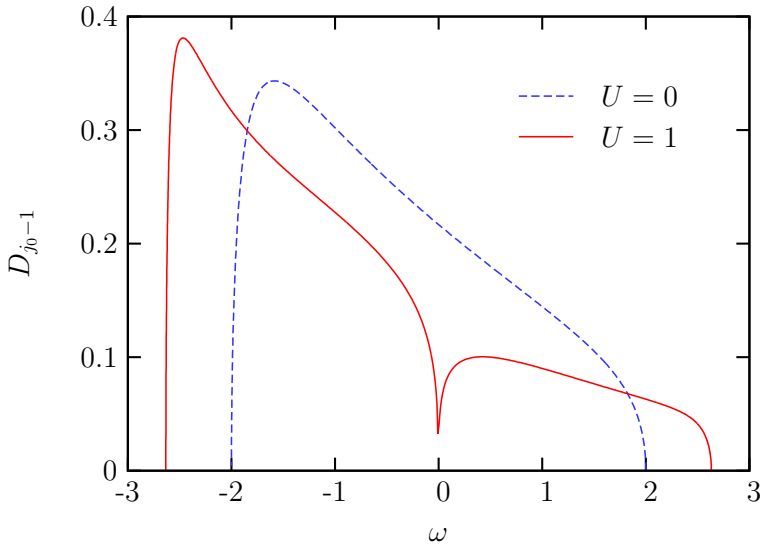

Abbildung D.1: *Lokale Zustandsdichte neben einer Störstelle der Stärke* $V = 1.5t$ *für spinlose Fermionen bei halber Füllung und Nächstnachbarwechselwirkung* $U = t$*; die Störstelle liegt in der Mitte einer Kette mit* 1025 *Gitterplätzen; zum Vergleich wird der wechselwirkungsfreie Fall* $U = 0$ *gezeigt. Die Wechselwirkung führt zu einer starken Unterdrückung der lokalen Zustandsdichte an der Fermienergie.*

selwirkungen und beliebige Störstellenpotentiale gerechtfertigt. Ein Vergleich mit exakten numerischen DMRG Daten für Systemgrößen mit bis zu 1000 Gitterplätzen zeigt jedoch, daß die fRG mit Vertexrenormierung auch für mittlere Wechselwirkungsstärken erstaunlich präzise ist, wobei für Spin-$\frac{1}{2}$ Fermionen eine nicht vernachlässigbare nackte Rückstreuamplitude zu deutlich größeren Abweichung von exakten Ergebnissen als für spinlose Fermionen führen. In diesem Fall ist in der Berechnung des nichtuniversellen Verhaltens auf mittleren Skalen der vernachlässigte Einfluß der Störstellen auf die Vertexrenormierung wahrscheinlich von Bedeutung.

Explizite Flußgleichungen wurden für verschiedene eindimensionale fermionische Gittermodelle mit unterschiedlichen Störstellenpotentialen hergeleitet. Die berechneten Observablen umfassen die lokale Zustandsdichte am Rand des Systems und in der Nähe von Störstellen, das Dichteprofil und die Temperaturabhängigkeit des linearen Leitwerts für Ketten mit bis zu 10^6 Gitterplätzen. Die Universalität des Randfixpunkts wird bestätigt, es stellt sich jedoch heraus, daß sehr große Systeme notwendig sind, um den Fixpunkt für mittlere Werte des Störstellenpotentials und der Wechselwirkung zu erreichen (s. Abbildungen D.1, D.2). Die spektralen Ei-

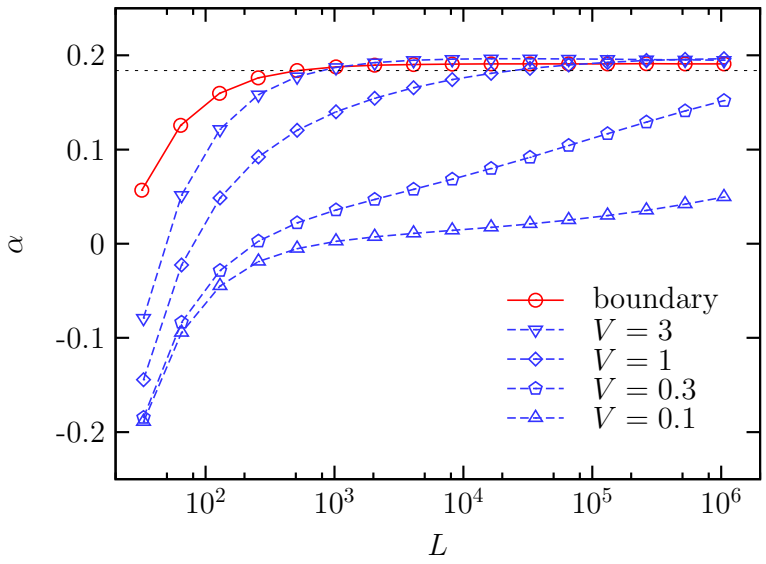

Abbildung D.2: *Effektiver Exponent des spektralen Gewichts an der Fermienergie in der Nähe eines Randes (durchgezogene Linie) oder einer Störstelle (gestrichelte Linien) in der Mitte der Kette der Länge L, für spinlose Fermionen bei viertel Füllung und Wechselwirkungsstärke $U = t$; die horizontale Linie stellt den exakten Randexponenten für $U = 1$ dar. Die verschiedenen Kurven zeigen, wie das universelle asymptotische Verhalten für schwache Störstellenpotentiale bei zunehmend großen Systemen eintritt.*

genschaften von Ein-Teilchen-Eigenschaften und der von Störstellen oder Rändern generierten Friedeloszillationen im Dichteprofil zeigen die charakteristischen Potenzgesetze bei niederen Energien oder großen Systemen. Für den linearen Leitwert von Luttingerflüssigkeiten mit einer einzelnen Störstelle mit nichtwechselwirkenden Zuleitungen liefert die fRG die erwarteten Potenzgesetze, sowie den durch eine Einparameterskalenfunktion bestimmten Übergang vom Schwach- zum Starkkopplungslimes. Für resonantes Tunneling durch eine Doppelbarriere, die einen Quantenpunkt umschließt, können in Abhängigkeit der Parameter unterschiedliche Temperaturbereiche mit ausgeprägtem Potenzgesetz- sowie nichtuniversellem Verhalten identifiziert werden [Enss et al. 2005; Meden et al. 2005].

Schließt man den Spinfreiheitsgrad mit ein, führt die Rückstreuung von Elektronen mit entgegengesetztem Spin an unterschiedlichen Fermipunkten zu unerwarteten Effekten, die bei spinlosen Fermionen nicht vorhanden waren. Insbesondere sind diese nicht in einer Beschreibung des Niederenergiefixpunktmodells, des Luttingermodells, erfaßt. Der erwarteten Unterdrückung des spektralen Gewichts an der

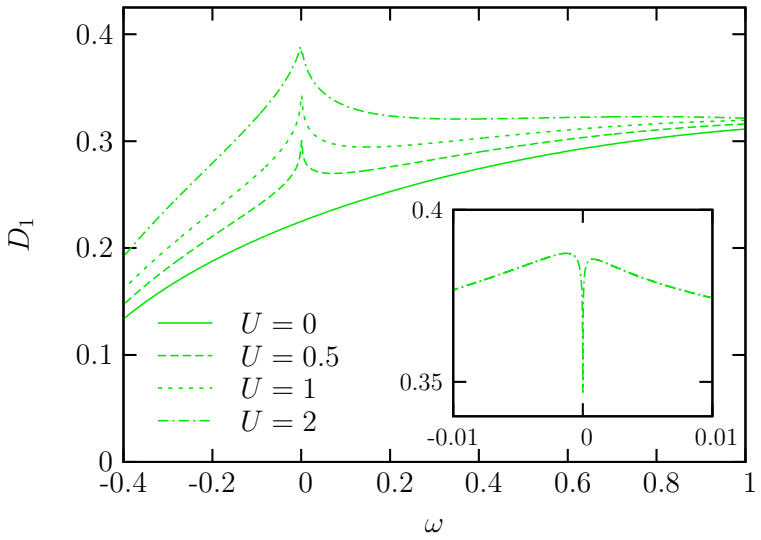

Abbildung D.3: *Lokale Zustandsdichte am Rand einer Hubbard Kette der Länge* $L = 4096$ *bei viertel Füllung und verschiedenen Wechselwirkungsstärken* U*; im kleinen Schaubild sind Ergebnisse für Hubbard Wechselwirkung* $U = 2t$ *und* $L = 10^6$ *für sehr kleine* ω *gezeigt. Im Gegensatz zur erwarteten asymptotischen Unterdrückung* steigt *das spektrale Gewicht an der Fermienergie* an*, eine Unterdrückung setzt erst bei sehr niederen Energien bzw. hinreichend großen Systemen ein.*

Störstelle und des Leitwerts bei niederen Energien geht oft ein deutlicher Anstieg voraus, der besonders in der lokalen Zustandsdichte in der Nähe einer Störstelle oder eines Randes als Funktion von ω ausgeprägt sein kann (s. Abbildungen D.3, D.4). Für die lokale Zustandsdichte in der Nähe eines Randes ist dieser Effekt bereits früher im Rahmen einer Untersuchung mit Hartree-Fock und DMRG [Meden et al. 2000; Schönhammer et al. 2000], und für den Leitwert mit einer Renormierungsgruppenanalyse des g-ology-Modells [Matveev et al. 1993; Yue et al. 1994] beobachtet worden. Ferner weisen die asymptotischen Potenzgesetze logarithmische Korrekturen auf. Im erweiterten Hubbard Modell mit einer zusätzlichen Nächstnachbarwechselwirkung zur lokalen Hubbard Wechselwirkung kann die Rückstreuamplitude für bestimmte Parameter unterdrückt werden. In diesem Fall sind die Ergebnisse ähnlich wie für spinlose Fermionen. Für schwache und mittlere Störstellenpotentiale wird das asymptotische Niederenergieverhalten nur bei verhältnismäßig niederen Energieskalen erreicht, die nur in sehr großen Systemen zugänglich sind (s. Abbildung D.5). Diese langsame Konvergenz wurde bereits für spinlose Fermionen wahrgenommen

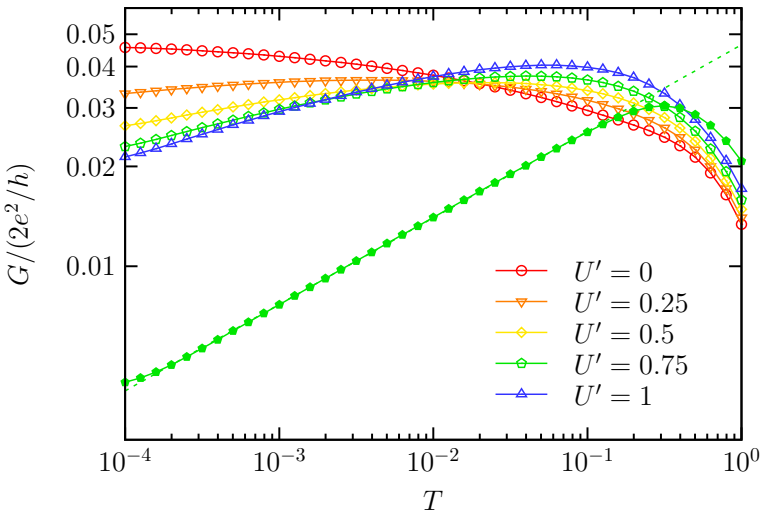

Abbildung D.4: *Temperaturabhängigkeit des Leitwerts für das erweiterte Hubbard Modell mit $L = 10^4$ Gitterplätzen mit einer Störstelle der Stärke $V = 10t$ in der Mitte, Hubbardwechselwirkung $U = t$ und verschiedenen Werten für die Nächstnachbarwechselwirkung U'; die Dichte beträgt $n = 1/2$, außer für die unterste Kurve, die mit $n = 3/4$ und $U' = 0.65t$ einer sehr kleinen nackten Rückstreuamplitude entspricht; die gestrichelte Linie stellt ein Potenzgesetz dar. Für das reine Hubbard Modell ($U' = 0$) steigt der Leitwert bei niedrigeren Temperaturen, mit zunehmender Nächstnachbarkomponente wird eine Unterdrückung sichtbar. Entsprechende Potenzgesetze sind aufgrund logarithmischer Korrekturen wesentlich schwächer ausgeprägt als vergleichsweise für einen Parametersatz mit dem gleichen Wert für K_ρ wie für $U' = 0.75t$, jedoch vernachlässigbarer Rückstreuamplitude.*

und bleibt auch ohne Zwei-Teilchen Rückstreuung erhalten.

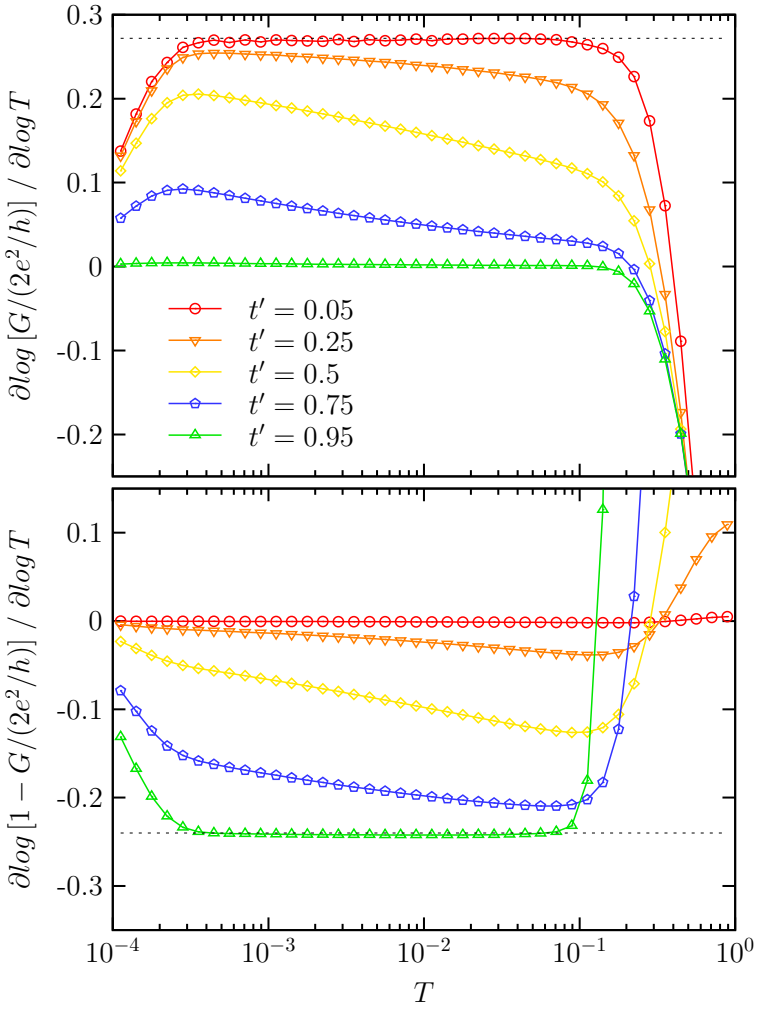

Abbildung D.5: *Effektiver Exponent des Leitwerts (oberes Schaubild) und der Abweichung vom unitären Limes e^2/h (unteres Schaubild) für das erweiterte Hubbard Modell mit $L = 10^4$ Gitterplätzen und Störstellen mit verschiedenen Hüpfamplituden t'; die Dichte ist $n = 3/4$, die Wechselwirkungen $U = t$ und $U' = 0.65t$; diese Parameter entsprechen einer sehr kleinen nackten Rückstreuamplitude; die gestrichelten Linien stellen Potenzgesetze dar. Für sehr starke Störstellen (kleines t') folgt der Leitwert einem wohl definierten Potenzgesetz, der für mittlere Werte von t' diesem näher kommt, jedoch nicht erreicht wird, bevor eine Sättigung aufgrund der endlichen Drahtlänge bei $T < \pi v_F/L$ einsetzt. Für sehr schwache Störstellen dagegen wird für $1 - G(T)/(2e^2/h)$ im unteren Schaubild ein Ansteigen mit einem Potenzgesetz beobachtet.*

Curriculum Vitae

Name	Sabine Andergassen
Date of birth	May 10th, 1976
Place of birth	Bozen, Italy
Nationality	Italian

Education

since 11/2001	Ph.D. studies supervised by Prof. Dr. Walter Metzner Max-Planck-Institut für Festkörperforschung, Stuttgart
03/2001	Laurea (M.S.) in Physics, 110/110 *cum laude* Università degli Studi di Roma "La Sapienza", Italy Thesis: *Fluctuation effects on charge instabilities in strongly correlated electron systems,* supervised by Prof. Dr. Carlo Di Castro
10/1995 - 03/2000	Studies of Physics Università degli Studi di Roma "La Sapienza", Italy
06/1995	Abitur Deutsche Schule Rom

Employment

since 11/2001	Research assistant, Department Metzner Max-Planck-Institut für Festkörperforschung, Stuttgart